Experimental exploration of cryogenic CO_2 capture utilising a moving bed

Thesis submitted in accordance with the requirements of the University of Chester for the degree of Doctor of Philosophy by:

David Gary Cann

MEng, AIChemE

April 2021

University of Chester

Thornton Science Park

Pool Lane

Ince

Chester

CH2 4NU

Declaration

The material being presented for examination is my own work and has not been submitted for an award of this or another HEI except in minor particulars which are explicitly noted in the body in the thesis. Where research pertaining to the thesis was undertaken collaboratively, the nature and extent of my individual contribution has been made explicit.

Signature……Date……

Acknowledgements

I would like to thank Carolina Font-Palma and Paul Willson, my academic and industrial supervisors, for their support throughout the PhD as well as providing opportunities to present my research at conferences such as GHGT-14. Their feedback and guidance throughout the project has been invaluable in my development as a researcher. I would also like to thank John Morris. His help in designing and constructing the purpose built rig for the experiments has been invaluable.

Nomenclature

a – surface area of bed material (m^2)

a_s – Specific surface area of bed material (m^2/m^3)

A – Cross sectional area (m^2)

Bi – Biot Number

C_p – Specific heat capacity (J/kgK)

d_p – Particle diameter (m)

D_{ab} – Binary diffusion coefficient

g – Desublimation rate constant (s/m)

h – Heat transfer coefficient (W/m^2K)

Δh – Latent heat (kJ/kg)

k – Thermal conductivity (W/mK)

k_{CO2} – Gas mass fraction

K_η – Non-dimensional conductivity in the y direction

K_ξ – Non-dimensional conductivity in the x direction

L – Characteristic length (m)

LCOE – Levelised cost of heat exchange

m – Mass (kg)

m'' – Frost deposition rate (kg/m^2s)

m' – Mass of frost per unit volume (kg/m^3)

$\dot{m}$ - Mass flow rate (kg/s)

MBHE – Moving bed heat exchanger

Nu – Nusselt Number

P – Pressure (atm)(Pa)

Pr – Prandtl Number

Q – Heat duty (kJ)

$\dot{Q}$– Volumetric flow rate (m^3/s)

Re – Reynolds Number

Sc – Schmidt Number

Sh – Sherwood Number

t – Time (s)

T – Temperature (K)

u – superficial velocity (m/s)

y – Gas mole fraction

Greek Symbols

δ – thickness (m)

ε – bed void fraction

η – Non-dimensional co-ordinate in the y direction

θ – Solid temperature (K)

ξ – Non-dimensional co-ordinate in the x direction

ρ – Density (kg/m^3)

μ – dynamic viscosity (kg/ms)

ψ – Pressure drop coefficient

Subscripts and superscripts

b - Bed

co2 – Carbon Dioxide

f – Fluid

f - Frost

g – Gas

σ - Saturation

s – Solid

s+ - Moving bed

sub - Sublimation

t – Triple point

w - Wall

x – x co-ordinate

y – y co-ordinate

Abstract

It is widely accepted that climate change is a result of the increase in greenhouse gases in the atmosphere. The continued combustion of fossil fuels and subsequent emission of CO_2 is leading to an increase in global temperatures, which has led to interest in decarbonising the energy sector. Carbon capture and storage (CCS) is a method of reducing carbon emissions from fossil fuel power plants by capturing CO_2 from exhaust gases and storing it in underground gas stores.

Carbon capture using chemical solvents is the most matured technology for capturing emissions from the energy sector, however as the energy sector continues to decarbonise with the arrival of renewable sources focus is shifting to other industries to reduce their carbon footprint. Solvent carbon capture has disadvantages including requiring large equipment and large amounts of heat to regenerate solvent for capture, meaning it would be difficult to scale the technology down and apply it to other industrial applications.

Cryogenic carbon capture (CCC) is one proposed method of CCS at smaller scale, which captures CO_2 by freezing CO_2 out of the exhaust gases as CO_2 forms a frost on a heat transfer surface. One disadvantage of CCC is the accumulation of CO_2 frost reduces the efficiency of the capture process. The process must be periodically shut down to regenerate the heat transfer surface and collect CO_2 that has been frozen out of exhaust gases. This thesis proposes to overcome the frost accumulation through the use of a moving packed bed of small spherical metal beads as the heat transfer surface. As CO_2 is fed into a capture column and freezes onto the metal beads, the metal beads are removed

from the column, regenerated to recover the CO_2, then cooled and recirculated back into the capture column. This prevents the accumulation of frost and allows continuous CO_2 capture.

There are many difficulties identified in this project, primarily a lack of knowledge on CO_2 frost formation and how heat transfer in a moving bed affects frost formation. The research done on a purpose built experimental rig is critical in improving the future design work of a next generation moving bed CCC system. The frost accumulation in a capture column is known as a frost front, which advanced through the capture column at a fixed velocity until the column is saturated with frost. Experimental results had shown that the frost front velocity is predictable for varying CO_2 concentrations and gas flow rates, with frost front velocities between 0.46-0.78 mm/s for CO_2 concentrations between 4-18% v/v and 0.36-0.98 mm/s for gas flow rates between 50-120 LPM. These frost front velocity experiments in a fixed packed bed allowed the design of a moving packed bed column to set the bed flow rate to match the frost front velocity. The moving bed experiments show that the excessive accumulation of CO_2 frost within the capture column can be prevented by utilising the moving bed.

The successful development of a moving bed CCC system would result in a cost effective solution to the requirements of certain smaller applications that need to capture CO_2, which make up a significant portion of emissions. In particular this technology is very economical for biogas upgrading, where the CO_2 content of biogas must be removed before the gas can be introduced to the UK's larger gas network. There is also a growing interest for use in shipping and other maritime applications, capturing CO_2 from ship exhaust emissions during transit.

Table of Contents

Figures

Tables

Chapter 1: Introduction

Rising emissions of carbon dioxide into the atmosphere has been closely linked to climate change. CO_2 emissions have increasingly become a concern due to increasing global temperatures. It is widely accepted that global warming is a result of the increase in greenhouse gases (GHG) (Houghton et al., 1996; Parmesan & Yohe, 2003). Greenhouse gases are gases that reside in the upper layers of our atmosphere, they absorb infra-red (IR) radiation and reflect this radiation back. When light from the sun reaches the Earth, the Earth is warmed by the effect of infra-red rays. When the Earth emits IR back to space, the radiation is instead absorbed by greenhouse gases and reflected back to Earth, this creates a greenhouse effect where heat is trapped within the Earth's atmosphere. (Houghton et al., 1996)

A worldwide effort is being made to reduce CO_2 emissions through the discontinued use or adaptation of carbon emitting sources in industrial sectors. Carbon capture and storage (CCS) is one such method of reducing carbon emissions, preventing the emission of CO_2 from point sources through chemical or physical separation from other gases and then storing concentrated CO_2 gas in underground stores.

This PhD thesis focuses on the development of a method of carbon capture and storage (CCS) utilising a cryogenic moving packed bed. Previous studies into cryogenic carbon capture have demonstrated that utilising a fixed packed bed is an effective method of carbon capture, however the fixed packed bed eventually becomes saturated with frost and requires the bed to be regenerated and the carbon dioxide frost to be recaptured for transport and/or storage. This drawback to the cryogenic packed bed concept is typically addressed by using multiple capture columns that can alternate between cooling, capture and regeneration stages of the packed bed to allow for a pseudo-continuous process.

The introduction of a moving packed bed seeks to address this issue of the cryogenic packed bed method of CCS. Utilising a moving bed for cryogenic carbon capture has not been covered previously in the available literature, this work investigates the conceptually proposed advanced cryogenic carbon capture known as A3C that uses a novel moving cryogenic packed bed system at technology readiness level (TRL) 2 (Willson et al., 2019). This thesis aims to demonstrate the cryogenic moving packed bed concept through experimental work, supported by theoretical work which is used to simulate and predict the behaviour of the experimental rig.

The main purpose of the experimental work within this thesis is to understand how quickly frost accumulates within a fixed packed bed and how to slow down, or halt entirely, the accumulation of CO_2 frost within a capture column. The major experimental objectives are summarised below:

- Design and construct a purpose built experimental rig for cryogenic carbon capture.

- Develop a method to predict the frost front velocity when varying CO_2 concentrations and gas flow rates.
- Demonstrate that a moving bed capture column can affect the frost front velocity and prevent excessive build-up of CO_2 frost.
- Balance flow rate of bed material and frost front velocity in order to create a thermal equilibrium within the capture column.
- Develop the technological readiness level (TRL) of the moving bed cryogenic carbon capture process to TRL 3.

A purpose built rig was constructed for the purpose of experimentation and was fed a mixed gas of CO_2 and N_2 to act as a simulated flue gas. The simulated flue gas was kept as a simple binary gas in order to reduce complexity, the purpose of the experimental work is to establish how to prevent the accumulation of CO_2 frost in a cryogenic capture column.

Experimental work began with the purpose built capture column being used to capture CO_2 frost as a fixed packed bed in order to understand the base case scenario. These experiments consisted of two stages; the first stage being a pre-cooling stage where the bed material in the capture column was cooled to near cryogenic temperatures, the second stage was the capture stage where CO_2 and N_2 mixed gas was fed into the bottom of the column where CO_2 would desublime out of the gas phase onto the packed bed. Once the build-up of frost within the fixed packed bed was understood, experimental work began on introducing the moving packed bed in order to mitigate the accumulation of CO_2 within the column. The purpose of these experimental runs was to observe whether the CO_2 frost would advance through the column in a steady predictable rate, known as the CO_2 frost front velocity. The rate of bed flow within the capture column was then set to match the frost front velocity in order to maintain a net frost front velocity of zero.

After establishing that the frost front can be controlled, further experimental work would combine the pre-cooling stage and capture stages of the experimental work into a simultaneous stage. Performing the two stages within the capture column simultaneously would demonstrate that the moving packed bed concept can capture CO_2 as a continuous process.

The structure of the thesis is as follows:

Chapter 2 covers the available literature and highlights the knowledge gaps in the area of cryogenic carbon capture. Different methods of carbon capture are also compared as well as the fundamentals of heat transfer and frost formation within fixed and moving packed beds.

Chapter 3 describes the experimental set up of the purpose built rig and outlines the experimental work that was conducted in this thesis. The experimental work focuses on the variation of gas flow rate and CO_2 concentration as the varying factors for experimental results.

Chapter 4 adapts available equations in the literature to the specifications for the purpose built rig given in the methodology chapter. The theoretical work provides comparative data for the experimental work in this thesis for discussion. Comparison between theoretical predictions and experimental data is important to validate the design of the experimental rig.

Chapter 5 displays results from fixed packed bed experiments, focusing on the frost front velocity within the fixed packed bed. Results from this chapter are compared to results in the literature and the compatibility of these results are discussed.

Chapter 6 discusses results for the moving bed experiments and shows that the frost front velocity can be controlled using the moving bed. Temperature profiles close to the gas injector show a significant change and delay in the characteristic temperature plateaus that indicate frost formation. This chapter also compares experimental results with simulated temperature profiles and discusses different methods of gathering data to construct simulated temperature profiles.

Finally, chapter 7 introduces a second gas injector to the capture column in order to allow bed cooling and CO_2 capture to occur simultaneously as opposed to operating in cycles. A significant step towards a continuous carbon capture process. The results from this chapter show promise, however results from experimental work are not as extensive as what would be ideal. The impact of Covid-19 on the UK had affected the progress of experimental work due to lockdowns and restrictions on working in the lab over the year.

Chapter 2: Literature Review

Introduction

The overview of this thesis has been provided in the introductory chapter, the development of a cryogenic carbon capture system which utilises a moving bed to avoid the problematic accumulation of CO_2 frost within the capture column.

In order to achieve the research aims of the PhD, the available literature must be studied thoroughly both to identify what research has been conducted that is applicable to this thesis and more crucially what research has not yet been conducted. This thesis will seek to identify research gaps that must be filled in order to progress the development of the proposed moving bed capture system. In particular,

this thesis focused research on the fundamentals of CO_2 frost formation and previous studies on fixed bed cryogenic carbon capture.

This chapter provides greater context behind the reasoning for developing the proposed moving bed capture system and discusses the relevant research that has been conducted in the literature.

2.1 Literature Overview and Background

While the greenhouse effect is a naturally occurring phenomenon that is vital to keeping the planet at a reasonable temperature, the continued combustion of fossil fuels since the industrial revolution has led to an increase in carbon dioxide emissions. The greater concentration of CO_2 in the atmosphere is causing an increase in global temperatures around the world beyond that which is sustainable for the environment.

In 2019, the UK government released an amendment to the 2008 Climate Change Act which increased the set target of 80% reduction of carbon emissions in the UK from the 1990 baseline by 2050 to a 100% reduction in carbon emissions (HM Government., 2019). With similar acts and carbon reduction targets being set around the world, it is clear that there has been extensive research into methods of meeting these targets.

This literature review will give a scope of the background of carbon capture and the need for it and cover the known methods of carbon capture that have been researched and published. In particular, of the methods of carbon capture to date, this literature review will analyse research made into cryogenic carbon capture and the factors affecting carbon capture in cryogenic packed beds. Namely; heat transfer, pressure drop, and desublimation of gases on packed bed surfaces.

2.2 Chemical Properties of Carbon Dioxide

Understanding the relevant chemical properties of carbon dioxide is critical in finding the most effective methods of separation to capture carbon dioxide from flue gases. Relevant chemical properties can be listed into two major categories; chemical reactive properties with sorbent and physical phase change properties.

Carbon dioxide is able to react and form carbonates and bicarbonates, which is the basis for various methods of CCS. Reaction between carbon dioxide with aqueous ammonia or with soluble carbonates is extensively researched in the literature. (Figueroa, Fout, Plasynski, McIlvried, & Srivastava, 2008).

Carbon dioxide is soluble in water, as well as other chemical solvents due to the chemical structure of CO_2. Although the structure of carbon dioxide is symmetrical and therefore non-polar, the oxygen present in the structure still contains a slight negative charge which allows it to be soluble in polar

solvents. There have been numerous tests on the solubility of carbon dioxide in various proposed solvents (Aronu et al., 2011; Krupiczka, Rotkegel, & Ziobrowski, 2015).

Carbon dioxide is also able to be captured by exploitation of its phase change properties compared to other components in flue gases.

CO_2 desublimes at -78.5^oC at atmospheric pressure and with increased pressure CO_2 can be condensed out of the gaseous phase. The desublimation temperature changes according to both pressure and the CO_2 concentration. CO_2 desublimation occurs at different temperatures, as can be seen in table 2.1.

Table 2.1. Desublimation temperatures under different CO2 concentrations at atmospheric pressure (Eide et al., 2005).

Concentration (% v/v)	100	15	10	5	2	1	0.1	0.002
Desublimation Temperature (^oC)	-78.5	-99.3	-103.1	-109.3	-116.7	-121.9	-136.7	-155.8

2.2 Carbon Capture Overview

Carbon capture methods can be divided into three major groups; pre-combustion, post combustion carbon and oxy-fuel combustion. Post-combustion capture involves processes that seek to capture CO_2 once combustion has been completed within the reactor, separating out CO_2 from a range of flue gases to store the CO_2 for either storage underground or for utilisation in industry if high purity. Pre-combustion carbon capture decarbonises the fuel source before it is combusted, oxy-fuel combustion utilises an air separation unit to burn fuel in a near pure oxygen environment leaving an easy to separate flue gas consisting of CO_2 and water.

The major methods of pre and post combustion carbon capture are; adsorption, chemical or physical absorption, cryogenic, membrane separations and chemical looping combustion (CLC).

2.2.1 Oxy-Fuel Combustion

Oxy-fuel combustion capture processes utilise an air separation unit to modify the oxygen content present in the combustion reaction to synthesise a flue gas that is easier to capture CO_2 from. Using a pure oxygen environment for combustion, the fuel is burned to create CO_2 and water. The flue gas is allowed to cool which will condense the water out of the flue gas and the resulting gas is a high purity

CO_2 gas, which could be stored underground via pipeline, used in enhanced oil recovery, or if pure enough it can be utilised in the chemical industry.

The Allam Cycle is an oxy-fuel combustion method designed by Rodney Allam that recirculates supercritical CO_2 created post-combustion back into the combustion chamber mixed with pure oxygen to control combustion rates and temperatures within the combustion chamber, while the rest of the near pure CO_2 formed in the process is stored underground. (Scaccabarozzi, Gatti, & Martelli, 2016). NET Power is constructing a power plant to demonstrate this technology in Texas, the power plant is a 300MWe natural gas fired plant and was expected to be fully in operation by 2020 (Allam et al., 2017). Progress continues to be made at the NET Power although the date has been delayed to 2022.

2.2.2 IGCC

IGCC stands for Integrated Gasification Combined Cycle, the principle is to combust fossil fuels at a high pressure in a low oxygen environment. This causes a gasification reaction which creates a syngas consisting of CO, CO_2, H_2, H_2O and COS. This syngas is then reacted with water in a water-gas shift reaction (Adams, Hoseinzade, Madabhushi, & Okeke, 2017).

$$H_2O + CO \rightarrow CO_2 + H_2 \quad (1)$$

$$H_2O + COS \rightarrow CO_2 + H_2S \quad (2)$$

The syngas, now consisting of CO_2, H_2, and H_2S can then be treated and separated using an absorber to capture CO_2 and create a combustible fuel in H_2. Since H_2 is used as the fuel gas for combustion, removing the CO_2 at this stage makes IGCC a pre-combustion technology.

2.2.3 Chemical Looping

Chemical looping combustion is another method of carbon capture where fuel is reacted in an oxygen rich environment. Unlike oxy-fuel combustion, which uses an air separation unit to purify oxygen out of the air, chemical looping combustion provides oxygen to the reactor by circulating metal oxides. These metal oxides are reduced when reacting with the fuel, fed into an air reactor to become oxidised, then recirculated back into the fuel reactor (Sreenivasulu, Gayatri, Sreedhar, & Raghavan, 2015). The reaction in the fuel reactor is similar to a water-gas shift reaction (Ohlemuller, Strohle, & Epple, 2017).

$$CH_4 + 4Me_xO_y \rightarrow CO_2 + 2H_2O + 4Me_xO_{y-1} \quad (3)$$

$$CO + Me_xO_y \rightarrow CO_2 + Me_xO_{y-1} \quad (4)$$

$$H_2 + Me_xO_y \rightarrow H_2O + Me_xO_{y-1} \quad (5)$$

A $1MW_{th}$ pilot scale CLC plant has been constructed at Technische Universität Darmstadt using coal and a fuel blend of coal and torrefied biomass. More volatile fuels resulted in a greater carbon capture efficiency of the plant and a CO_2 reduction efficiency compared to conventional coal plants of 122%, meaning negative emissions when compared to coal. However the actual capture efficiency of carbon was low due to char leaving the fuel reactor, reacting in the air reactor and forming CO_2. (Ohlemuller et al., 2017).

Calcium looping also uses a similar set up but instead focuses on the dry carbonation reaction between metal oxides and CO_2 under high temperature (~650^oC)(Diego, Arias, & Abanades, 2020). Post combustion calcium looping cycles a metal oxide into a carbonator which reacts with CO_2 present in the flue gas, then the resulting carbonate is fed into a calciner which is heated to decompose the carbonate back into the metal oxide and a CO_2 rich gas stream (Diego et al., 2020). Using metals such as lithium oxide or calcium oxide for the carbonation reaction with CO_2. The advantages of this proposed method is the abundance of high temperatures leading to reduced energy penalties involved in the regeneration of the sorbent (Eide et al., 2005).

$$MeO_{(s)} + CO_{2(g)} \leftrightarrow MeCO_{3(s)} \quad (6)$$

A similar reaction can be complete using carbonates such as sodium and lithium carbonate. Sodium carbonate can react with CO_2 and water to create sodium bicarbonate. This bicarbonate can also be regenerated under high temperatures. This carbon capture process is known as alkali-metal carbonate process (M. Zhao, Minett, & Harris, 2013).

$$Na_2CO_3 + CO_2 + H_2O \leftrightarrow 2NaHCO_3 \quad (7)$$

2.2.4 Cryogenic

Cryogenic carbon capture utilises the difference in the temperature and pressure of the triple point of constituent gases in the flue gas stream to physically separate out CO_2 by desublimating out CO_2 forming a frost. Cryogenic carbon capture has advantages of being able to run effectively at near atmospheric pressure but has issues relating to heat transfer efficiency. As the carbon dioxide is captured as a frost on the heat transfer surface, the accumulation of frost reduces heat transfer efficiency of the process over time. Furthermore, the frost must be recovered from the heat transfer surface which requires periodic shut down of the capture system for regeneration.

Other forms of cryogenic carbon capture will instead use a method of cryogenic distillation to separate CO_2 from other components in its liquid state to avoid frost related issues. However the increased pressure and lower temperatures requires to liquefy the carbon dioxide increases operating costs for separation.

2.2.5 Absorption

Absorption uses an absorbent solution to capture CO_2 by chemical or physical reaction. For low pressure systems, amine based absorbents such as monoethanolamine (MEA) is the preferred selection. In high pressure systems or flue gases with high concentrations of CO_2, organic solvents such as Selexol and Rectisol are used for physical absorption instead due to their higher absorption capability. (Sreenivasulu et al., 2015).

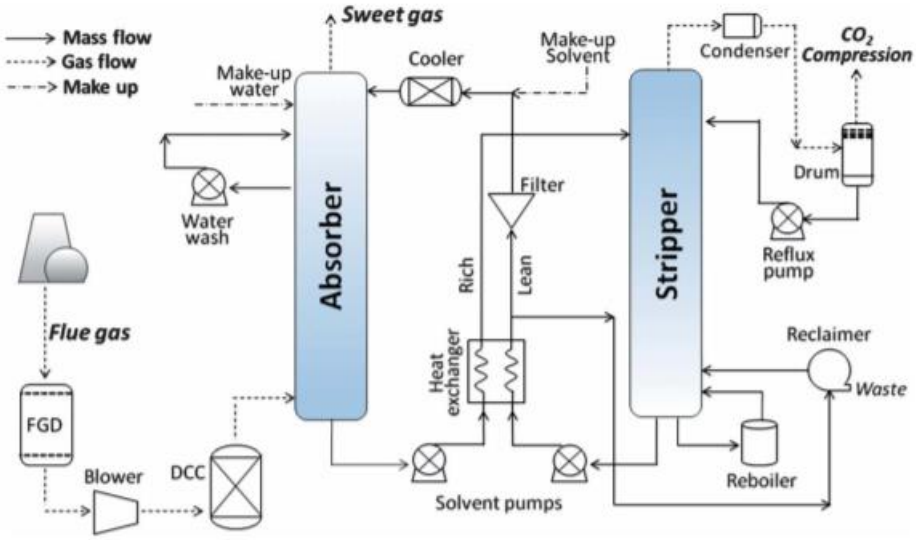

Figure 2.1. Diagram of typical MEA process. Republished with permission of Energy & Environmental Science, from A review of techno-economic models for the retrofitting of conventional pulverised-coal power plants for post-combustion capture (PCC) of CO2, M.Zhao et al., volume 6, 2012; permission conveyed through Copyright Clearance Center, Inc.

Of the carbon capture technologies, chemical absorption is the most developed and widely employed due to its capture efficiency at low CO_2 concentration and higher selectivity (Sreenivasulu et al., 2015). The previously mentioned methods of carbon capture are the main methods researched in the literature. The main disadvantages of absorption technology is the energy intensive requirements to regenerate the solvent and desorb CO_2 which has large impacts on the operational costs, as well as the requirement for large quantities of amine and large absorber columns for the solvent to effectively capture CO_2 (Haszeldine, 2009). However, MEA is the baseline chemical solvent for absorption technology and investigation into more effective solvents is ongoing in the literature. Solvents such as

piperazine, various ionic liquids, 2-amino-2-methyl-propanol (AMP), diethanolamine (DEA) and methydiethanolamine (MDEA) (Ma, Gao, Wang, Hu, & Cui, 2018; MacDowell et al., 2010; Rochelle et al., 2011).

Absorbents are sprayed into a contact column with flue gas, the solvent removes CO_2 from the flue gas stream by absorbing the CO_2 into its structure. The absorbent is then collected from the bottom of the contact column and regenerated through high temperatures to separate solvent and CO_2. The CO_2 is collected and stored and the solvent is recycled back into the contact column.

An example of a successful chemical absorption CCS pilot plant is the Tomakomai CCS demonstration project. It was constructed in October 2015 with the aim of capturing and storing 100,000 tonnes of CO_2 per year. A test run of the plant was completed in February and injection of CO_2 into underground stores has been continuing since April 2016 for 3 years. This project is an example of chemical absorption being done at large scale and aims to demonstrate the effectiveness of absorption based CCS as well as demonstrate that leaking does not occur from the chosen underground storage location by monitoring the storage site until 2020 (JapanCCS, 2016).

2.2.5.1 Aqueous Ammonia

Ammonia can be reacted with carbon dioxide to produce carbonates. The simplified overall reaction for the absorption of CO_2 by ammonia is governed by the following reversible reaction (Liu, Wang, Zhao, Tong, & Chen, 2009).

$$CO_{2(g)} + NH_{3(aq)} + H_2O_{(l)} \leftrightarrow NH_4HCO_{3(aq)} \quad (8)$$

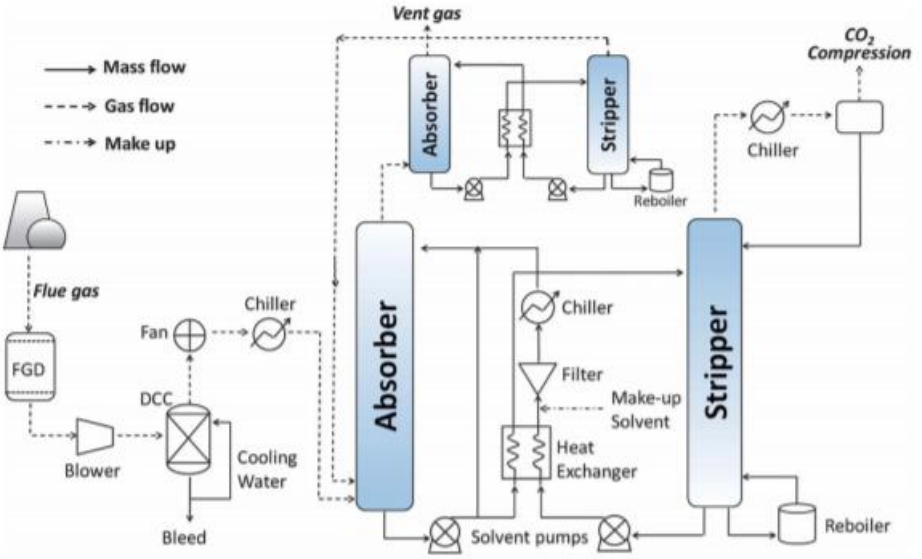

Figure 2.2. Diagram of chilled ammonia process. Republished with permission of Energy & Environmental Science, from A review of techno-economic models for the retrofitting of

conventional pulverised-coal power plants for post-combustion capture (PCC) of CO2, M.Zhao et al., volume 6, 2012; permission conveyed through Copyright Clearance Center, Inc.

The process functions similarly to absorption processes, where aqueous ammonia is sprayed into a stripping column to react with CO_2 gas. Literature reports that aqueous ammonia can reach a greater level of capture efficiency and a higher capacity than the typical MEA absorbent (Liu et al., 2009).

2.2.7 Membranes

Membrane separations use polymer or ceramic membranes to filter CO_2 out of the flue gas. (Ben-Mansour et al., 2016). Utilising a semi-permeable membrane to allow CO_2 to flow through the membrane from the flue gas into an absorbing fluid. Membrane separation requires a difference in partial pressure on both sides of the membrane to act as the driving force for separation (Tan, Nookuea, Li, Thorin, & Yan, 2016).

For a membrane to be effective at CO_2 capture, it requires a list of properties (Powell & Qiao, 2006):

- High carbon dioxide permeability.
- High carbon dioxide/nitrogen selectivity.
- Thermally and chemically resistant.
- Plasticisation resistance.
- Aging resistance.
- Cost effective.
- Ability to be cheaply manufactured.

The permeability and CO_2/N_2 selectivity of the membrane are the two leading factors and usually come at a trade-off between another, membranes that offer high permeability have low selectivity and vice versa. It is possible to manufacture high selectivity membranes on a support structure with high permeability to overcome this issue however there is currently a lack of study on the long-term stability of membranes and their resistance to water vapour present in flue gases (Kárászová et al., 2020).

2.2.8 Adsorption

Adsorption is a physical process that removes CO_2 from a flue gas stream with the use of adsorption/desorption properties of CO_2 (Ben-Mansour et al., 2016). Unlike absorption which utilises the entire volume of the sorbent, adsorption only utilises the surface volume of the sorbent due to the heterogeneous nature of the process (Aaron & Tsouris, 2005). Adsorption generally has an advantage over absorption by having lower energy requirements for regeneration of the sorbent (Ben-Mansour et al., 2016).

Different methods of adsorption have been proposed in the literature, which include pressure swing adsorption (PSA), temperature swing adsorption (TSA) and electrothermal swing adsorption (ESA). PSA takes advantage of the reduced adsorption capacity of adsorbent material at low pressure, adsorbent material captures CO_2 under high pressure and is regenerated by reducing the pressure. Sometimes a purge gas stream is introduced to further reduce the partial pressure of the adsorbed CO_2. TSA similarly regenerates the adsorbent material using a heated gas stream such as steam to recover CO_2, where steam can be easily condensed to recover CO_2. ESA uses an electric current to deliver heating to the adsorbent material, which can offer higher CO_2 concentrations after regeneration as purge gas streams and heating can be applied together (Ribeiro, Grande, & Rodrigues, 2014).

One particular type of adsorbent are metal organic frameworks (MOFs), these components are able to selectively allow CO_2 to pass through its porous structure while excluding molecules with a larger kinetic diameter such as nitrogen and methane. Granting high levels of CO_2 adsorption due to the quadrupole moment CO_2 exerts along with strong selectivity of CO_2 due to the kinetic diameter being smaller than the likes of N_2 and CH_4. MOFs face issues due to thermal stability and a lack of resistance to water (Ghanbari, Abnisa, & Wan Daud, 2020).

2.2.9 Direct Air Capture

While not specifically a method of flue gas treatment, direct air capture (DAC) is a process that uses a similar process to common CCS technology but has a unique outlook. DAC filters carbon dioxide out of ambient air rather than focusing on point sources like power plants. Roughly half of carbon dioxide emissions are not emitted from point sources and CCS is not effective at capturing carbon dioxide from distributed sources. DAC not requiring to be attached to point sources allows the set up and operation of plants in a much greater number of locations (Sanz-Perez, Murdock, Didas, & Jones, 2016).

An example of direct air capture commercially available through Climeworks. Climeworks use direct air capture to capture CO_2 from atmospheric air on a filter bed of amines supported on granulates. The filter bed captures atmospheric CO_2 that is drawn into the filter by a large fan. When the filter is saturated with CO_2, the filter is regenerated by heating to 100^{o}C. CO_2 is then transferred from the filter into a storage vessel (McGrath, 2017).

2.2.10 Comparisons for carbon capture

The previously listed CCS technologies have different advantages and disadvantages, the application of these technologies into different industries is dependent on the compatibility with the present flue

gases in industry. Tables 2.2 and 2.3 show the general compositions of typical flue gas streams and the relative advantages and disadvantages of CCS technologies respectively.

Table 2.2. CO_2 concentration of various point sources.

Flue gas source	**CO_2 concentration**	**Reference**
Gas turbine	4% 8-10%	
Coal fired plant	10-11%(wet) 12.5-14.5%(dry)	(Aouini, Ledoux, Estel, & Mary, 2014)
Cement kiln	14-33%	(Bosoaga, Masek, & Oakey, 2009)
Diesel engine	12%	(Sharma & Maréchal, 2019)
Biogas	20-50%	(Chen, Vinh, Avalos Ramirez, Rodrigue, & Kaliaguine, 2015)

Carbon capture technology	Advantages	Challenges	Ideal environment	References
Chemical absorption	High technological readiness level. Most matured technology.	MEA is the most well researched solvent but also relatively expensive. Development of new solvents can be difficult to scale up.	High temperature, low pressure, low CO_2%, large flow rates.	(Sreenivasulu et al., 2015; M. Zhao et al., 2013)
Adsorption	Low energy requirement for regeneration.	Generally less CO_2 capacity. Intermittent process with capture and regeneration cycles.	High pressure, low temperature, dry gas.	(Ben-Mansour et al., 2016)
Chemical looping			High temperature.	(Diego et al., 2020; M. Zhao et al., 2013)
Cryogenic	No requirement for specialist materials for absorption. Can operate at atmospheric pressure.	Frost accumulation and regeneration makes the process intermittent.	High CO_2%, dry gas.	(Tuinier, Annaland, Kramer, & Kuipers, 2010)
Membranes		The most effective membranes require more testing to demonstrate robustness.		(Kárászová et al., 2020)

Table 2.3. Summary of carbon capture processes.

Post-combustion carbon capture is the most mature of the currently known carbon capture methods and are suitable for being retrofitted onto existing power plants as opposed to requiring a new fleet power plants to be constructed, with the added benefit of being able to be applied to other industries such as hydrogen gas production, steel and cement manufacturing. This advantage also allows post combustion CCS to be installed on other industrial emitters, with interest in CCS from cement, marine shipping and hydrogen production. This advantage gives post-combustion capture systems an advantage for short and medium term CCS projects. The ability to be retrofitted makes it easier to compare different technologies in the literature as technologies can be evaluated through using data from existing power plants as a base case. Comparison of a base case power plant with a power plant with CCS allows for a clear understanding of the magnitude of effect for different CCS technologies. One key method of comparing the different post combustion CCS processes in the power sector is the specific energy of CO_2 capture, the amount of energy required to capture a kg of CO_2. Absorption technologies have made significant improvements to their technological readiness level (TRL), making it the most mature of available CCS technologies. Amine based absorption is used as a typical benchmark to compare other technologies. Cryogenic carbon capture compares very well to these technologies, being lower in energy penalty and comparable to membrane technology.

Two major factors are compared when performing techno-economic evaluations of power plants, these are the levelised cost of electricity (LCOE) and the cost of CO_2 avoided or cost of CO_2 captured (M. Zhao et al., 2013).

$$LCOE = \frac{capital\ costs\ \times levelisation\ factor}{net\ power\ output\ \times capacity\ factor\ \times 8760} + variable\ operating\ costs + fuel\ costs \quad (9)$$

$$Cost\ of\ CO_2\ avoided = \frac{LCOE\ (capture) - LCOE\ (ref.)}{CO_2\ emissions\ (ref.) - CO_2\ emissions\ (capture)} \quad (10)$$

Evaluations of carbon capture technologies have been conducted in the literature (Adams et al., 2017; Goto, Yogo, & Higashii, 2013; Tuinier, Hamers, & Annaland, 2011; M. Zhao et al., 2013). These evaluations work under different assumptions and do not consider all carbon capture technologies.

Goto et al (2013) investigated the regeneration energies and efficiency penalties of known solvents in chemical absorption. The results, shown in table 2.4, show that most solvents are roughly equal in their efficiencies. The work also notes that while retrofitting CCS onto an existing plant provides no

noticeable advantage in energy efficiency over newly built plants, retrofitting has a cost advantage of 33 euros/t-CO_2 vs 44 euros/t-CO_2 (Goto et al., 2013).

Table 2.4. Performance of advanced solvents (Goto et al., 2013).

Solvent	Regeneration energy (GJ/t-CO_2)	Efficiency penalty (%)
Econmaine FG+	3.12	9.2
KS-1	3.08	8.4
KS-2	3.00	9.3
CANSOLV	2.33	7.8
H3	2.80	7.8
NH_3 (10^oC)	2.2-2.8	8-11.2
NH_3 (4^oC)	2.46	8.5
MDEA-TETA	2.55	9.3
MDEA-PZ	2.52	8.46

Zhao et al. (2013) investigated the LCOE and cost of CO_2 avoided among various different techno-economic case studies of coal power plants. Zhao et al. collected different economic evaluations of CCS technologies for analysis. These individual economic analyses were based on a base case of pulverised coal power plant and compared the base case power plant and CCS retrofitted power plant for each individual study. The average percentage differences were compared between different CCS technologies. Comparing the percentage difference between LCOE reference base case and the case with CCS retrofitted produced the table of results summarised in table 2.5.

Table 2.5. LCOE and cost of CO2 avoided from techno-economic studies (M. Zhao et al., 2013).

	MEA	Chilled ammonia	Alkali metal carbonate	Membrane	Calcium looping
CO_2 emissions reference (kg/MWh)	807	799	774	781	788
CO_2 emissions capture (kg/MWh)	112	109	84	92	125
Reference LCOE ($/MWh)	57	64	65	63	52
Capture LCOE ($/MWh)	100	99	88	106	71

Difference in LCOE compared to base plant without retrofitted CCS (%)	+75.1	+55.5	+36.2	+69.6	36.3
Cost of CO_2 avoided ($/t-$CO_2$)	61	53	34	68	29

The results in table 2 show that from the techno-economic studies Zhao et al had reviewed, calcium looping and alkali metal carbonate are the most cost-effective technology for post combustion capture on pulverised coal plants. In addition to the economic comparisons of different capture technologies, typical capture technologies are also compared on a MJ/kg CO_2 basis in appendix A.

Tuinier et al (2011) conducted a techno-economic evaluation of cryogenic, membrane and amine absorption capture technologies. Comparing their estimated costs of CO_2 abatement under different methods of operation. The flue gas streams in this techno-economic evaluation are kept at roughly the same flow rates; being fed at 635kg/s, 666kg/s and 602kg/s for cryogenic, absorption and membrane technologies respectively. The figure 2.3 shows the results of their evaluation. The graph shows that given favourable assumptions; such as low pressure steam being readily available for amine scrubbing, or a cold source being readily available for cryogenic capture, these technologies are favourable. Therefore, the efficiency and cost related impacts of carbon capture depend on the conditions and resources available at the site where carbon capture would be constructed. The work suggests that under similarly favourable conditions of a readily available cold source, cryogenic carbon capture would be the most cost effective method of carbon capture out of the methods evaluated in their work.

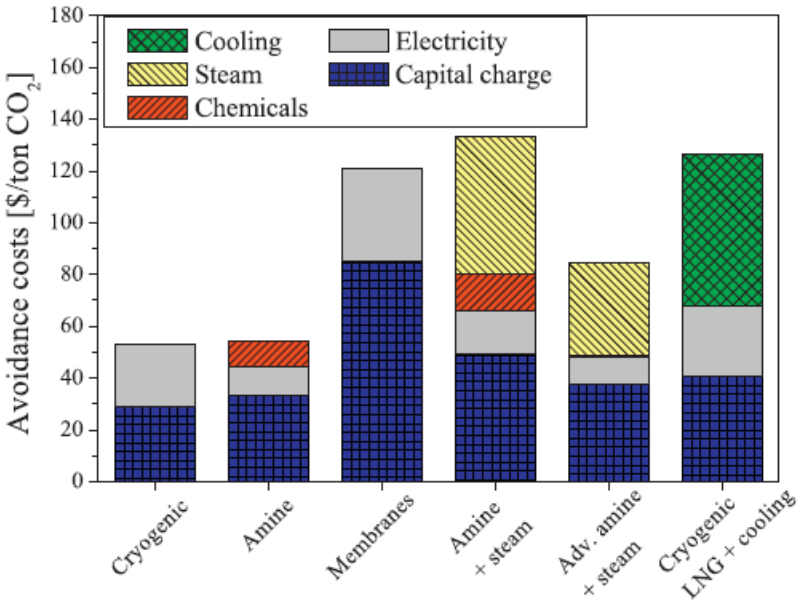

Figure 2.3. Avoidance costs for different technologies. Republished with permission of International Journal of Greenhouse Gas Control, from Techno-economic evaluation of cryogenic CO2 capture—A comparison with absorption and membrane technology, Tuinier, Hamers et al., volume 5, 2011; permission conveyed through Copyright Clearance Center, Inc.

Okeke and Adams collate a number of techno-economic evaluations of proposed post combustion CCS approaches in the US. The paper collects techno-economic data and makes comparisons between the proposed approaches and their economic benefits compared to unabated carbon power plants. The findings on the comparative differences between capture approaches were inconclusive in regards to which solvents or membranes were more suitable due to the many differences in methodology and assumptions in each study. Instead, Adams et al. determine that improvements made to power generation plants through post combustion capture methods are insufficient to improve key metrics such as cost of CO_2 emissions avoided, stating that the fundamental separation problem of CO_2/N_2 limits how effective these technologies can be economically. Instead, technologies such as oxy-fuel combustion which separates CO_2/H_2O, can achieve greater efficiency due to an easier separation step for CO_2 recovery. Figure 2.4 demonstrates the results of the paper's findings, typically post combustion capture processes had a wide variation in cradle to grave emissions and LCOE compared to pre-combustion capture techniques.

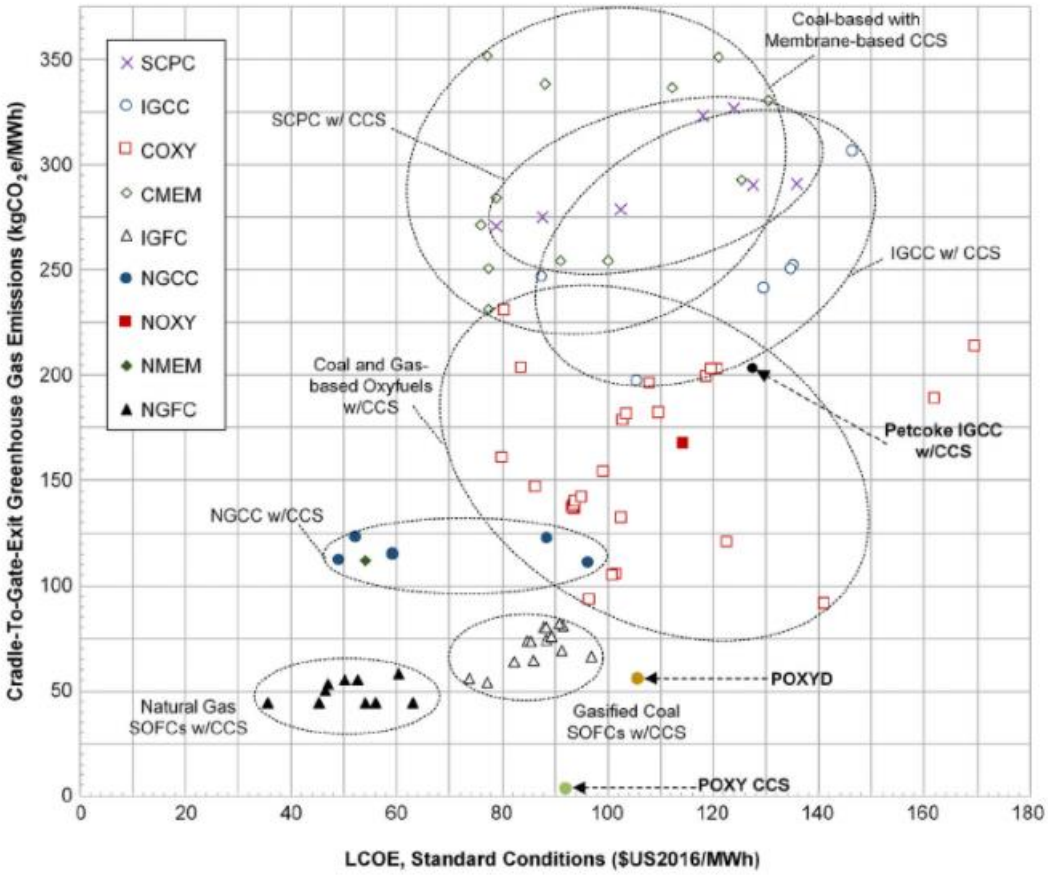

Figure 2.4. LCOE vs CO2e emissions for various capture proposals. SCPC – supercritical pulverised coal, IGCC – integrated gasification combined cycle, COXY/NOXY – coal/natural gas based oxy-fuel, CMEM/NMEM – coal/natural gas based membranes, IGFC – integrated gasification fuel cell, CaL – calcium looping, CCLC/NCLC – coal/natural gas based chemical looping combustion, NGCC – natural gas combined cycle, NGFC – natural gas fuel cell. (Okeke & Adams II).

It can be seen that there are discrepancies between findings between Okeke and Adams (Okeke & Adams II) and Zhao et al. (M. Zhao et al., 2013) between CO_2 emissions and the LCOE considering membrane and calcium looping post combustion capture. There are some important differences between the calculations of emissions between the two published papers. Firstly, Okeke and Adams took into consideration the cradle to grave emissions, the total emissions released by the plant including construction and decommissioning of the plant. Whereas Zhao et al. does not cite cradle to grave emissions. Furthermore, Okeke and Adams give emissions of CO_{2e} would include other greenhouse gases whereas Zhao et al. only considers the CO_2 emissions of the plant. This would explain why Adams et al. reported the emissions of calcium looping and membranes to be significantly higher than Zhao et al. The LCOE discrepancies could be explained by the different assumptions in referenced published papers used in their respective review articles.

Amine based carbon capture is recognised as the most matured technology, however the size requirement of amine absorption columns to achieve a high capture rate of CO_2 is large. This is suitable for large scale power plants where the scale of the process is large as well, but for smaller scale industrial sectors an amine absorber cannot be scaled down as effectively without sacrificing the capture efficiency of the process. This indicates a gap in the market where already existing industrial sectors outside of power generation require a modular addition to their process to scrub flue gases of CO_2 of an appropriate size for their process.

This paper aims to investigate cryogenic carbon capture (CCC) as a method of CO_2 separation. Cryogenic carbon capture is a post combustion capture process that allows for the separation of CO_2 from flue gas through a physical phase change instead of a chemical separation process. Cryogenic carbon capture has gathered interest in a range of potential applications such as hydrogen production and biogas upgrading.

2.3 Cryogenic carbon capture

The concept of cryogenic carbon capture utilises a cold source to sufficiently cool down a flue gas containing CO_2 sufficiently to cause CO_2 to separate from the gas phase by phase change. This is usually done through either cryogenic distillation or uses the difference in the location of the triple point of CO_2 compared with other components of a flue gas stream to act as the driving force for separation. At near atmospheric pressure, the sublimation temperature of CO_2 occurs at a relatively high temperature compared to the point of sublimation temperatures of other gas components.

Cryogenics have been gaining interest in both carbon capture and biogas upgrading to liquefied natural gas (LNG). Biogas upgrading utilises cryogenics as a means of removing impurities, such as CO_2 and H_2S (Spitoni, Pierantozzi, Comodi, Polonara, & Arteconi, 2019).

Cryogenic carbon capture has a unique advantage in that the nature of separation means that the carbon dioxide recovered from the process is of high purity in comparison to the likes of carbon dioxide from chemical absorption that has traces of amines, so long as water is removed from the process before going to near cryogenic conditions. This means that the CO_2 formed is of a useable purity in industrial or commercial processes, meaning it could be used as a commercial product.

Attaining a high efficiency cryogenic cooler requires minimal exergy losses during cooling processes. Irreversibility in cryogenic cooling comes from the convective heat transfer between the hot and cold streams. Heat transfer between the cold stream and ambient conditions and pressure drop due to fluid flow (Sahoo & Das, 1994). Reducing energy losses in heat transfer relies on effectively integrating heat transfer throughout the system, creating the smallest minimum temperature approach possible.

Temperature approach is the temperature difference of hot and cold fluid streams entering a heat exchanger, typically the temperature of the process fluid at the outlet of the heat exchanger and the service fluid temperature at the inlet; heat transfer between the two fluids causes the two fluids to approach the temperature of the other. A temperature approach of zero indicates that the temperature of the two streams are equal, so all possible heat transfer has occurred and no exergy is lost.

The current cryogenic capture technologies being researched are listed (C. Song, Liu, Deng, Li, & Kitamura, 2019); cryogenic distillation, controlled freezing zone (Kelley, Valencia, Northrop, & Mart, 2011), cryogenic carbon capture via compressed flue gas (CCC-CFG), cryogenic carbon capture via external cooling loop (CCCECL) (Baxter, Baxter, & Burt, 2009), CryoCell® (Hart & Gnanendran, 2009), Stirling coolers (C.-F. Song, Kitamura, Li, & Ogasawara, 2012), cryogenic packed beds (Ali, Maqsood, Syahera, Shariff, & Ganguly, 2014; Tuinier, Annaland, & Kuipers, 2011), anti-sublimation (Clodic, El Hitti, Younes, Bill, & Casier, 2005). Details of a feasibility study regarding the moving bed cryogenic packed bed technology this work seeks to demonstrate experimentally, known as A3C is included as well (Willson et al., 2019).

Distillation is a common method of separation and purification of product; cryogenic distillation is the application of distillation under cryogenic temperatures, -80 to -90 ^{o}C approximately (Maqsood, Pal, Turunawarasu, Pal, & Ganguly, 2014), this process has been proposed for natural gas purification. The flue gas is pre-cooled before entering the distillation column. For biogas upgrading, CO_2 separation produces methane as a gas and CO_2 is recovered as a liquid from the bottom product.

Controlled freezing zone (CFZ) is a similar in concept to cryogenic distillation which has been used to purify natural gas that contains CO_2 (Michael E. Parker, Northrop, Valencia, Foglesong, & Duncan, 2011). Controlled freezing zone is a cryogenic distillation setup with the central section of the column being an open space that allows CO_2 to freeze and melt as part of the distillation process. The bottom tray of the freezing zone is the melting tray, kept slightly above the freezing temperature of CO_2. The distillation liquid above the freezing zone is sprayed into the freezing zone as liquid droplets, the lighter components that encounter the warmer temperatures vaporize and the increased CO_2 concentration in the droplets freeze. Gas from the distillation section below the freezing zone meet with colder temperatures as they pass through the freezing zone and CO_2 desublimes out. One advantage of the CFZ process is that H_2S and CO_2 are both removed by the same process (Haut & Thomas, 1989).

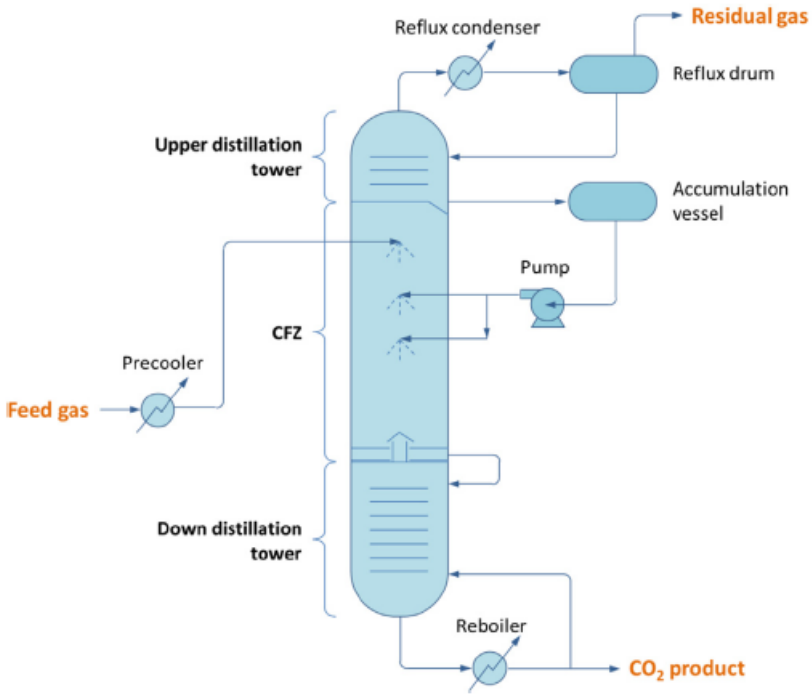

Figure 2.5. Diagram of controlled freezing zone (CFZ). Republished with permission of Renewable and Sustainable Energy Reviews, from Cryogenic-based CO2 capture technologies: State-of-the-art developments and current challenges, C.Song et al., volume 101, 2019; permission conveyed through Copyright Clearance Center, Inc.

CCC-CFG technology functions through expansion of a dehydrated gas. CCC-CFG dries and compresses the flue gas, uses heat exchange to cool the flue gas, then expands the gas to flash out as solid CO_2, and the CO_2 product is heated through heat exchange to form a liquid CO_2 product (Baxter et al., 2009). The CCC-CFG process is shown in figure 2.6.

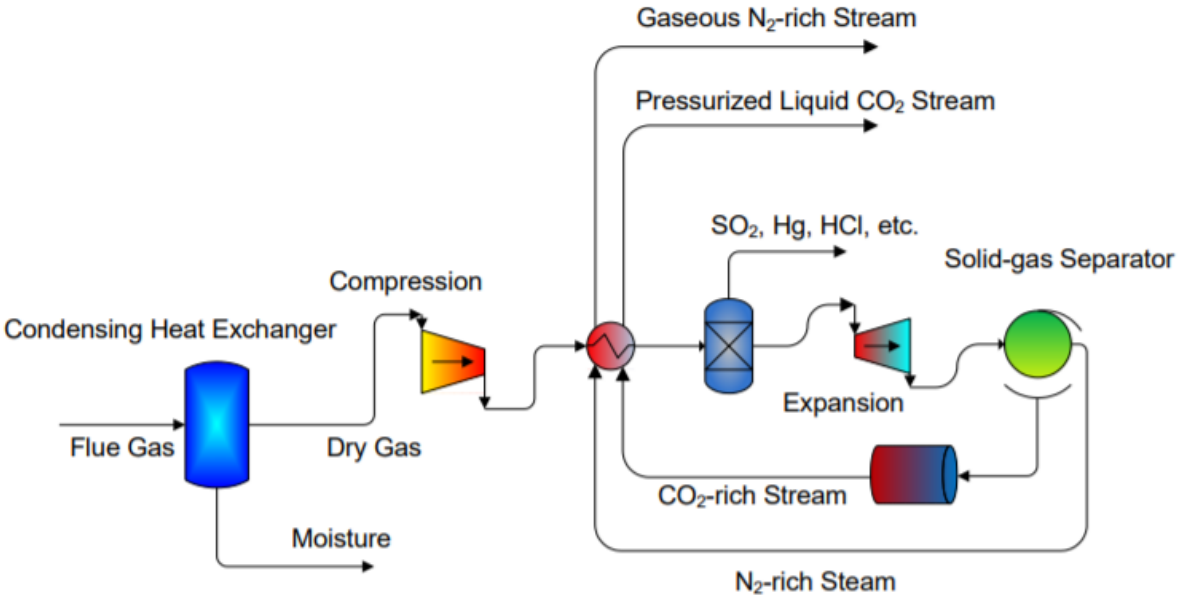

Figure 2.6. Diagram of CCC-CFG process (Baxter et al., 2009).

CCC-ECL similarly also uses a dryer to remove water content of incoming flue gas as CCC-CFG does. A cooling loop of cryogenic liquid is used as to cool the flue gas and desublime CO_2 from the flue gas, the external loop is then also used for heat recovery to warm the compressed solid CO_2 stream to sufficiently melt and form a liquid CO_2 stream (NETL, 2016).

The CryoCell® process is similar in principle to the CCCECL process. The CryoCell® process creates a CO_2 stream that consists of three phases after expansion. The three phase separator after expansion of the gas separates out liquid and solid CO_2 (Hart & Gnanendran, 2009). The thermodynamic pathway for the CryoCell® process is shown in figure 2.7; after initial dehydration of the flue gas to remove water the flue gas is cooled under high pressure until it condenses, then the liquid is expanded across a Joule-Thompson expansion valve to create a three phase mixture, this mixture is then separated using a three phase separator. The solid phase is melted and combined with the liquid phase and the combined CO_2 stream is used as a cold source for heat exchange.

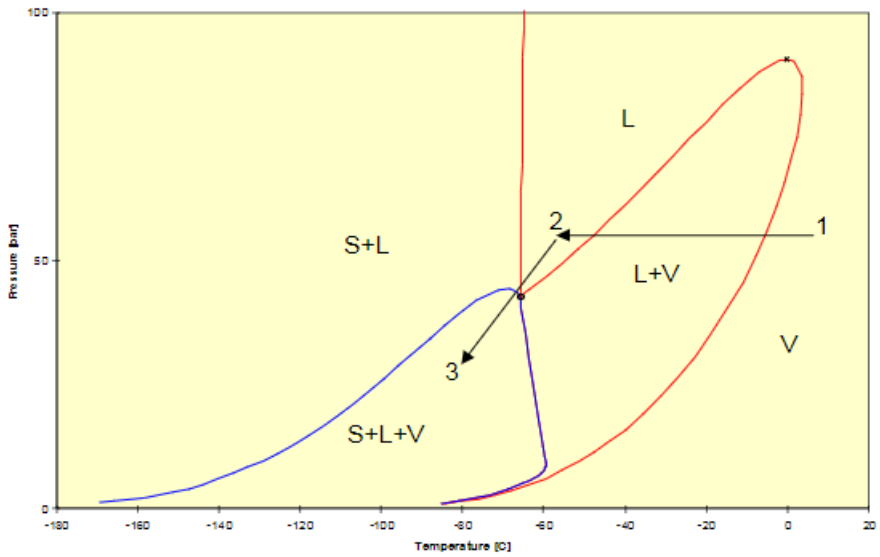

Figure 2.7. Phase envelope of CryoCell® process**.** Republished with permission of Energy Procedia, from Cryogenic CO2 capture in Natural Gas, Hart & Gnanendran, volume 1, 2009; permission conveyed through Copyright Clearance Center, Inc.

Stirling coolers for CO_2 capture have been designed by Song et al. (C.-F. Song et al., 2012; Chun Feng Song, Kitamura, & Li, 2012). The design uses three Stirling coolers in series as can be seen in figure 2.8. The first cooler, in the pre-freezing tower, dehydrates the incoming gas, the second Stirling cooler inside the main freezing tower, removes CO_2 from the gas phase by frosting onto the fins of the cooler. The third Stirling cooler, inside the storage tower, stores captured CO_2 that is recovered from Stirling cooler 2 and acts as a heat exchanger to cool incoming flue gas.

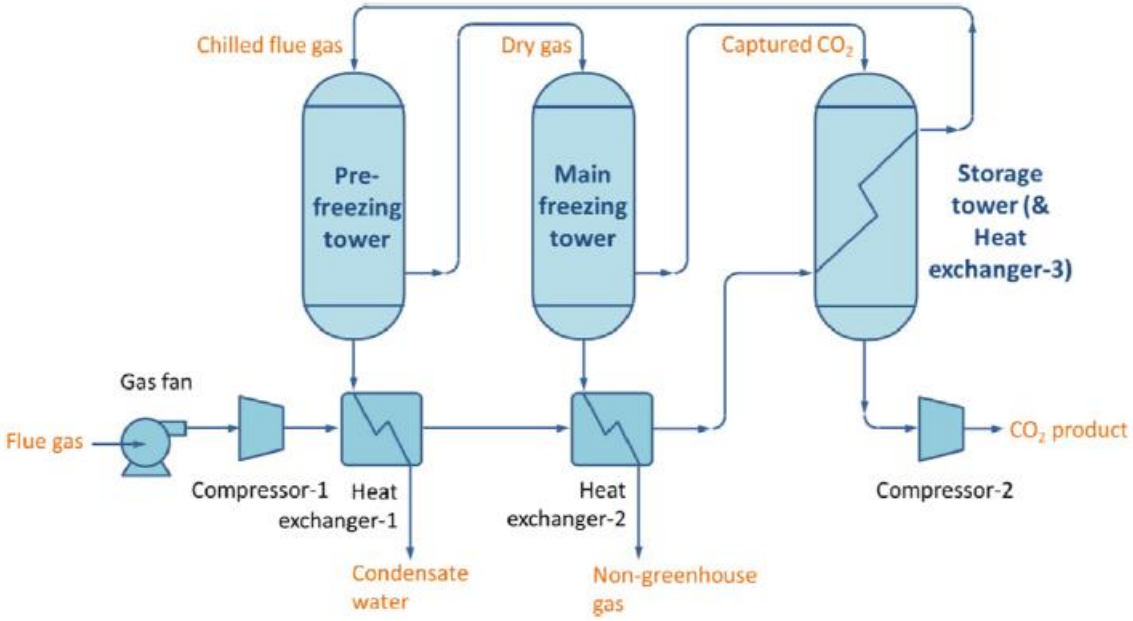

Figure 2.8. Diagram of Stirling cooler capture setup**.** Republished with permission of Renewable and Sustainable Energy Reviews, from Cryogenic-based CO2 capture technologies: State-of-the-art developments and current challenges, C.Song et al., volume 101, 2019; permission conveyed through Copyright Clearance Center, Inc.

Current research into packed beds for cryogenic carbon capture has been evaluated by using heat exchangers or static beds to cool flue gas streams and deposit CO_2 onto the heat transfer surface (Ali et al., 2014; Tuinier et al., 2010). This process leads to a build-up of CO_2 frost on the heat exchanger surface, degrading the efficiency of the heat exchanger until the heat exchanger is saturated with frost (Ali et al., 2014). The process of rectifying this would be to replace the frosted heat exchanger with a fresh one or to have multiple heat exchangers cycling between capture and regeneration cycles to create a pseudo-continuous process (Tuinier, Annaland, et al., 2011). Both of these processes are presented with the challenges of reduced efficiency the more the heat exchanger becomes saturated with frost, reduced equipment lifespan due to the thermal stresses of freeze-thaw operation and thermodynamic losses due to the irreversibility of the capture and regeneration cycle.

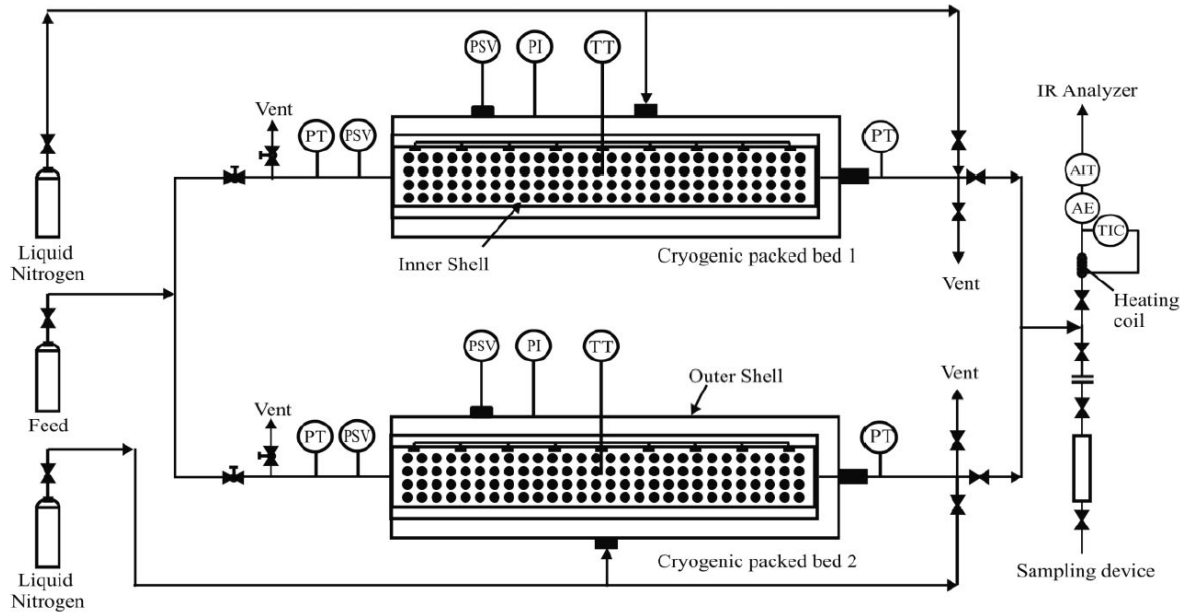

Figure 2.9. Diagram of cryogenic packed bed arrangement**.** Chemical Engineering & Technology: Ali et al.: Energy Minimization in Cryogenic Packed Beds during Purification of Natural Gas with High CO2 Content. Chemical Engineering & Technology. 2014. Volume 37. Pages 1675-1685. Copyright Wiley-VCH GmbH.

Clodic et al (2005) have developed a method of cryogenic carbon capture at the *Centre for Energy and Processes* using a pseudo-continuous anti-sublimation (AnSU) carbon capture cycle at atmospheric pressure (Eide et al., 2005). This process uses a series of expanders and evaporators to frost CO_2 on

low temperature frost evaporators (LTFE). The process runs multiple frost evaporators and alternates the capture and defrosting cycles on each one to create a pseudo-continuous process.

A diagram of the anti-sublimation process is provided in figure 2.10. The flue gas is cooled by a series of heat exchangers to roughly 0°C, cooling stages 1 and 2, to dehydrate the flue gas. The dehydrated flue gas is cooled further to -40°C via the first flue gas/flue gas heat exchanger and cooling stage 3. This removes any remaining water by freezing it out of the flue gas. The flue gas then enters the second flue gas/flue gas heat exchanger to pre-cool the gas to -100°C before going into the low temperature frost evaporator (LTFE). Multiple LTFEs running successively allows CO_2 to be captured continuously, while one LTFE undergoes regeneration, the other LTFE can be used to capture CO_2 (Eide et al., 2005).

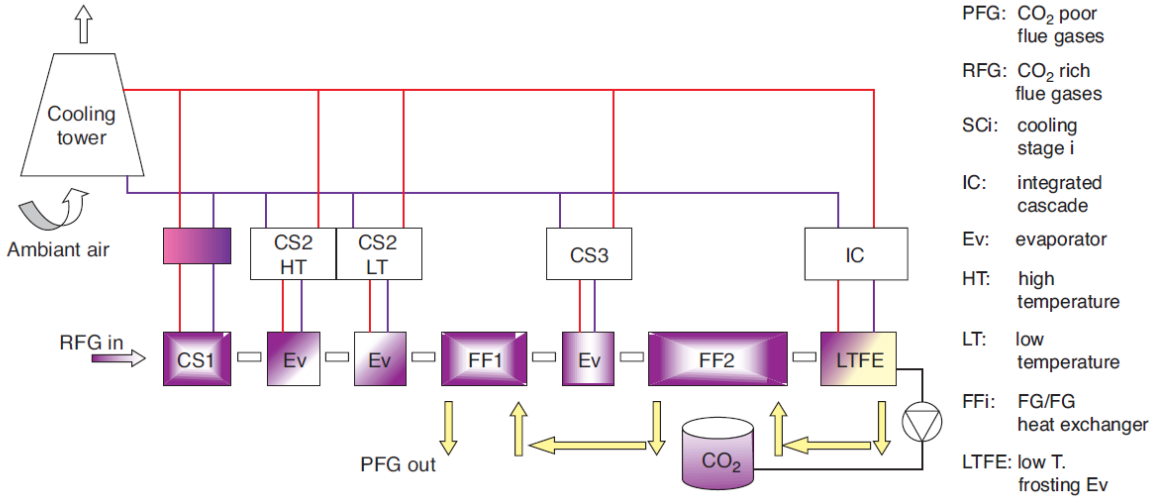

Figure 2.10 Representation of CO2 capture system. Republished from (Eide et al., 2005) with permission of Oil & Gas Science and Technology.

A lab scale design has been constructed in order to demonstrate the principle of the AnSU design. The rig was tested with inlet concentrations of CO_2 ranging from 1% to 23% CO_2. The results from tests on the rig showed that the energy penalty for this process is dependent on the refrigeration cycle efficiency and on the CO_2 concentration in the flue gas (Eide et al., 2005). Experimental results from this lab scale rig show that the rig can achieve roughly 90% capture rate.

Table 2.6: CO2 capture rates for anti-sublimation. Adapted from (Clodic et al., 2005).

Volumetric CO_2 concentration inlet (%)	Volumetric CO_2 concentration outlet (%)	Length of time (s)
13	1	600s
3	0.5	450s

The investigation into the energy requirement of CO_2 capture through this cryogenic process has been shown in table 2.7. The energy required to capture CO_2 per kg of CO_2 increases as the initial CO_2 concentration in the flue gas decreases. It can be seen that the energy requirement makes a sharp increase when the CO_2 concentration is below 10%.

Table 2.7. Energy cost of CO2 with 90% capture rate. Adapted from (Clodic et al., 2005).

CO_2 (% v/v)	Energy duty (kJ/kgCO_2)
5	1250
10	950
15	800
20	700
30	650
40	600

While most work done on cryogenic carbon capture focuses on binary mixtures of CO_2 and N_2/CH_4, Brigham Young University and SES Innovation have begun work on capturing flue gases and have reached the demonstration stage for cryogenic carbon capture (Baxter & Stitt, 2016). Their process captures CO_2, NO_x and SO_x from flue gases at very high capture rates; 95% for CO_2 and 99% for NO_x and SO_x. Their research suggests that cryogenic based carbon capture is more cost effective than the other, more mature, methods of carbon capture currently available (Baxter et al., 2009).

The current work on cryogenic moving packed bed capture is summarised by a feasibility study on the A3C process (Willson et al., 2019). The moving packed bed system operates in a similar fashion to the cryogenic packed bed work done by Tunier et al. As a flue gas containing CO_2 is fed into a capture column filled with sufficiently cold bed material, the gas is cooled to a temperature where CO_2 desublimates out of the gas phase and forms as a frost on the bed material. The moving bed removes CO_2 frost covered bed material at a flow rate that matches the accumulation of frost within the capture column. The feasibility study compares the A3C process with a base case MEA capture system of a similar scale, the feasibility study finds that for an application such as biogas upgrading A3C is a favourable technology.

The range of cryogenic capture techniques publicly available are summarised in table 2.8.

Table 2.8. Summary of cryogenic carbon capture processes.

Technology	Description of process	Benefits and Challenges	Energy duty (kJ/kg CO_2)	References
Cryogenic packed bed	-CO_2 is sufficiently cooled to desublimtate at atmospheric conditions. CO_2 frost is formed on heat transfer surface.	-Low pressure -CO_2 frost must be regenerated for storage. -Efficiency reduces as frost accumulates on heat transfer surface.	-2000 (15% CO_2 flue gas)	(C. Song et al., 2019; Tuinier et al., 2010; Tuinier, Annaland, et al., 2011)
CCCECL	-CO_2 containing flue gas is compressed, cooled, and then expanded to flash CO_2 out of flue gas.	-CO_2 is produced in liquid phase which allows for easy transport compared to solid CO_2 frost.		(Baxter et al., 2009)
CryoCell®	-CO_2 containing flue gas is compressed, cooled, and then expanded to create a three phase mixture of CO_2.	-Final CO_2 product is in liquid phase after solid CO_2 has been melted.		(Hart & Gnanendran, 2009)

Stirling coolers	-Stirling coolers in series desublime CO_2 out of flue gas as frost on the fins of the coolers.	-Can be operated at atmospheric pressure.	-3400 (thermal)		(C.-F. Song et al., 2012; C. Song et al., 2019)
Anti-Sublimation	-Flue gas is dehydrated using heat exchangers and CO_2 is frosted on LTFEs.	-Frost formation negatively affects the capture process.	-800 (15% CO_2 flue gas)		(Clodic et al., 2005)
Cryogenic distillation	-CO_2 is separated via a distillation column.	-High capital costs.			(C. Song et al., 2019)
Controlled freezing zone	-CO_2 is separated from methane via distillation modified for CO_2 freezing.	-CO_2 and H_2S is both removed from methane by the same process.		(Haut & Thomas, 1989)	
A3C	Capture of CO_2 frost utilising a moving packed bed.	-prevents excessive build-up of CO_2 frost on packed bed -lack of experimental validation of process leads to a low TRL.	-946.8	(Willson et al., 2019)	

The capture of solid CO_2 using packed beds is rather well detailed in the literature. For the purpose of addressing CO_2 capture in various industries, cryogenic packed beds were highlighted as a method of capture due to its attractive energy duty. The research into packed bed cryogenic carbon capture shows that the process is competitive with chemical absorption technology in terms of energy penalties and costs of avoidance for CO_2 captured. The build-up of CO_2 frost on the heat transfer surface over time reduces the efficiency of the capture step until the heat transfer surface is saturated with frost and requires a regeneration step. This paper investigates a moving packed bed. Allowing the bed material to capture CO_2 in the capture column, leave the capture column to be reheated in a sublime, cooled and recirculated back into the capture column to create a closed cycle of bed material. A moving bed will avoid capture and regeneration cycles because the frost that is formed in the capture stage will be removed continuously by the moving bed, preventing a saturation of frost.

An outline of the proposed cryogenic moving bed process is provided in figure 2.11. A carbon rich gas is pre-cooled then fed into the capture column with a separate cooling gas is introduced to the bed further up the column to bring the bed down to suitable temperatures for CO_2 capture. CO_2 is frosted on the moving bed and lean gas escapes the column. Bed material covered with CO_2 frost is fed into a bed warmer to regenerate the bed material and collect CO_2 for storage. Bed material is then recycled back into the column by the use of a screw conveyor.

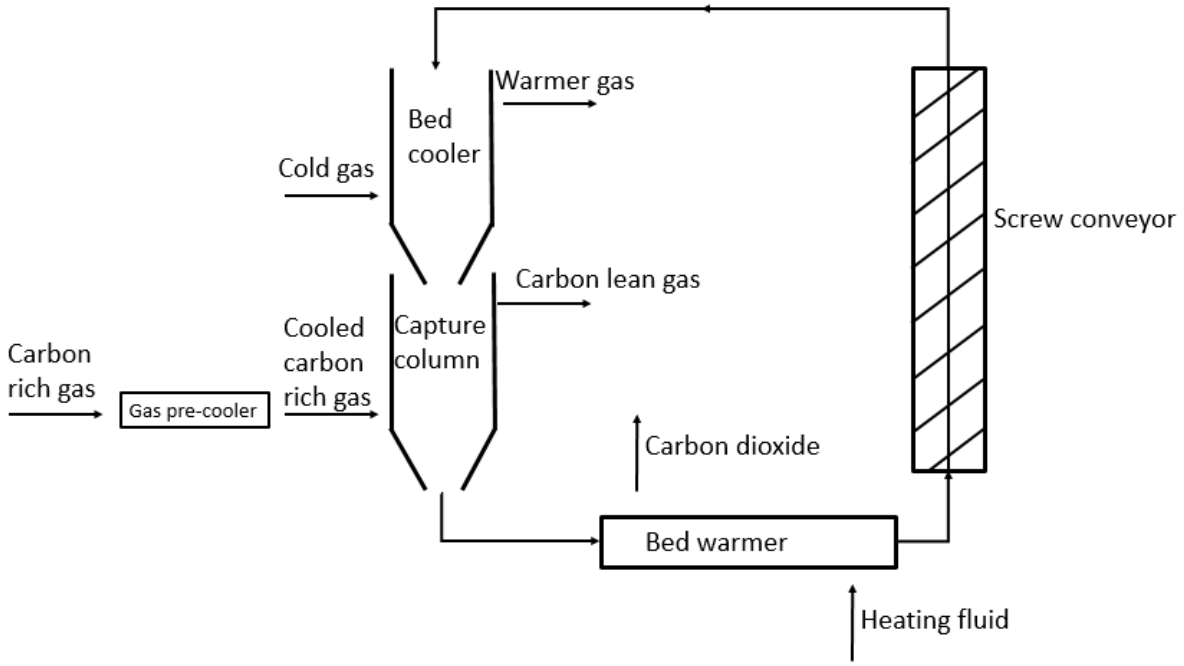

Figure 2.11. Diagram of proposed moving bed cryogenic capture rig.

Various carbon capture technologies have been discussed in this thesis. The fundamentals of pressure drop and heat transfer within a packed bed have yet to be detailed within this literature review. Understanding the pressure drop within a packed bed system aids in the design of a new cryogenic carbon capture rig.

2.3.1 Pressure drop within packed beds

Pressure drop occurs when the flow of a fluid is resisted by frictional forces, frictional forces in a packed bed are exerted on the fluid mainly by the wall of the pipe and the particles that make up the packed bed. The fluid will attempt to resist the frictional forces where possible by traveling through the channels present within the packed bed structure that offer the least resistance to fluid flow. This is demonstrated by pressure drop correlations linking the relationship between the superficial velocity of a fluid or Reynolds number in a column to the pressure drop within the column.

The most common pressure drop calculation is the Ergun equation, which simultaneously factors kinetic and viscous energy losses within the system due to fluid flow (Ergun, 1952):

$$\frac{\Delta P}{L} = 150\frac{(1-\varepsilon)^2}{\varepsilon^3}\frac{\mu U_f}{D_p^2} + 1.75\frac{1-\varepsilon}{\varepsilon^3}\frac{\dot{m}_f U_m}{d_p} \tag{11}$$

Where U_f is the superficial velocity of the fluid, d_p is the particle diameter of bed material, ε is the bed voidage and $\dot{m}_f$ is the mass flowrate of the fluid. The first term in the equation represents the viscous energy losses within the system and the second term represents the kinetic energy losses within the system (Ergun, 1952). While this equation is applicable to many scenarios, work has been done by other researchers to derive pressure drop equations for specific fields.

The nuclear industry has utilized packed bed reactors for decades, the German nuclear safety commission known as KTA has developed its own correlation for pressure drop in high temperature packed bed reactors within specific ranges of bed voidage $0.36<\varepsilon<0.42$ and $Re/(1-\varepsilon)<10^5$ (KTA, 1981).

$$\Psi = \frac{320}{\left(\frac{Re}{1-\varepsilon}\right)} + \frac{6}{\left(\frac{Re}{1-\varepsilon}\right)^{0.1}} \tag{12}$$

Where Ψ represents the coefficient of pressure loss due to friction, the first term in the equation is the asymptotic solution for laminar flow whereas the second term in the equation is the asymptotic solution for turbulent flow. For reference to section 2.9, the terms can be rewritten into the form:

$$\Psi = A\left(\frac{Re}{1-\varepsilon}\right)^{-n} \tag{13}$$

Where n=1 for laminar flow regimes and n=0.1 for turbulent flow regimes (Achenbach, 1995). For the KTA equation of pressure drop in a packed bed, the Reynolds number is calculated by:

$$Re = \frac{(\dot{m}/A)d_p}{\eta} \tag{14}$$

Where η is the dynamic viscosity and d_p is the diameter of the particles within the bed.

$$\psi = \frac{\Delta p}{\left(\frac{L}{d_h}\right)\left(\frac{\rho}{2}\right)v^2}\left(\frac{\varepsilon^3}{1-\varepsilon}\right) \tag{15}$$

The literature also gives another example of pressure drop in a packed bed column due to friction between the gas and solid particles and can be expressed as the following (Fenech, 1981).

$$\Delta P = \Psi \frac{L}{d_h}\frac{\rho}{2}V^2 = \Psi \frac{L}{d_p}\frac{\rho}{2}V_g^2\left(\frac{1-\varepsilon_b}{\varepsilon_b}\right) \tag{16}$$

Which can be rearranged for:

$$\Psi = \frac{\Delta P}{L}\frac{d_h}{(\rho/2)V^2} \tag{17}$$

Where V_g is the superficial velocity of the as flowing through an empty pipe and V is the superficial velocity of the gas flowing through a pipe filled with granular material. d_h is the hydraulic diameter, which is a relationship between the diameter of the spherical particles in the packed bed and the bed voidage, or porosity, of the packed bed (Abdulmohsin, 2013).

$$d_h = d_p\left(\frac{\varepsilon}{1-\varepsilon}\right) \tag{18}$$

Eisfeld and Schnitzlein (2001) compared many correlations within the literature and concluded on an improved correlation by Reichelt that accounts for the wall effect present for low tube to particle diameter ratios $1.624 \leq D/D_p \leq 250$.

$$\Psi = \frac{K_1 A_w^2}{Re_{dp}}\frac{(1-\bar{\varepsilon})^2}{\bar{\varepsilon}^3} + \frac{A_w}{B_w}\frac{(1-\bar{\varepsilon})}{\bar{\varepsilon}^3} \tag{19}$$

$$A_w = 1 + \frac{2}{3(D/d_p)(1-\varepsilon)} \tag{20}$$

$$B_w = \left[k_1\left(\frac{d_p}{D}\right)^2 + k_2\right]^2 \tag{21}$$

2.3.2 Heat transfer in packed beds

The current literature on heat transfer focuses on heat transfer in stationary fixed packed beds. Heat transfer within a packed bed occurs mostly through the convective heat transfer of the gas flowing through the void of the packed bed, partly through conduction between the packed bed particles and partly through thermal radiation (Abdulmohsin, 2013). While these three methods of heat transfer are present, in most operations where the Reynolds number is high, the convection heat transfer mechanism is dominant (Abdulmohsin, 2013). Convective heat transfer in packed beds is quantifiable through the Nusselt number Nu (Chhabra & Shankar, 2017).

$$Nu = \frac{hL}{k} \tag{22}$$

where h is the heat transfer coefficient, L is a characteristic length and k is thermal conductivity of the flowing gas. The Nusselt number can be adjusted for packed bed or pebble bed reactors by using the characteristic length L as the diameter of the bed particles (Abdulmohsin, 2013).

$$Nu = \frac{hd_p}{k} \tag{23}$$

The Nusselt number is a dimensionless number that quantifies convective heat transfer within a closed system. Literature presents numerous models for calculating Nusselt number for a packed bed system (Achenbach, 1995; Gunn, 1978; Wakao & Kaguei, 1983) as described below.

Wakao and Kaguei (1983) proposed the following semi empirical correlation for the calculation of the Nusselt number in a packed bed:

$$Nu = 2 + 1.1Pr^{0.33}Re^{0.6} \tag{24}$$

Where Pr is the Prantl number, given by:

$$Pr = \frac{\mu C_p}{k} \tag{25}$$

Nielinski (1978) developed a semi-empirical method of determining heat transfer within a packed bed by assuming the heat transfer around a single spherical particle given of given diameter and applying an interstitial velocity, which is the velocity of the fluid through the packed bed.

$$U_p = \frac{U}{\varepsilon} \tag{26}$$

The Nusselt number for a single sphere is calculated combining two asymptotic solutions for the laminar and turbulent regime (Gnielinski, 1978). Achenbach (1995) comments that this semi-empirical method is very successful, going on to state that although this method was first suitable for Reynold numbers up to $Re/\varepsilon=2x10^4$, further experimental work extended the applicable range to $Re/\varepsilon=7.7x10^5$.

$$Nu_{laminar} = 0.664 Pr^{1/3} (Re/\varepsilon)^{1/2} \tag{27}$$

$$Nu_{turbulent} = \frac{0.037 (Re/\varepsilon)^{0.8} Pr}{1 + 2.443 (Re/\varepsilon)^{-0.1} (Pr^{2/3} - 1)} \tag{28}$$

$$Nu_{sp} = 2 + (Nu_l^2 + Nu_t^2)^{1/2} \tag{29}$$

This equation for heat transfer for a single particle can be related to the heat transfer of a packed bed of particles by introducing an empirical arrangement form factor.

$$f(\varepsilon) = 1 + 1.5(1 - \varepsilon) \tag{30}$$

Therefore:

$$Nu = f(\varepsilon) Nu_{sp} \tag{31}$$

A method of determining the wall to bed heat transfer coefficient has been developed in Germany (Hahn & Achenbach, 1986). The applicable range of Reynold numbers in this work is between 50-$2x10^4$, although Achenbach (1995) notes that the model loses its justification for Reynolds numbers below 100 since diffusion effects in the system dominate over convective heat transfer.

$$Nu_w = \left(1 - \frac{1}{D/d}\right) Re^{0.61} Pr^{1/3} \tag{32}$$

Work by Gunn (1978) determined a correlation of heat transfer within fixed beds of particles suitable for Reynolds numbers up to 10^5 and porosity above 0.35.

$$Nu = \left(7 - 10\varepsilon_g + 5\varepsilon_g^2\right)\left(1 + 0.7 Re^{0.7} Pr^{1/3}\right) + \left(1.33 - 2.4\varepsilon_g + 1.2\varepsilon_g^2\right) Re^{0.7} Pr^{1/3} \tag{33}$$

KTA Standards (1983) released a standard for the design of gas cooled pebble bed reactors, following the restrictions within their standards document that the equation is suitable for Reynolds numbers between 100-10^5 and a porosity between 0.36-0.42. The Nusselt number for the calculation of heat transfer coefficient was calculated as follows:

$$Nu = 1.27 \left(\frac{Pr^{1/3}}{\varepsilon^{1.18}}\right) Re^{0.36} + 0.033 \left(\frac{Pr^{1/3}}{\varepsilon^{1.07}}\right) Re^{0.86} \tag{34}$$

This chapter gives an extensive review of the current methods of heat transfer calculation for packed beds, however this chapter has not yet investigated the validity of such heat transfer equations in moving bed systems.

Tuinier et al provide the following energy balance equation for packed beds.

$$\left(\varepsilon\rho_g C_{pg} + \rho_s(1-\varepsilon)C_{ps}\right)\frac{dT}{dt} = -\rho_g v_g C_{pg}\frac{dT}{dz} + \frac{dT}{dz}\left(k_{eff}\frac{dT}{dz}\right) - \sum_{i=1}^{n_c}\dot{m}_i^{"}a_b\Delta H_i \qquad (35)$$

When comparing experimental results to the provided energy balance equation, they noticed that the energy balance was insufficient and required an extra term to include wall effects within the column. Bed material close to the wall was seen to be roughly 20 degrees hotter in temperature than bulk material in the centre of the column.

The literature grants a good foundation of understanding for the calculation of pressure drop and heat transfer within a packed bed, as well as giving reasonable confidence that cryogenic carbon capture is a feasible process. The concept of a moving packed bed for CCC has not been considered by others before. A moving packed bed would avoid the issue of multiple packed beds being required to alternate capture and regeneration cycles by instead circulating bed material through a continuous cycle. Cold bed material would flow through the column, CO_2 would form a layer of frost on the bed material as it leaves the column, a heat exchanger would heat the bed leaving the cooling column to sublimate and capture CO_2 frost, and then the bed material is cooled again and recirculated back into the cooling column.

2.4 Flow in moving beds

The bed material for the moving bed design will function as hoppers, allowing for a steady flow of bed material through the heat transfer column. Hoppers can experience two flow regimes, mass flow and core flow.

Mass flow is characterised by relative velocity of all particles on the same horizontal plane equivalent to each other, meaning that the residence time of all particles travelling through the hopper is the same. Core flow is characterised by solid particles near the wall moving at a slower rate due to the shear forces exerted by the wall than the particles in the centre of the hopper. The bed material closer to the centre of the hopper moving faster and discharging from the hopper creates a pit in the top layer of bed material, this is called rat-holing. To ensure stable and controllable heat transfer, it is desirable to ensure that mass flow is achieved (Rhodes, 2008).

The literature provides extensive work on the discharge rates and conditions affecting mass flow in angled hoppers which can be found in (Nicolin Govender, Wilke, Pizette, & Abriak; Jia, Gui, Yang, Tu, Jia, et al., 2017).

Govender (2018) simulated the flow of materials in 2 dimensional hoppers with hopper angles of 0°, 30° and 60° from the horizontal plane. A strong similarity between the simulated models and experimental flows under the same conditions was observed. The results from Govender showed evidence of core flow present at angle 0°, the flat bottom angled hopper, and mass flow in the 30° and 60° hoppers. The flow out of these hoppers was tested for spherical particles and for non-spherical particles, for the non-spherical particles the hoppers still showed the same flow regimes for their respective angles; however the rate of mass flow of the particles had dropped.

The flow rate of granular materials through a hopper orifice in the literature is calculated through the Beverloo equation (Beverloo, Leniger, & van de Velde, 1961).

$$\dot{m} = C\rho_b\sqrt{g}(d_c - kd_p)^{5/2} \tag{36}$$

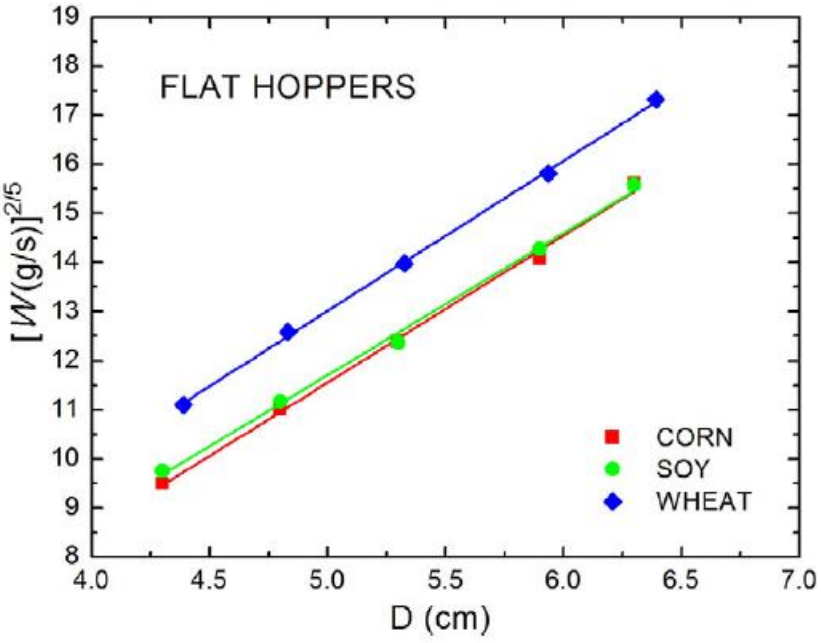

Figure 2.12. Correlation between discharge rate and diameter of outlet . Republished with permission of Powder Technology, from Correlations between flow rate parameters and the shape of the grains in a silo discharge, Calderón, Villagrán Olivares, Uñac, & Vidales, volume 320, 2017; permission conveyed through Copyright Clearance Center, Inc.

The k and C are empirical values dependent on the geometry of the hopper and are calculated by determining the discharge rate of bed material from a hopper with varying outlet diameters. The

Beverloo equation will result in a linear correlation between the diameter of the hopper outlet and the discharge rate $\dot{m}^{2/5}$ as demonstrated in figure 2.12, the linear correlation allows C to be determined from the gradient and k to be determined by the intercept of the line with the y axis (Calderón et al., 2017).

The Beverloo equation holds best for particle sizes that are not coarse (Hui, Jia, Gui-Ping, & Hai-Feng, 2018; Mankoc et al., 2007). Hui et al (2018) summarises 6 variations of the equation found in the literature with various particle and outlet diameters and different hopper structures. Their work summarises the work related to the Beverloo equation over the last few decades and investigates the effect of surface roughness of fine particles and of Van der Waals forces on the discharge rates of the material through a conical hopper. Their work suggests that varying the particle size of the material inside the hopper has little effect on the overall discharge rate observed, while increasing the diameter of the hopper outlet will lead to an increased discharge rate.

There are various mechanisms by which a hopper will experience alterations to flow, one major issue is arching (Jia, Gui, Yang, Tu, & Jiang, 2017). Arching occurs near the outlet of a hopper and is the result of particles forming an instantaneous bridge which effectively clogs the outlet and halt particle flow (Nicolas, Garcimartin, & Zuriguel, 2018). The cause of an arching is typically due to the diameter of the outlet being too small relative to the diameter of the particles stored in the hopper. These arches can form and break instantaneously or the formation of an arch can cause particle flow to cease entirely. Arches can be broken by applying a force to the hopper which disrupts the arch. Typical methods of breaking an arch include; aeration of the bed using gas streams to fluidise the bed and vibration of the hopper to destabilise the arch.

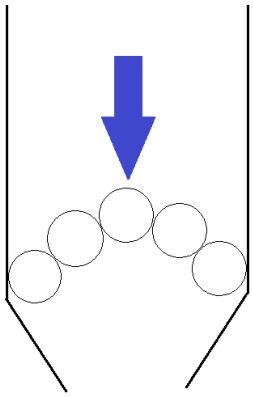

Figure 2.13. Representation of particles causing an arch by compression under gravity.

There are two types of arches that can occur in hoppers; mechanical arches and cohesive arches. A mechanical arch occurs instantaneously by the movement of particles, an arch is randomly formed while particles are in transit. Cohesive arches occur when the superficial velocity of particles within the hopper is very low. Over periods of time, materials that are undisturbed can form a more dense packing and become more cohesive. This causes the hopper to become clogged (Rhodes, 2008).

The issue of arching in hoppers can be addressed by adding an obstruction near the end of the outlet of the hopper. The inclusion of an obstruction makes the formation of an instantaneous arch less likely.

Investigations have been conducted in the literature to determine the effect of discharge rates of hoppers when the particle sizes are not uniform (Y. Zhao, Yang, Zhang, & Chew, 2018). Zhao et al determine that discharge rate decreases as the particle size distribution increases. It is important to note that while the discharge rate changes, the discharge rate for each experimental run is still constant. This is shown in figure 2.14.

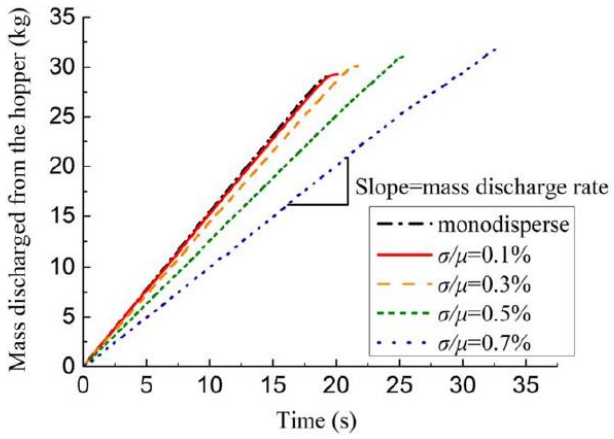

Figure 2.14. Mass discharge vs time profiles. Republished with permission of AICheE Journal, from DEM Study on the Discharge Characteristics of Lognormal Particle Size Distributions from a Conical Hopper, Y.Zhao et al., volume 64, 2018; permission conveyed through Copyright Clearance Center, Inc.

This phenomenon is the cause of particle segregation, in effect when particles of varying sizes are agitated the smaller particles sink down through the voidage of larger particles, creating a separation of particles by particle size (Xu, Sandali, Sun, Zheng, & Shi, 2017).

Although the shape of hoppers is very simple, the nature of particle flow within hoppers is far more complex than expected, many factors can affect the flow rate of particles within a hopper. Furthermore, the change from packed bed to moving bed will have an impact on the pressure drop and heat transfer equations. While the literature covering the fundamentals of pressure drop and heat

transfer in moving beds is sparse, there is some information on the subject matter. The information relevant to pressure drop and heat transfer within a moving bed system is discussed in the next section.

2.4.1 Pressure drop across moving packed beds

Similar to pressure drop in packed beds, pressure drop in moving beds occurs from the frictional forces exerted onto the fluid by the bed material and walls of the packed bed. However, a moving packed bed causes the channels and paths of least frictional resistance to constantly change due to the movement of the bed material. The topic of pressure drop in moving beds is less extensive than the research on fixed beds. Furthermore, the research on the topic does not seem to be in agreement. While some research has been conducted on pressure drop within moving packed beds, in some cases regarding moving beds the pressure drop is considered to be approximately equal to the fixed bed pressure drop due to the solids flow rate being far smaller than the gas flow rate through the bed and therefore having a negligible effect on pressure drop.

Work done by Happel (1949) included investigation on pressure drops in moving bed systems, both counter current and co-current and identified a modified Reynolds number and friction factor for the Ergun equation (Happel, 1949). Happel divided the friction factor equations into three separate regimes for laminar, turbulent and the transition region of fluid flow.

$$Re_m = Re(1-\varepsilon) \tag{37}$$

$$f_m = \frac{1630}{Re_m} \; for \; Re_m < 5 \tag{38}$$

$$f_m = \frac{1000}{Re_m} + \frac{200}{Re_m^{0.22}} for \; 5 < Re_m < 200 \tag{39}$$

$$f_m = \frac{207}{Re_m^{0.22}} \; for \; Re_m > 200 \tag{40}$$

Not all sources agree with this correlation though. (Yoon & Kunii, 1970) noted that the friction factor correlations suggested shows that the gas velocity is independent of the solids flow velocity in the moving bed. Whether this is the case is debateable due to work by Yoon and Kunii (1970) that suggests that at a fixed pressure drop, an increasing solids velocity through a column results in a decreasing gas velocity in a linear correlation.

Yoon and Kunii (1970) conclude in their work that the Ergun equation can be used for pressure drop in moving beds as long as the superficial velocity for gas is substituted with the slip velocity.

$$\Delta u = \frac{u_g}{\varepsilon + u_s} \tag{41}$$

$$\frac{\Delta P}{L} = 150\frac{(1-\varepsilon)^2}{\varepsilon^3}\frac{\mu u_g}{d_p^2(\varepsilon + u_s)} + 1.75\frac{1-\varepsilon}{\varepsilon^3}\frac{\dot{m}_g u_g}{d_p(\varepsilon + u_s)} \tag{42}$$

The lack of a consensus between sources found in the literature on pressure drop in moving packed beds requires an investigation into which model for pressure drop best fits the experimental results in this project. This work establishes a suitable pressure drop equation for fixed packed bed experiments, the pressure drop through the packed bed is tested to establish whether pressure drop is low enough to satisfy the assumption that the moving bed experiments would not heavily affect pressure drop.

2.4.2 Heat transfer in moving packed beds

The major difference between a fixed bed and a moving bed is the solids flux, the solids flux within a fixed bed is zero since there is no appreciable movement of the bed material (R. J. Wang, Fan, & Lu, 2017).

Heat transfer coefficients in moving beds are mainly determined by two different methods; using a heated plate at the wall of the vessel containing the solid to achieve heat transfer (Baird, Rao, Tackie, & Vahed, 2008), or by using a heated gas or solid phase flow to achieve heat transfer (Crawshaw, Paterson, & Scott, 2000; Feng, Dong, Gao, Li, & Liu, 2016). Moving beds can be used as heat exchangers which are used for waste heat recovery. Moving bed heat exchangers (MBHEs) utilise cross flow between the bed material and the gas phase.

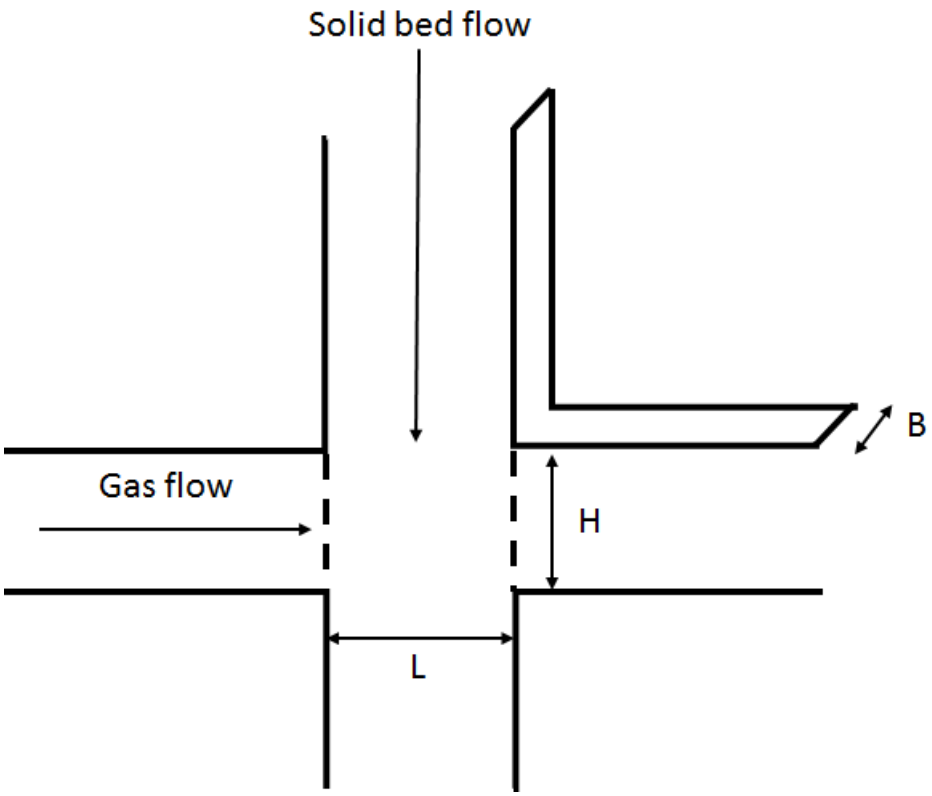

Figure 2.15. Diagram of Moving bed heat exchanger (MBHE)**.** Adapted from Applied Thermal Engineering, from Solid conduction effects and design criteria in moving bed heat exchangers, Almendros-Ibáñez, Soria-Verdugo, Ruiz-Rivas, & Santana, 2011, volume 31, 2011; permission conveyed through Copyright Clearance Center, Inc.

The governing equations of the moving bed heat exchanger for the gas and solid phase heat transfer are as follows:

$$\varepsilon\rho_g c_{pg}\left(\frac{dT}{dt}+u_g\cdot\nabla\mathrm{T}\right)=\nabla\cdot\left(k_g\nabla T\right)+h_s a_s(\theta-T) \tag{43}$$

$$(1-\varepsilon)\rho_s c_{ps}\left(\frac{d\theta}{dt}+u_s\cdot\nabla\theta\right)=\nabla\cdot(k_s\nabla\theta)+h_s a_s(T-\theta) \tag{44}$$

Θ and T represent the solid and gas phase temperatures respectively. In these heat transfer equations; heat losses to the surroundings, heat transfer by radiation and loss of potential energy in the solid phase are neglected. Furthermore, when a gas is used in the MBHE the gas thermal conductivity is orders of magnitude lower than the gas convection term, meaning it can usually be neglected in gas solid operations (Almendros-Ibáñez et al., 2011).

In general, these heat transfer equations for the moving bed heat exchanger will use the assumption of plug flow for both the gas and solid phase, this assumption is considered acceptable so long as the diameter of the column is at least 10 times larger than the particle diameter of the bed material. This assumption is fair as previously mentioned when discussing flow of bed material in hoppers, in order

to maintain mass flow as opposed to core flow within the bed material the particle diameter is required to be at least 10 times smaller than the column diameter as well.

These general equations can then be converted into a non-dimensional form assuming 2D geometry of the gas and solid flows respectively.

$$\frac{d\hat{\theta}}{d\eta} - K_{\xi}\frac{d^2\hat{\theta}}{d\xi^2} - K_{\eta}\frac{d^2\hat{\theta}}{d\eta^2} = \hat{T} - \hat{\theta} = -\frac{dT}{d\xi} \tag{45}$$

Where:

$$\hat{\theta} = \frac{\theta - \hat{\theta}_{in}}{\hat{T}_{in} - \hat{\theta}_{in}}, \hat{T} = \frac{T - \hat{\theta}_{in}}{\hat{T}_{in} - \hat{\theta}_{in}} \tag{46}$$

Represent the non-dimensional temperatures and:

$$\xi = \frac{xh_s a_s}{\varepsilon\rho_g u_g c_{pg}}, \eta = \frac{yh_s a_s}{(1-\varepsilon)\rho_s u_s c_{ps}} \tag{47}$$

Represent the non-dimensional co-ordinates.

$$K_{\xi} = \frac{h_s a_s k_{sx}}{\left(\varepsilon\rho_g u_g c_{pg}\right)^2}, K_{\eta} = \frac{h_s a_s k_{sy}}{\left((1-\varepsilon)\rho_s u_s c_{ps}\right)^2} \tag{48}$$

Represents the non-dimensional conductivities of the gas and solid flows respectively. The heat transfer is optimised when the non-dimensional co-ordinates are equal (Soria, Almendros-Ibáñez, Ruiz-Rivas, & Santana, 2009).

$$\xi_{x=L} = \eta_{y=H} \tag{49}$$

If the non-dimensional co-ordinates are unbalanced then a certain part of the flow entering the larger of the two lengths will not experience complete heat transfer. For example, if the vertical non-dimensional co-ordinate is larger than the horizontal then certain portions of the gas entering the heat exchanger horizontally will leave the column at roughly the same inlet temperature. Due to the high density of the solid bed material compared to the gas phase generally, the height of the heat exchanger is larger than the width of the column to allow the bed material more contact time with the gas. This will allow for the bed material to have the contact time required to ensure maximum exergy recovery.

The non-dimensional co-ordinates when balanced can be manipulated into an equation that balances the flow rates and specific heat capacities of both the solid and the gas phases.

$$\dot{m}_s c_{ps} = LB(1-\varepsilon)\rho_s u_s c_{ps} = \dot{m}_g c_{pg} = HB\varepsilon\rho_g u_g c_{pg} \tag{50}$$

Where B is the width of the heat exchanger.

For short distances of the non-dimensional co-ordinates, conduction effects have an important effect on reducing the efficiency of heat exchange, in order to maintain efficiency in a heat exchanger with conductive material the size of the heat exchanger must be increased in order to maintain efficiency. The conduction term of the solid bed material must also require to be sufficient enough to maintain an equivalent temperature of the bed material at the core and surface of the bed material in order to prevent impacting convection heat transfer. Therefore, the optimal conductivity for the bed material would be required to maximise the efficiency of the conduction and convection heat transfer, the literature suggests that the Biot number should be approximately 0.1 in order to achieve this.

$$Bi = \frac{h_s d_p}{k_s} \leq 0.1 \tag{51}$$

The correlation given by Wakao and Kaguei (1983) has been used in works by Crawshaw (2000), Kim (2013) as a decent approximation for heat transfer within moving beds.

Baird, Rao, Tackie and Vahed (2008) used heated bed material to transfer heat to a surrounding of nickel carbonyl gas. Their equation for the Nusselt number is as follows, where the subscript z relates to the z direction:

$$Nu = 0.332 Re_z^{0.5} Pr^{1/3} \tag{52}$$

Feng, Dong, Gao, Li and Liu (2016) investigated counter flow heat transfer for sinter waste heat recovery. Their numerical model for heat transfer was as follows:

$$Nu = 0.2\varepsilon^{0.055} Re_p^{0.657} Pr^{1/3} \tag{53}$$

Crawshaw et al. (2000) have conducted heat transfer experiments within a moving bed, the method of calculating heat transfer was done using a logarithmic mean temperature difference.

$$\Delta T_{LM} = \frac{\left(T_{g,b} - T_{s,b}\right) - \left(T_{g,t} - T_{s,t}\right)}{ln\left(\frac{T_{g,b} - T_{s,b}}{T_{g,t} - T_{s,t}}\right)} \tag{54}$$

where the subscripts g, s, t and b represent the gas and solid phase and top and bottom of the heat transfer region respectively. The heat transfer coefficient can then by calculated by:

$$h = \frac{Q_g}{a_s \Delta T_{LM}} \tag{55}$$

This heat transfer coefficient can then be related to the Nusselt number or Biot number using equations (21) or (49) respectively.

The heat transfer equations provided in the literature are extensive and, the heat transfer correlations in the literature relate to two-phase heat transfer between a solid and a liquid or gaseous phase. These current equations however may not be suitable for scenarios where phase change occurs, such as with desublimation or condensation. More information regarding heat transfer when desublimation occurs is required to use these equations effectively, so information regarding the effects of desublimation are discussed in the next section.

2.5 Effect of frost deposition on heat exchange in packed beds

When carbon dioxide in the gas stream is sufficiently cooled by the cold packed bed, carbon dioxide forms a frost on the surface of the packed bed. This phase change affects the heat transfer within a packed bed in two ways; firstly by requiring latent energy to undergo phase change, and secondly by reducing thermal conductivity between the bed material and the gas phase.

Frost growth can be categorized into 3 major stages; crystal growth period, frost growth period and frost densification period (C. F. Song, Kitamura, Li, & Jiang, 2013). The crystal growth period is a relatively short period where CO_2 crystals nucleate onto the surface of the packed bed material. The frost growth period is a period where the CO_2 forms a porous layer of frost as crystals grow on top of other crystals and increase the thickness of the frost present on the packed bed. The frost densification period is where the deposition rate of new frost slows down while the density of the frost layer gradually increases. It is during this period that an equilibrium between sublimation and deposition of frost is achieved (C. F. Song et al., 2013).

Frost formation is affected by the partial pressure of CO_2, as can be seen by table 2.1. Increasing the partial pressure of CO_2 present means that the gas becomes saturated with CO_2 at relatively higher temperatures. This has been demonstrated by Tuinier et al. (2011) in figure 2.16, where the graphs plot the temperature profiles of a packed bed capture column. Where the stable temperature region of the graphs indicate that CO_2 frost is forming inside the experimental capture column. On the left graph, with a feed gas of 20% CO_2 the temperature plateau forms at is roughly -90^oC, whereas on the right graph, the temperature plateau forms at is roughly -98^oC. The temperatures of desublimation provided by Tuinier et al. (2011) are slightly differing from the figures given in table 2.1. However this difference regarding the desublimation temperature of CO_2 at 10% concentration v/v is only of a few degrees.

Due to the latent energy in phase change, the temperature within the column remain stable while frost is desublimating onto the packed bed material. These temperature plateaus indicate the presence of frost and by plotting temperature profiles at different points in time, the plateaus can be used to deduce how quickly the column is being saturated with frost.

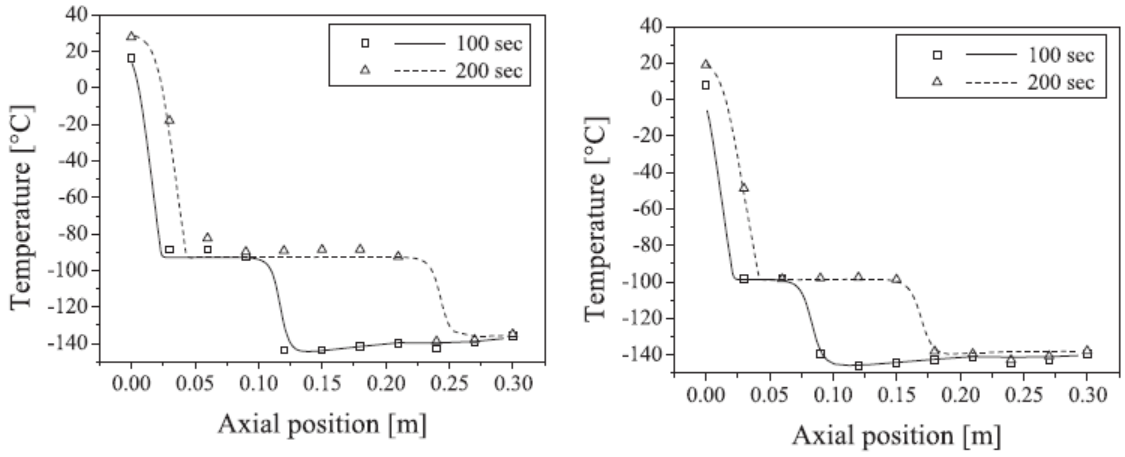

Figure 2.16. Temperature profiles of packed bed column with 20% CO_2 concentration (left) and 10% CO2 concentration (right). Republished with permission of International Journal of Greenhouse Gas Control, from A novel process for cryogenic CO2 capture using dynamically operated packed beds—An experimental and numerical study, Tuinier, Annaland et al., volume 5, 2011; permission conveyed through Copyright Clearance Center, Inc.

An estimation of rate of frost formation can be achieved by difference in partial pressure of CO_2 and saturated vapour pressure of solid CO_2. If the partial pressure of CO_2 is higher than the saturated vapour pressure then CO_2 must desublime out of the gaseous phase.

The CO_2 saturation pressure can be calculated by the Antoine equation for CO_2 (Giauque & Egan, 1937).

$$log_{10}P = A - \left(\frac{B}{T - C}\right) \tag{56}$$

Where A=6.81228, B=1301.679, C=-3.494, T is temperature in Kelvin and P is pressure in bar.

Earlier work was done by Span and Wagner on another equation of state for CO_2 (Span & Wagner, 1996).

$$ln\left(\frac{P_{sub}}{P_t}\right) = \frac{T_t}{T} \cdot \left\{a_1\left(1 - \frac{T}{T_t}\right) + a_2\left(1 - \frac{T}{T_t}\right)^{1.9} + a_3\left(1 - \frac{T}{T_t}\right)^{2.9}\right\} \tag{57}$$

where a_1=-14.740846, a_2=2.4327015 and a_3=-5.3061778. Span and Wagner's equation of state gives the saturation pressure in MPa.

An example of the saturated vapour pressure equation for CO_2 is given by ZareNezhad (2006). This equation is only suitable for temperatures below the triple point of CO_2.

$$P^{\sigma} = 9.94 \times 10^8 e^{\left(\frac{-3108.2}{T}\right)} (kPa) \tag{58}$$

Since CO_2 is not an ideal gas then partial pressure must be substituted for the fugacity of CO_2 to obtain accurate data. Fugacity coefficients for CO_2 mixtures were calculated by ZareNezhad (2006) using the Peng Robinson equation of state.

Tuinier et al (2010) worked on the partial pressure method to create a CO_2 desublimation rate equation with a desublimation rate constant g.

$$\dot{m}_i^{"} = \begin{cases} g\left(y_{CO_2}P - P_{CO_2}^{\sigma}\right) & if\ y_{CO_2}P \geq P_{CO_2}^{\sigma} \\ g\left(y_{CO_2}P - P_{CO_2}^{\sigma}\right)\dfrac{m_i}{m_i + 0.1} & if\ y_{CO_2}P < P_{CO_2}^{\sigma} \end{cases} \tag{59}$$

The desublimation rate constant was determined to be $1x10^{-6}$ s/m which was what best fit the experimental results. Without using the rate constant models a sharp temperature frost front. The rate constant models the temperature change as opposed to a sharp change from an unsaturated to a saturated bed.

Research has been conducted to estimate the latent heat of desublimation for frosts. Fossa and Tanda (2002) determined the following equation.

$$\Delta h_{CO_2}^{sub} = 2.88 \times 10^6 - 195 T_f \frac{\mathrm{J}}{\mathrm{kg}} \tag{60}$$

Where T_f is the temperature of the frost. The units for L_{sub} in this equation are J/kg. Alternatively, Tuinier (2010) gives a different value for latent heat of desublimation of CO_2, one that is a constant value independent of temperature.

$$\Delta h_{CO_2}^{sub} = 5.682 \times 10^5 \frac{\mathrm{J}}{\mathrm{kg}}$$

Work was done in North America to determine the vapour pressure and sublimation rates of various organic compounds, the work conducted and published by NIST shows the latent heat of sublimation is as follows. .

Table 2.9. Latent heats of sublimation for CO2.

Latent heat of sublimation (kJ/mol)	Reference temperature (K)	Reference
25.9	207	(Ambrose, 1956)
27.2 ± 0.4	70-102	(Bryson, Cazcarra, & Levenson, 1974)
25.2	195	(Giauque & Egan, 1937)
26.3	167	(Stull, 1947)

These standards all seem to give large differences for the latent heat of sublimation. The work by Fossa and Tanda is based on frost formation from moisture in ambient air, so discrepancies between their data and data specifically related to CO_2 is not entirely surprising.

As the CO_2 is deposited onto the bed material, the thermal conductivity of the packed bed will reduce. The impact of frost formation on the overall heat transfer coefficient is primarily dependent on the density of the frost that is formed on the surface of the solid material.

When predicting frost thermal conductivity, water frost formation experiments have previously used a flat plate of aluminium as a test plate to allow frost formation. Yun, Kim & Min (2002) provided the following equation for the calculation of thermal conductivity in a frost:

$$k_{total} = \frac{k_{frost,surface} k_{frost,inner} \left(\delta_{frost,surface} \delta_{frost,inner}\right)}{k_{frost,inner} \delta_{frost,surface} + k_{frost,surface} \delta_{frost,inner}} \tag{61}$$

The subscripts inner and surface relate to the inner layer and surface layer of the frost, representing a rough frost as the surface layer (Yun et al., 2002). Since the density of the frost is not constant throughout frost growth, this equation gives an averaged thermal conductivity for the frost within the system.

Many alternative empirical models have been suggested for the relation between frost density and frost thermal conductivity.

(Yonko & Sepsy, 1967):

$$k_{frost} = 0.024248 + 0.00072311 \rho_{frost} + 0.000001183 \rho_{frost}^2 \tag{62}$$

(Sanders, 1974):

$$k_{frost} = 1.202 \times 10^{-3} \rho_{frost}^{0.963} \tag{63}$$

(Lee, Jhee, & Yang, 2003) correlation was found from their work to be more accurate to experimental data than other compared models, the provided model is less accurate during the initial stages of frosting.

$$k_{frost} = 0.132 + 3.13 \times 10^{-4} \rho_{frost} + 1.6 \times 10^{-7} \rho_{frost}^2 \tag{64}$$

Study of the effects that frost deposition has on the heat transfer efficiency of a heat exchanger require the mass and thickness of the frost deposited to understand the level of effect that the frost has. Taking the column that holds the bed material as an example, the thermal resistance of the wall as frost is deposited can be modelled by the following equation (Wang et al., 2013).

$$R_{total} = \frac{1}{h_r \pi d_1} + \frac{1}{2\pi k_w} ln \frac{d_2}{d_1} + \frac{1}{2\pi k_{frost}} ln \frac{d_x}{d_2} + \frac{1}{h_a \pi d_x} \quad (65)$$

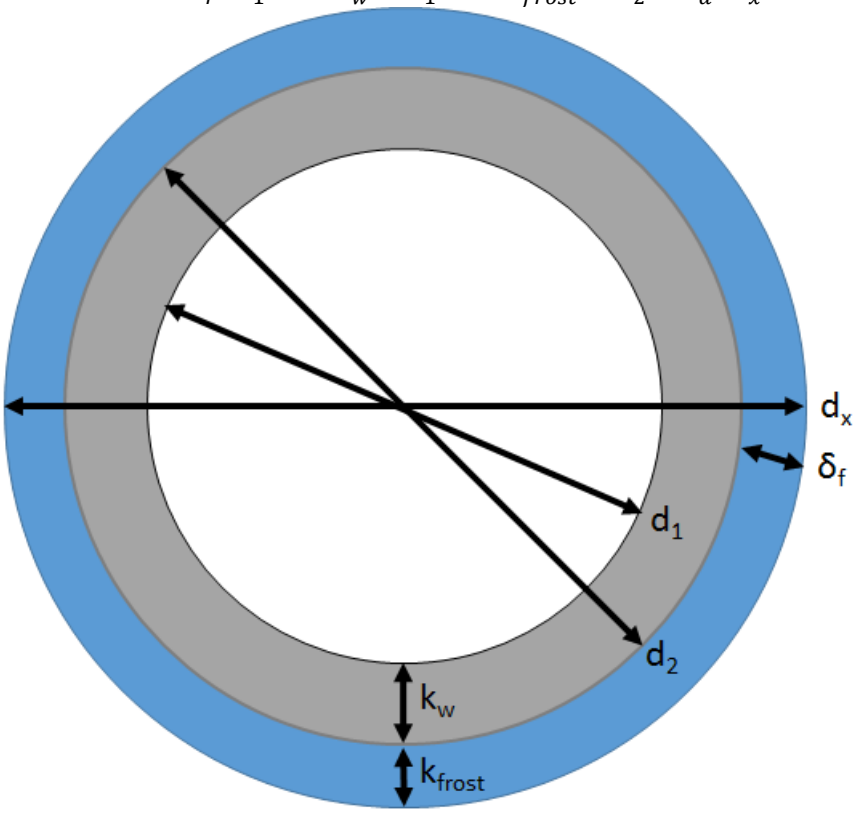

Figure 2.17. Representation of thermal resistance equation. Adapted from Applied Thermal Engineering, from Theoretical study on the critical heat and mass transfer characteristics of a frosting tube, Wang et al., volume 54, 2013; permission conveyed through Copyright Clearance Center, Inc.

The above equation requires modification to become applicable to the work this paper conducts. Primarily due to two reasons; firstly frost formation will occur on the inside wall and secondly, frost formation on a moving packed bed will lead to a large quantity of irregularities in the heat transfer from the cooling gas to the wall.

An interesting phenomenon of frost formation is that the early stages of frost formation on a heat exchanger is noted to cause an increase in heat transfer capacity instead of a decrease (Wang et al., 2013).The reason as to why this phenomenon occurs is a topic of debate within the literature.

The critical frost thickness for maximum heat transfer can be calculated by taking the derivative of the thermal resistance equation.

$$\frac{dR_{total}}{dd_x} = \frac{1}{\pi d_x} \left(\frac{1}{2k_{frost}} - \frac{1}{h_a d_x} \right) \quad (66)$$

As it has been noted earlier, the densification of frost is the latest stage of frost growth, so the critical frost thickness calculation is suitable for the initial stage of frost growth; the density, and therefore thermal conductivity, of the frost can be assumed to be constant. To achieve the critical frost thickness, the left hand side of the equation must be set to zero (Wang et al., 2013).

$$d_x = \frac{2k_{frost}}{h_a} \tag{67}$$

To determine if this value is a local maximum or minimum, the second derivative of the thermal resistance equation is taken.

$$\frac{d^2R_{total}}{dd_x^2} = \frac{1}{\pi d_x^2}\left(\frac{2}{h_a d_x} - \frac{1}{2k_{frost}}\right) \tag{68}$$

When substituting the value for d_x:

$$\frac{d^2R_{total}}{dd_x^2} = \frac{h_a^2}{8\pi k_{frost}^3} > 0 \tag{69}$$

2.6: Effect of desublimation and porosity on pressure drop and heat transfer

As carbon dioxide desublimes onto the packed bed, the porosity of the bed will slowly decrease over time as the voidage in the column is filled with frost. Utilising a moving bed prevents the formation of CO_2 frost from increasing past the equilibrium line; however the effects of frost formation within the frosted section of the contact column will be present in an alteration of the pressure drop and reduction of heat transfer across the frosted section of the bed.

The effect of frost growth on the packed beds can likely be interpreted either as an increase of surface roughness of the packed bed material or as a decrease in bed porosity. The literature shows no clear consensus on the level of effect that surface roughness of particles has on pressure drop within a packed bed. Eisfeld and Schnitzlein (2001) claim that surface roughness having an observable impact on pressure drop is hardly plausible, whereas others (Allen, von Backstrom, & Kroger, 2013; Crawford & Plumb, 1986) claim that surface roughness of particles results in a noticeable increase in the pressure drop across the packed beds.

The act of frost desublimation onto a packed bed will reduce the bed porosity present within the packed bed. Since pressure drop across a packed bed and heat transfer within a packed bed is affected by the porosity of the bed, this means that frost accumulation on the packed bed will have an effect on the pressure drop and heat transfer across the packed bed over time.

Achenbach (1995) states in his work that the combination of two previously stated equations (13) and (15) for pressure drop with an equation for the variation of pressure drop in relation to porosity results in the following equation.

$$\frac{d(\Delta P)}{\Delta P} = \frac{d(\Delta P)}{d\varepsilon}\frac{d\varepsilon}{dP} \tag{70}$$

$$\frac{d(\Delta P)}{\Delta P} = -\frac{3-\varepsilon(2-n)}{1-\varepsilon}\frac{d\varepsilon}{\varepsilon} \tag{71}$$

Where n=1 represents the low Reynolds number range and n=0.1 represents the high Reynolds number range. This equation shows that a positive relative variation of porosity causes a negative relative variation in pressure drop.

Conclusions

Of the main carbon capture technologies that are being researched, post-combustion capture technologies appear to have the greatest potential for short to mid-term impact by being able to be retrofitted onto existing power plants. Of the post combustion technologies, amine-based capture is the most mature yet studies suggest that amine based absorption has nearly reached the maximum efficiency that can be achieved, whereas other technologies such as cryogenic carbon capture has potential room for improvement beyond what amine capture can achieve.

The nature of pressure drop and heat transfer within packed beds is quite well established, however using a moving bed instead leaves less of a clear understanding on the fundamentals that are required to know. Furthermore, the impact of desublimation of frost onto a moving packed bed is unknown. Therefore, while a lot of the individual fundamentals can be referenced to in the literature, combining the phenomena together into a single model has not yet been attempted.

Chapter 3: Methodology

Introduction

The current literature shows a significant research gap around frost formation in moving beds. The moving bed cryogenic carbon capture system proposed requires the frost formation mechanism in moving beds to be explored. Therefore, it is clear that the aim of this PhD thesis was to be able to quantify the differences between the fixed packed bed cases in the literature and the moving packed case proposed by this work. This would require experimental work using a capture column which is able to be used as both a fixed bed and moving bed capture column in order to easily compare the differences in behaviour.

This chapter provides a detailed description on the design of the purpose built experimental rig and the roadmap of experimental work conducted in order to address the major research gaps that have been highlighted by the literature review.

Section 3.1: Motivations for experiments

Current CCC technologies utilise either a fixed packed bed or heat transfer surface to produce a cold surface at which sufficiently cold CO_2 can desublime out of the gaseous phase onto the cold surface to form CO_2 frost. The main disadvantage of this technology is the increased frost production leads to a decrease in available nucleation sites for frost to form. This leads to the cold heat transfer surface to eventually become saturated with frost and desublimation of CO_2 no longer occurs, the process must be temporarily stopped to recover CO_2 frost and allow for more desublimation to occur. Developing a CCC system unit that does not require periodic downtime for defrosting is potentially a useful engineering solution.

Understanding the mechanics of heat transfer within the packed bed is critical in understanding what factors determine the rate of frost growth within the cooling column. The design of a moving bed would require the bed velocity to be equal to the velocity of the frost front advance in order to create a net 0 velocity for the frost front, preventing the build-up of frost within the column.

Achieving a net zero frost front velocity requires an understanding of the different effects that operating conditions have on the development of frost within the cooling column. Therefore, it was identified that once desublimation was being achieved and a frost front was forming, performing experiments to conduct a sensitivity analysis on frost front velocity would be critical in to prevent frost build up within the bed. Testing how the conditions of gas flow rate and CO_2 composition would affect how fast the frost front advanced up the column, which would be predicted by constructing a calibration curve.

From the literature review performed, the major factors that would affect frost formation are the CO_2 concentration in the flue gas, the initial temperature of the bed, the flow rate of the flue gas and the bed material (Ali et al., 2014; Tuinier et al., 2010). The major variables investigated in the experimental work of this thesis are the flow rate of gas through the bed and the concentration of CO_2 in the gas, with some investigation on different materials used as the bed material.

In the literature, there is a lack of understanding as to how frost growth behaviour is affected by a moving bed or how heat transfer in a moving bed is affected by frost growth within a moving bed. The motivation for this work is to establish the fundamentals of desublimation within a moving bed to aid in future designs of CCC technology. A moving bed CCC system prevents the excessive build-up of frost

within the capture column, reducing capital cost by eliminating the need for multiple packed bed capture columns operating cyclically to create a pseudo-continuous process. Furthermore, improved understanding of the desublimation process will lead to improved energy efficiency for heat transfer. The excessive build-up of frost on the packed bed surface reduces heat transfer efficiency which results in a more intensive sublimation step to regenerate the bed material.

Section 3.2: Experimental setup

3.2.1 Ambient condition experiments

Determining heat transfer coefficients and moving bed experiments are complex in nature. To simplify the experimental work to be undertaken, some assumptions were made considering the bed material. The bed material was assumed to be spherical in shape and consists entirely of bed material with a diameter of 1.4-1.7mm. Furthermore, the bed voidage within the column was calculated to 0.42 by weighing test samples of bed material occupying a known volume.

Two bed columns were constructed, the first one was constructed out of Perspex with an ID=0.1m, OD=0.105m, which can be seen in figure 3.1. This column was used in experiments regarding fluidisation ranges of the selected bed material and the heat transfer coefficient of bed material under ambient conditions. The Perspex column would allow these initial trial experiments to be performed with the bed material being observed through the clear wall of the column. This was important to establish two important factors; whether the bed material would show signs of fluidisation during the trial experiments, and whether the bed material within the column would be subjected to core or mass flow.

Figure 3.1. Photo of bed fluidisation experimental setup.

The first of the trial experiments aimed to determine whether the bed material would experience fluidisation, particularly local fluidisation near the gas injector. The effect of fluidisation would lead to less predictable heat transfer within the bed and would cause a lot more unpredictability, leading to a lessened understanding of heat transfer experiments. Compressed air at 4 bar was fed into the column via the copper gas injector at various flow rates from 100 LPM up to 400 LPM in increments of 50 LPM. The flow rate was used to estimate the pressure drop across the length of bed material in the column using a pressure drop equation (16) from section 2.3.1 (Fenech, 1981) and compared against the pressure drop recorded by the pressure gauge in the column.

When it was determined that the bed material did not experience fluidisation under these flow rates, then experiments began to investigate the heat transfer coefficient of the bed material. This could be experimentally determined without requiring cryogenic conditions, calculation of the heat transfer coefficient would also be beneficial in designing the cryogenic moving bed. Determining the heat transfer coefficient between the bed material and a heated stream of compressed air could be done using a similar method used by Crawshaw (2000) to calculate the logarithmic mean temperature difference and derive the heat transfer coefficient from it.

The experimental set up for the trial heat transfer experiments, shown in figure 3.2, was a simplified version of the rig used in the cryogenic experiments. A compreFssed gas line was used as the gas supply for the heat transfer experiments. The gas supply fed into the heat transfer column was heated using a copper coil submerged in a water bath. Thermocouples measure the temperature of the heated gas and the bed material, one measuring the gas inside the feed pipe before entering the column, two measuring temperature of 30mm above the gas injector and one measuring the temperature of the bed material 5mm below the injector. Bed flow through the heat transfer column was set by designing the column with a tapered end to allow mass flow of the bed material through the column at a rate of 40 g/s.

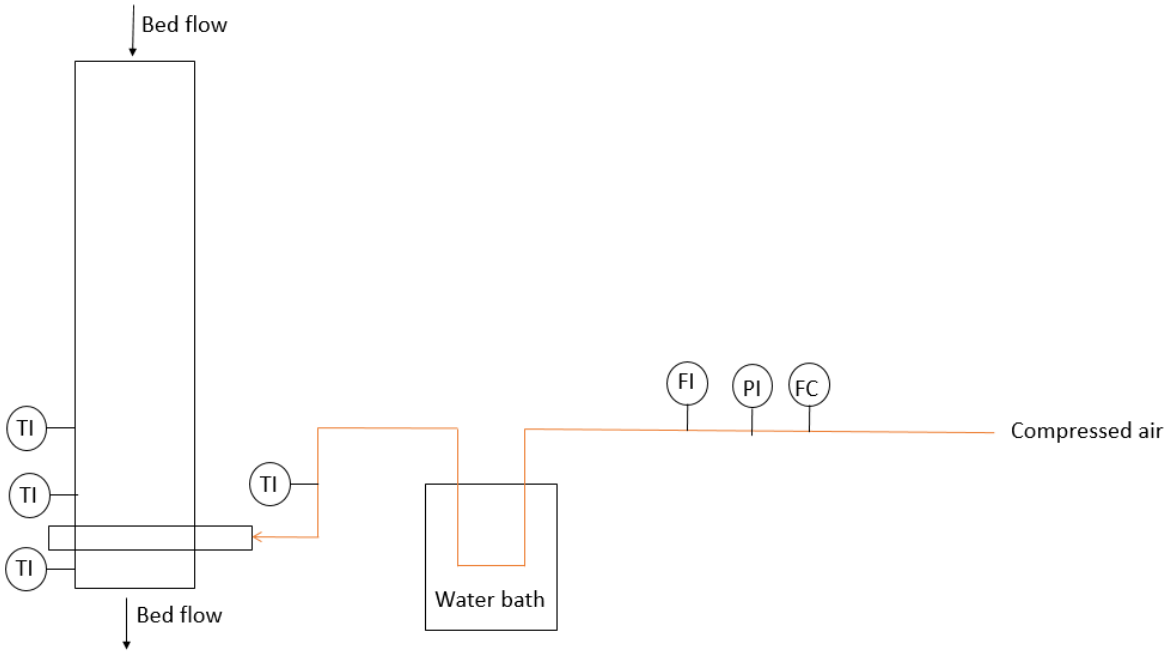

Figure 3.2. Sketch of ambient condition heat transfer rig.

A shroud was placed over one of the thermocouples placed 30mm above the gas injector, shown in figure 3.3, which would limit heat transfer by conduction as the bed material would not be able to come into contact with the probe, whereas the gas would. This modification would allow for a more accurate reading of the gas temperature within the bed. At this early stage of experiments, instead of using a screw conveyor to control the bed material, a funnel was fashioned with a tapered end and exit orifice 14mm in size. The purpose of these experiments was to keep bed temperature within the column stable as bed material that was heated by the compressed air stream would also leave the column, thus creating thermal equilibrium.

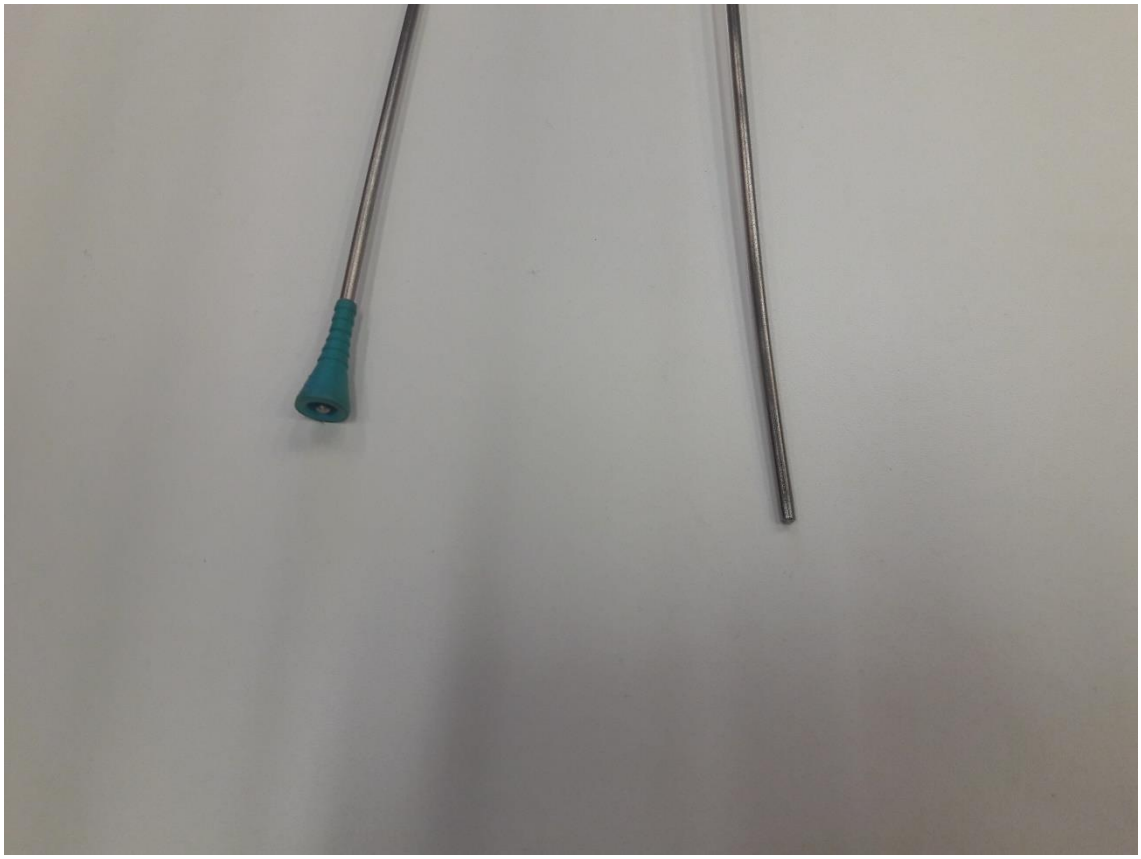

Figure 3.3. Image of thermocouple with shroud.

The second stage of experiments after the trial experiments would require the Perspex column to be replaced with the PTFE column in preparation for cryogenic experiments. Furthermore, the mixed gas line of CO_2 and N_2 and the liquid nitrogen dewar were also installed to replace the water bath in the previous trial experiments. Lastly, insulation was applied to the outer surface of the PTFE column in order to minimise the effect of heat leakage into the cryogenic column.

3.2.2 Cryogenic condition fixed packed bed experiments

After trial experiments were completed the Perspex column was replaced with the cryogenic cooling column, which was a 1m long vertical column made out of plastic polytetrafluoroethylene (PTFE), ID=0.072m, OD=0.095m. The size of the column was selected from available sizes that can be purchased. The internal diameter of 72mm provides a bed material to column diameter ratio of 1:36. The column was held between two aluminium plates with orifices to allow the filling and emptying of bed material in the column. This column was used for cryogenic experiments, PTFE was chosen as the material as it would be able to withstand cryogenic temperatures. A diagram of the cryogenic rig setup is provided in figure 3.4 and a photograph of the physical rig is provided in figure 3.5.

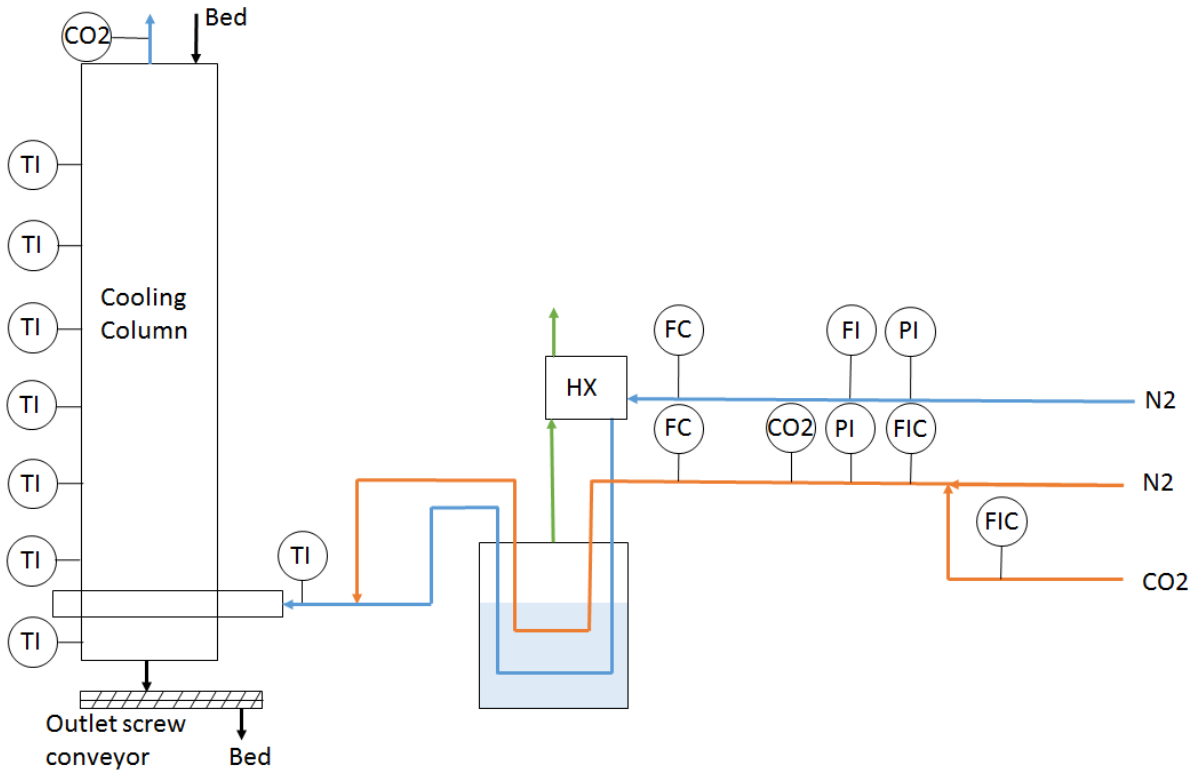

Figure 3.4. Diagram of moving bed rig set up.

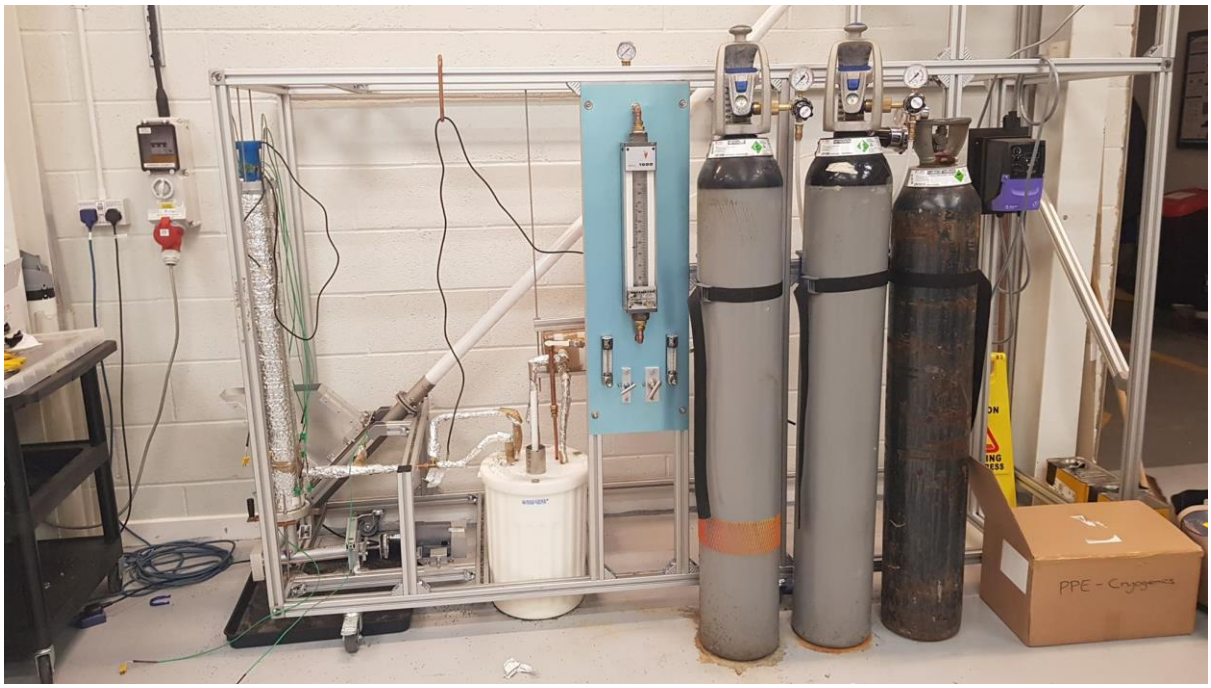

Figure 3.5. Photograph of cryogenic rig setup.

The piping that would convey the gases to the cooling column were required to be able to withstand cryogenic conditions, for this reason copper was chosen as the construction material for the gas pipes. A copper pipe served as the gas injector into the column, the pipe was cut to create multiple 1mm

wide slits within the pipe to allow gas to flow into the column while preventing a misdirected flow of bed material from the column into the gas pipeline. A photograph of an example of the gas injector design is provided in figure 3.6. The column has a small conical tapered end at the bottom made from a plastic insert to create a 14mm outlet at the bottom of the column.

Figure 3.6. Photograph of copper pipe gas injector design.

The gas injector is connected to two gas lines; the first gas line being a pure nitrogen gas line (shown as the blue line in figure 3.4) which is cooled to -140˚C by passing through a coil submerged in a liquid nitrogen dewar, which can be seen in figure 3.5 as the white dewar in the experimental rig, the second gas line was a mixed gas line of nitrogen and carbon dioxide (shown as the orange line in figure 3.4) which is cooled to -60˚C by passing through a separate coil submerged in the same liquid nitrogen dewar bath. The flow rate and CO_2 composition of this mixed gas line was controlled by two ball control valves, the control valves and rotameter for the mixed gas line can be seen in figure 3.5 on the blue control panel. The heat exchanger (HX) pre-cools the pure nitrogen gas line with evaporated liquid nitrogen from the liquid nitrogen dewar, to recover as much cooling duty as possible.

Two CO_2 sensors record the CO_2 concentration of the mixed gas line before being injected into the column and after travelling through the column. The CO_2 composition entering the cooling column and leaving the cooling column was measured using GSS ExplorIR®-W CO_2 sensors which have an accuracy of 0.001%. The sensor measuring concentration of CO_2 in the feed gas measures up to 20% CO_2 and the sensor measuring the concentration of CO_2 of the gas exiting the column measures up to 5% CO_2.

A small moving bed screw conveyor was set up at the bottom outlet of the capture column in order to control bed flow rate. The screw conveyor can be seen in figure 3.4 below the bottom of the cryogenic capture column and a more detailed picture of the screw conveyor is provided in figure 3.7. The required bed flow rate for cryogenic experiments, 20 g/s, was lower than what could be achievable through hopper design, so the screw conveyor was constructed in order to provide a greater level of control over the flow rate of bed material in moving bed experiments.

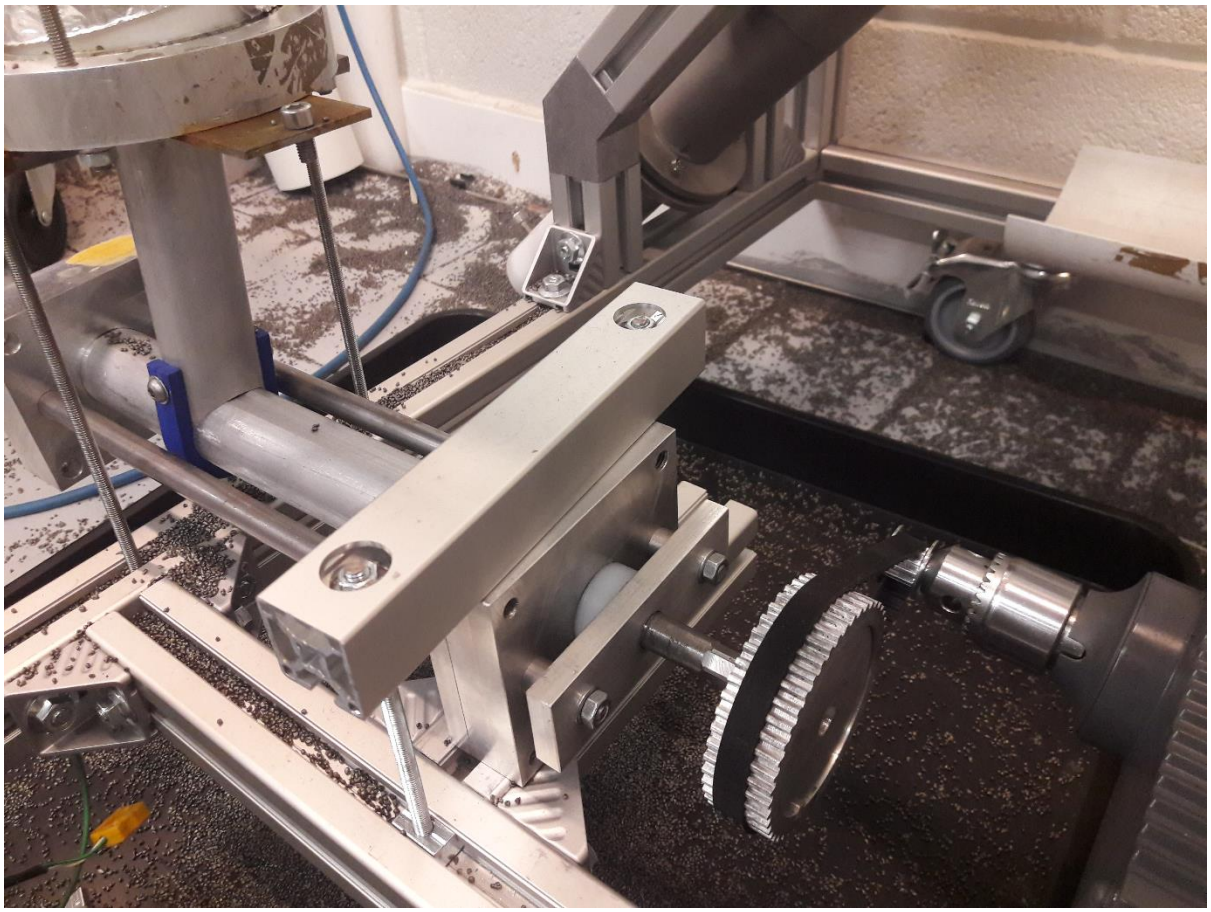

Figure 3.7. Purpose built screw conveyor.

Section 3.3: Development of moving bed methodology

The cryogenic experimental rig would operate in two stages, both with precooling. In the first stage, N_2 gas is cooled by passing through a liquid nitrogen bath before being fed into the capture column to precool the bed material; the second, a capture stage where the feed gas into the capture column is switched to a CO_2 and N_2 mixed gas. The precooling step lasts roughly 30 minutes where 250mm depth of bed material is cooled down to a temperature range of -140^{o}C to -120^{o}C., which would provide sufficient cooling duty to the mixed gas that would be injected into the capture column during the capture stage of the experimental runs.

Advancing to the moving bed experiments was broken down further into four major steps; i) precooling stage experiments in order to establish the fundamentals of the precooling stage, ii) frost front velocity experiments in a fixed bed to determine the rate of CO_2 frost front advance within the capture column and construct calibration curves to predict frost front velocity, iii) moving bed experiments to balance the flow rate of bed material in the column with the frost front velocity in order to achieve a net zero frost front velocity, and iv) finally combining the precooling and capture stages in order to provide a continuous process.

The main goal of the moving bed is to prevent frost accumulation. In order to achieve this, the flow rate of the bed material flowing down the column must be equal to the rate at which the frost accumulates within column. Since there is a lack of sufficient knowledge on moving bed CCC, experimental work first begins on a fixed bed case which can be compared to both theoretical modelling work provided in this work and experimental results for fixed bed CCC in the literature in order to provide validation for the moving bed experimental work. Since the frost front for the fixed packed bed case is expected to develop similar to the work done by Tuinier et al. (2011) shown in figure 2.18, thermocouples were placed 5mm, 30mm, 150 and 250mm above the gas injector.

As CO_2 frost forms, most heat transfer is occurring as latent energy. This means that the frost front can be identified by a characteristic constant temperature over time. The temperature at which the bed material should remain stable would be the temperature where CO_2 desublimation occurs. Since each thermocouple would be expected to record a temperature rise from the desublimation of CO_2 to form the characteristic plateau, recording the time at which each thermocouple records CO_2 deposition would indicate how fast the frost front advances through the capture column. This would be known as the frost front velocity.

The frost front velocity was measured under a range of different gas flow rates and CO_2 concentrations, listed in table 3.1.

Table 3.1. Frost front velocity experimental conditions.

Inlet gas flow rate (LPM)	Inlet gas CO_2 concentration (%)
100	18
100	8
100	4
120	18
80	18
50	18

Altering the flow rate and CO_2 composition of the gas and the initial bed temperature of the bed would give an understanding of the frost front velocity under the range of conditions that the rig could provide. These experiments were performed in triplicate to test for repeatability and a calibration curve was constructed in order to be able to predict frost front velocity in future experiments under conditions not previously tested.

After frost front velocity was determined to be predictable by the calibration curves, the next step in the moving bed experiments was to prevent the accumulation of frost by introducing a bed flow rate which would give a velocity to match the frost growth. This was organised to be done by a screw conveyor which would draw bed material out of the column, shown in figure 3.4. With the moving bed designed to prevent frost build up within the column, further experiments will test whether the design is working effectively. It is expected that with a moving bed, the frost front will not advance through the column, due to the removal rate of frosted bed material being equal to the rate of frost accumulation in the capture column. So the temperature profile of the bed material in the capture column should remain constant as temperature rise throughout the capture column, if not this would indicate the frost front velocity is not at a net zero velocity.

Thermocouples were placed in the same arrangement as in the previous frost front velocity experiments, at 5mm, 30mm, 150mm and 250mm above the injector. The frost front velocity and bed flow rate were set to match each other. Instead of fine tuning the RPM of the screw conveyor to an arbitrary gas flow rate and composition, the frost front velocity calibration curve was to be tested by altering the gas flow rates to match specified bed flow rates. Since it is possible greater level of control over the flow rate of gas entering the column than to control the bed flow rate utilising the screw conveyor. The temperature of the thermocouples around the 5mm and 30mm points were used to assess the progress of experiments.

The GSS sensor at the outlet of the cooling column would be used to estimate the temperature of the gas exiting the column after desublimation and create a theoretical temperature profile. The CO_2 composition measured by the GSS sensor would be estimated to be the saturated vapour pressure of the gas after desublimation in the frosted region of the bed had occurred. This could be compared to the temperature profiles of the thermocouples in place in the column.

The CO_2 concentration of the gas past the frost front boundary was measured by two separate methods. First method was to place the CO_2 sensor at the outlet of the column and measure the CO_2 concentration at the outlet. The second method was to create a small pipeline at the 30mm mark above the gas injector with a thermocouple sheathed inside the pipe with the GSS sensor attached to the outlet of the pipe. This second method would allow a sample of gas closer to the frost front

boundary to be measured by a thermocouple and the GSS sensor and should allow for a more direct comparison between the experimental and theoretical temperature measurements.

The final set of experiments was the combination of the precooling and capture stages. The limitation of a cryogenic fixed packed bed is the requirement to cycle between cooling, capture and regeneration steps. In order to demonstrate that the proposed moving bed capture column addressed this limitation, the experimental rig was upgraded to perform the cooling and capture stages simultaneously. This stage of experiments would require the introduction of a second injector, which will allow the injection of cooling gas from the precooling stage above the section of the bed where the CO_2 frost region occurs. The second injector is a vertical injector placed 100mm above the original injector, a photograph of the injector is shown in figure 3.7. The vertically placed injector will cool the bed material down as it flows through the column, the injector is placed vertically to allow ample contact time between the cooling gas and the bed material. The original injector will continue to feed the N_2/CO_2 mixed gas into the column. A stable CO_2 frost equilibrium should form in between the two injectors.

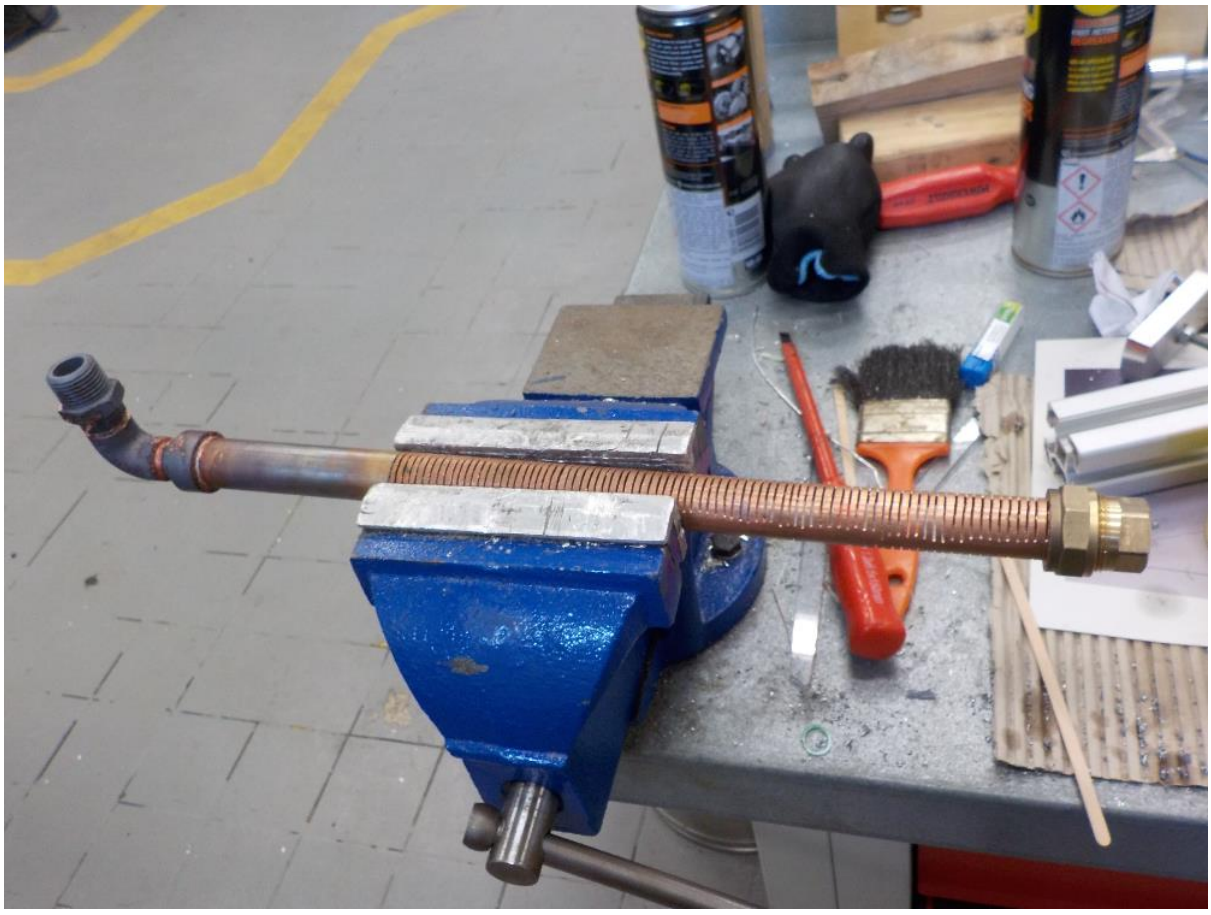

Figure 3.7. Photograph of the second injector.

The second injector was tested to judge how the second injector cools down the moving bed, repeating the experimental procedure of the precooling stage experiments. Thermocouples recorded the temperature of the bed in multiple regions of the column, both above the injector, below the injector and within the region of the injector. After gaining a clear understanding of the characteristics of the moving bed being cooled by the second injector, the new rig was set up to capture CO_2 continuously.

Due to a lack of circulation of bed material into the top of the column, the capture column will experience a depletion of bed material over the duration of each experiment. Whereas the fully developed design of the proposed capture system would be able to circulate bed material from the bottom of the column to a regeneration unit and then back into the column to be precooled by the vertical injector, the vertical injector in the current experimental rig will lose efficiency over time due to the loss of bed material in the column. Therefore, the precooling stage is not eliminated entirely, the precooling step would ensure that the bed material between the cooling stage injector and the capture stage injector is sufficiently cooled in order for the frosted region of the capture column to form before the capture stage injector and the moving bed are initiated.

It is expected from these final experiments that the cooling stage injector will maintain a stable temperature of fresh bed material approaching the frosted region of the capture column and that the frosted region of the bed material will not advance up the column due to the moving bed maintaining a net zero frost front velocity.

Conclusions

The experimental rig has been designed with the intention of facilitating experiments that will explore the research gaps highlighted by the literature review chapter.

The methodology for experiments was to approach the research gaps in incremental stages, with each stage of experiments in the methodology establishing empirical data from experiments which would be compared with theoretical data derived from available literature. i) first stage focused on testing bed material for fluidisation and heat transfer with the gas phase, in order to verify the suitability of the selected bed material ii) cryogenic experiments under fixed packed bed conditions in order to validate experimental work with fixed packed bed data found in literature and finally iii) cryogenic moving bed experiments to demonstrate that the frost front velocity can be controlled and thus excessive build-up of frost within the capture column can be prevented.

After each stage of experiments, comparative work between theoretical and empirical data would be used to facilitate the progression of experiments to the next stages within the methodology.

The methodology and experimental rig set up have been established in this chapter and equations of heat transfer and frost deposition have been discussed in the previous literature review chapter. The equations found in the literature need to be adapted and applied to the experimental rig design discussed in this chapter.

The following chapter will use theoretical modelling to predict the behaviours of the experimental rig, these results will be compared with experimental results which are presented in chapter 5.

Chapter 4: Theoretical modelling

Introduction

The CCC system design and experimental work proposed by the methodology provides a roadmap of the development of the moving bed design through the use of sequential experiments that build on from the knowledge gained from previous experimental work.

This work aims to understand the behaviour of the moving packed bed in a CCC system, since the literature review revealed that only the behaviour of a fixed bed CCC process has been investigated. The design of the purpose built experimental rig is based on this available information to make the first design decisions.

It should therefore be the case that the behaviour of the experimental rig in fixed bed experiments follows closely to what would be predicted by the available literature. The simulated experimental work provided in this chapter is important due to a lack of data available in the literature to compare with experimental results shown in this thesis. This chapter predicts the behaviour of the experimental rig, in particular the frost front velocity, to be later compared with experimental results from the purpose built rig in order to test accuracy and validity of the experimental results under fixed packed bed conditions. This chapter also begins to predict how the given theoretical equations governing fixed bed CCC systems would be adapted in order to model moving bed scenarios.

4.1. Theoretical modelling of frost front velocity

The purpose of creating a theoretical model for the frost front velocity within the column is to predict the rate at which CO_2 deposits on the bed material. Accumulation of CO_2 frost within the column stops once the bed is fully saturated with frost and the proposed method of utilising a moving bed to prevent

the saturation of the column would require an accurate prediction of the frost front velocity to operate a continuous moving bed effectively.

As the CO_2 and N_2 is fed into the column, the gas phase will be cooled down by the cold bed material. When the gas phase is cooled down the saturated vapour pressure of CO_2 will decrease. When the saturated vapour pressure drops below the partial pressure of CO_2 in the gas phase then the difference in pressures provide the driving force behind the desublimation of CO_2. CO_2 will continue to form on the bed material as a frost as long as the bed material can provide sufficient cooling duty to the gas for desublimation of CO_2 to occur. This means that the energy density of the bed material is a critical limiting factor in the rate of frost formation. Therefore, the rate of frost advance through the column can be estimated by an energy balance equation around the bed material.

The energy balance is focused around the frosted region of the bed material. As the gas enters the column it will be cooled down by the bed material and desublime CO_2 as a frost on the bed material. Therefore, the gas entering the column before the frosted region of the bed will still contain the same mass concentration of CO_2 as its feed composition. Under the assumption that all CO_2 in the gas phase will desublime as a frost after passing through the frosted region of the bed, the mass composition of CO_2 in the vapour phase leaving the frosted region would be zero.

When CO_2 desublimes out of the gas phase the bed material will begin to accumulate CO_2 frost on its surface. The accumulation of CO_2 will result in the frosted region of the bed expanding over time. This expansion of the frosted region can be estimated through the frost front velocity. The advancement of the frost front does not affect the simple estimate of frost front velocity. This is due to the assumption that all CO_2 is deposited inside the frosted region of the column. The frost front velocity can be estimated using the conditions of the bed material and the gas phase before and after exiting the frosted region.

The mixed gas requires cooling duty (Q_g) in order to bring the temperature of the gas down to the desublimation temperature of the CO_2 and requires further cooling duty to facilitate CO_2 desublimation. Equation (72) and further derivations to frost front velocity and energy balance are provided by Tuinier (2011).

$$Q_g = \dot{m}_g c_{pg} \Delta T + \dot{m}_g \left(k_{CO_2 in} - k_{CO_2 out}\right) \Delta h_{CO_2}^{sub} \tag{72}$$

Where k_{CO2out} will be zero due to the assumption that all CO_2 is being desublimed.

As already stated, since the bed material provides the required cooling duty to the gas and facilitates CO_2 desublimation, the frost front will advance through the column at a steady rate:

$$Q_s = U_{frost} A \rho_s c_{ps} \Delta T \tag{73}$$

Since the energy change between the gas phase and the bed material must be equivalent this equation can be rearranged to estimate the frost front velocity within the column.

$$U_{frost} = \frac{Q_g}{A \rho_s c_{ps} \Delta T} \tag{74}$$

Assuming no exergy is destroyed the temperature change for the gas and solid phases will be equal to each other. The bed material will no longer be able to cause CO_2 frost formation once the cooling duty is entirely spent. In other words, once the temperature of the bed material has reached equilibrium with the mixed gas feed further CO_2 deposition cannot occur. So the bed material will continue to increase in temperature until it is in equilibrium with the desublimation temperature of CO_2 in the mixed gas.

This assumption of no exergy loss during heat transfer has been assumed due to the high heat transfer coefficient between the gas and the bed. This high heat transfer coefficient means that heat transfer is completed within a 5mm depth of bed. The available excess of bed material within the column and excess cooling duty would be sufficient to bring the temperature of the gas leaving the frosted region roughly equivalent to the initial temperature of the bed material.

There is a finite amount of available cooling duty from the bed material. The amount of CO_2 that is deposited on the surface of the bed material will be dependent on the CO_2 concentration of the feed gas. When taking into account the dimensions of the capture column, the mass of frost can be determined per metre depth of column as shown:

$$m_{CO_2}\left(\frac{kg}{m}\right) = \frac{\dot{m}_g\left(k_{CO_2 in} - k_{CO_2 out}\right)}{u_{frost}} \tag{75}$$

Where k_{CO2out} is still zero. The mass flow rate of the gas and the frost front velocity are directly proportional so in the above equation the mass of frost deposited in the frosted region of the column is dependent on the CO_2 concentration of the feed gas.

Figure 4.1a shows the impact that the feed gas CO_2 composition has on the mass of frost deposited after using equation 73. It can be seen that with increasing CO_2 concentrations the mass of frost deposited also increases. This relationship is more significant at lower concentrations of CO_2 between 0-0.2 before adopting a near linear relationship for concentrations above 0.4. The mass of frost deposited on the bed material decreases the lower the feed concentration of CO_2 is. The trend seen in figure 4.1a closely matches the trend observed between the cooling duty required by the gas and the mass of frost deposited, shown in figure 4.1b.

This is due to cooling duty from the bed material being wasted by cooling down the gas which is of a lower CO_2 purity. The other constituents of the gas being cooled down which will not desublime as a frost, this combined with the knowledge that low CO_2 purity in the gas phase decreases the saturated vapour pressure of CO_2 means that more cooling duty must be supplied to the gas at lower CO_2 concentrations. The effect that the CO_2 purity has on the saturation pressure is greater at lower concentrations of CO_2. This then means that the desublimation temperature is more significantly affected by lower CO_2 concentrations in the gas.

a)

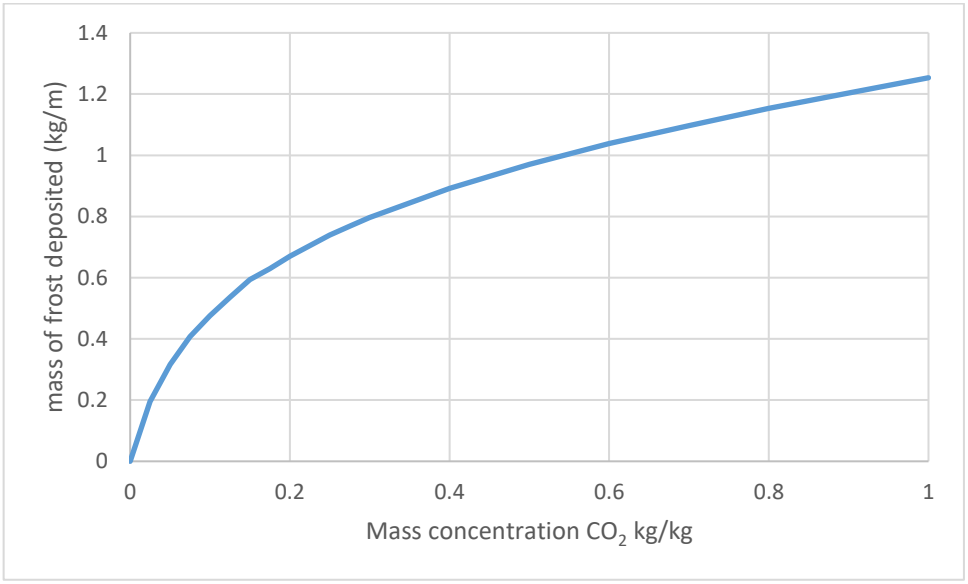

b)

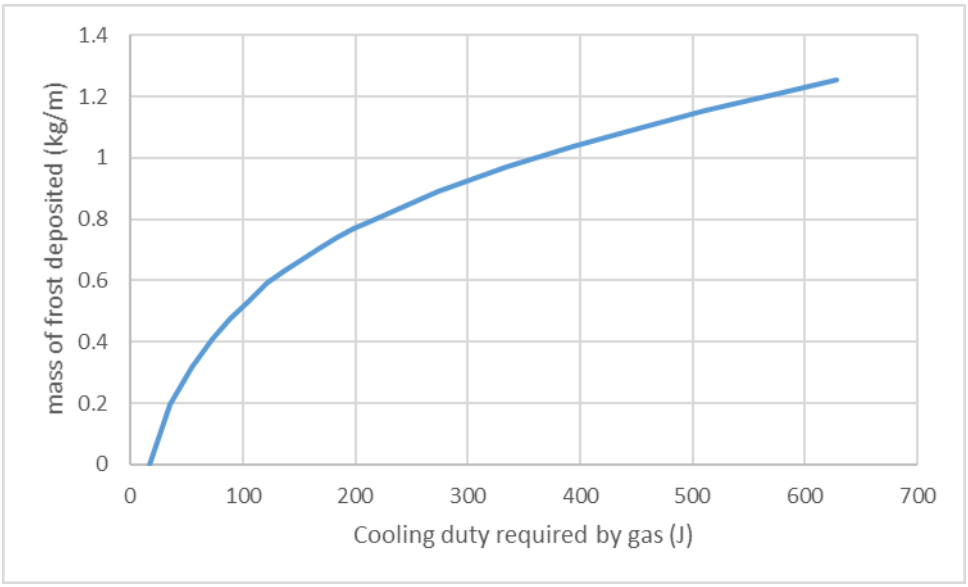

Figure 4.1. Mass of CO_2 deposited in frosted region of bed with varying CO_2 mass concentrations in the gas phase.

Higher concentrations of CO_2 in the feed gas would naturally lead to a greater mass of CO_2 frost, this is due to greater masses of CO_2 being deposited in the same depth of bed material, the same

conclusion is reached by (Tuinier, 2011). What is currently unknown is whether the increase in mass would result in an increase in the thickness of the frost or the density of the frost. Given the three stages of CO_2 frost formation it is clear that the frost growth stage is a relatively short stage so it is unlikely that the frost growth in the column would not progress past this stage (C. F. Song et al., 2013). The frost densification stage occurs once the sublimation and desublimation rates of CO_2 are in equilibrium with each other, so the frost densification stage likely would occur in the frosted bed section after the frost front has advanced through the entire column. So it can be assumed that the relationship between the mass of frost deposited is proportional to the thickness of the frost.

a)

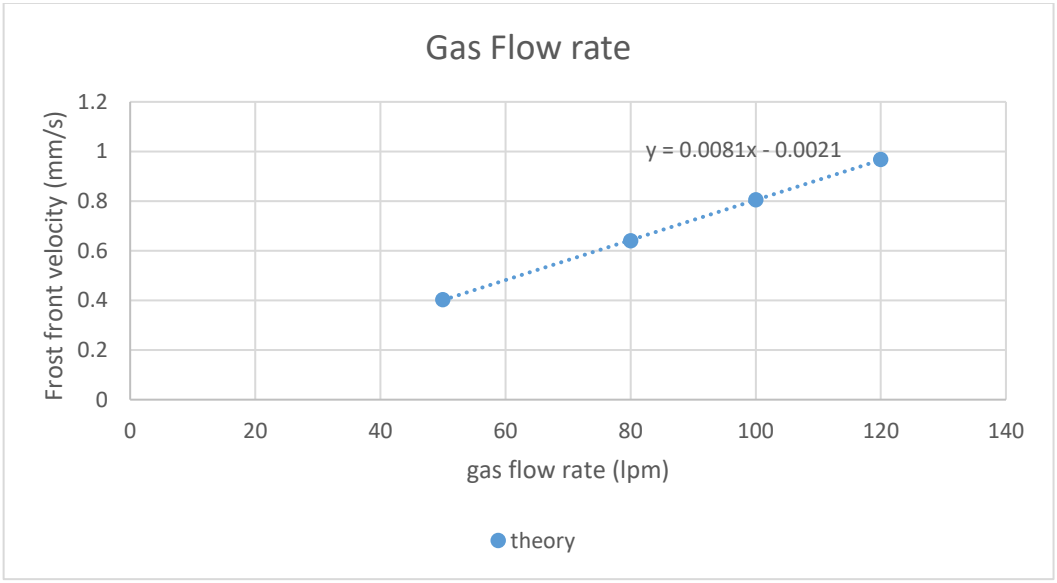

b)

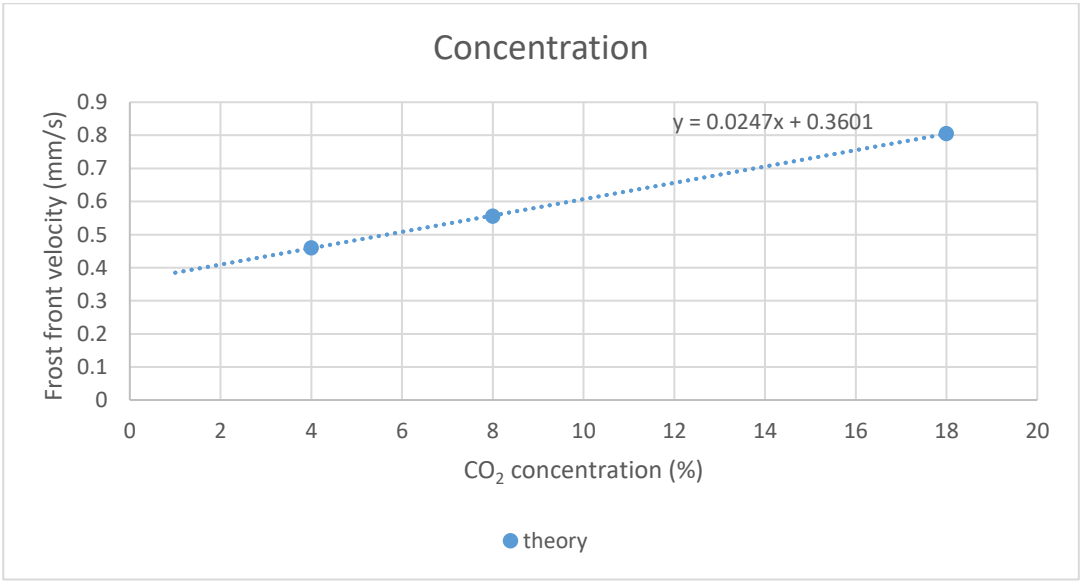

c)

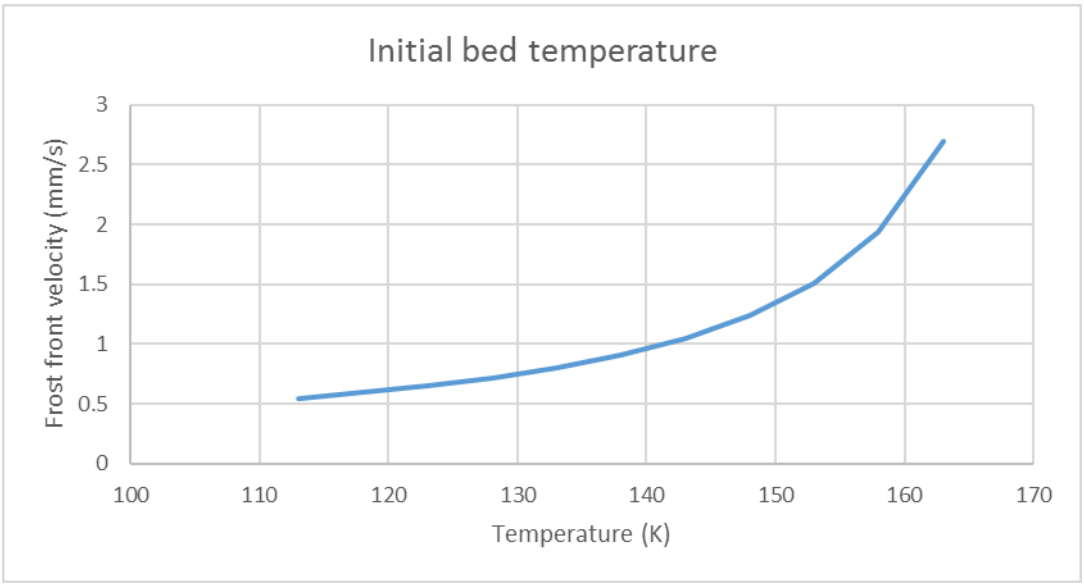

Figure 4.2. Graphs comparing theoretical flowrates under different conditions. a) Different total gas flow rates. b) Different CO_2 concentrations. c) Different initial bed temperatures.

The variation of frost front velocity is directly proportional to the variation in concentration or the flow rate of gas. A linear relationship means the frost front velocity is easier to predict under different conditions. The calibration curves were expected to intercept the (0,0) point of the graphs, while the calibration curve for gas flow rate is relatively accurate, the concentration calibration curve does not intercept close to the (0,0) point of the graph. This is due to two major reasons; firstly, the effect of the nitrogen concentration in the gas phase being a source of wasted cooling duty for the bed material. Secondly, a decrease in CO_2 concentration lowers the desublimation temperature of CO_2 which affects the available cooling duty the bed material can provide.

For figure 4.3, results from equation (74) are calculated for a base case of 100LPM 18% CO_2 v/v gas flow under a range of different initial bed temperatures. The difference between the initial bed temperature and the CO_2 desublimation temperature is then plotted against the frost front velocity. In contrast to the linear relationships between the gas flow rate and concentrations and the overall frost front velocity, altering the initial bed temperature changes the available cooling duty and as such the closer the initial bed temperature approaches the desublimation temperature for CO_2 the frost front velocity approaches infinity. The equation for the trend in figure 4.3 can be approximated as follows:

$$y = \frac{U_{frost}}{dT} \tag{76}$$

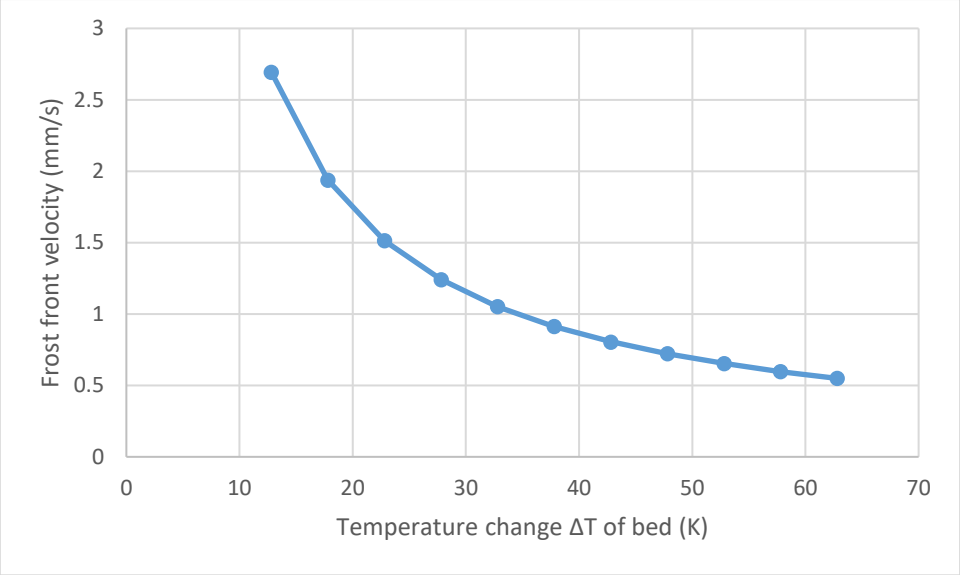

Figure 4.3. Graph of relationship between temperature change of bed and frost front velocity.

Where the constant C_1=34.5. Referring back to the equation for frost front velocity (74) it can be seen that the constant for C_1 can be calculated from the temperature change in the bed material and the frost front velocity.

$$\Delta T U_{frost} = \frac{Q_g}{A\rho_s c_{ps}} = C_1 \tag{77}$$

4.2. Frost thickness

The thickness of the frost influences the change in the bed porosity as frost accumulation increases the total diameter of the bed material. The frost will also impact the heat transfer characteristics of the bed as the frost will alter the overall thermal conductivity of the bed material. The accumulation of frost is also likely to affect the flow of bed material under moving bed conditions.

The accumulation of frost affecting the flow of bed material in a moving bed would require experimental work to determine the level of effect. Estimating the frost thickness would be useful in determining the effective thermal conductivity of the frosted bed material and overall affect frost has on heat transfer within the moving bed, particularly when regenerating the frosted bed material for CO_2 storage and bed recirculation.

It can be assumed that within the frosted region of the cryogenic cooling column the frost would be deposited uniformly across the bed material providing that there are no irregularities in gas flow or bed material temperature. Working with this assumption in mind, the thickness of the frost would be

estimated by taking Tuinier's (2011) experimental results for the density of the frost and the overall surface area of the bed within the frosted region. Density of frost for 10% CO_2 v/v ranges between 400-800 kg/m^3 and 50% v/v CO_2 ranges between 400-900 kg/m^3.

$$\delta_f = \frac{m_{CO_2}}{a_b \rho_f} \tag{78}$$

Where a_b is the available surface area of the bed material. The relationship between frost density and frost thickness would be inversely linear. An increase in frost thickness will be matched with a decrease in frost density. Furthermore the frost density is related to the thermal conductivity of the frost, as mentioned in chapter 2.5, a higher density frost would result in a higher thermal conductivity within the frost.

$$a_b = \frac{6(1-\varepsilon)V}{d_p} \tag{79}$$

The thickness of the frost is dependent on the available surface area of the bed material inside the capture column, which is dependent on the diameter of the bed material. The relationship between frost thickness and bed particle diameter is shown in figure 4.4. Figure 4.4 was constructed using equations (78) and (79) using a range of bed material diameters and a fixed mass of CO_2 frost calculated from theoretical models based on equation (75) for 25% CO_2 kg/kg and 100LPM. The thickness of the frost formed during the capture step and the diameter of the bed material in the capture column form a fixed ratio as can be seen by the linear relationship, in other words the thickness of the frost is a fixed percentage of the diameter of the bed material that is used in the capture column.

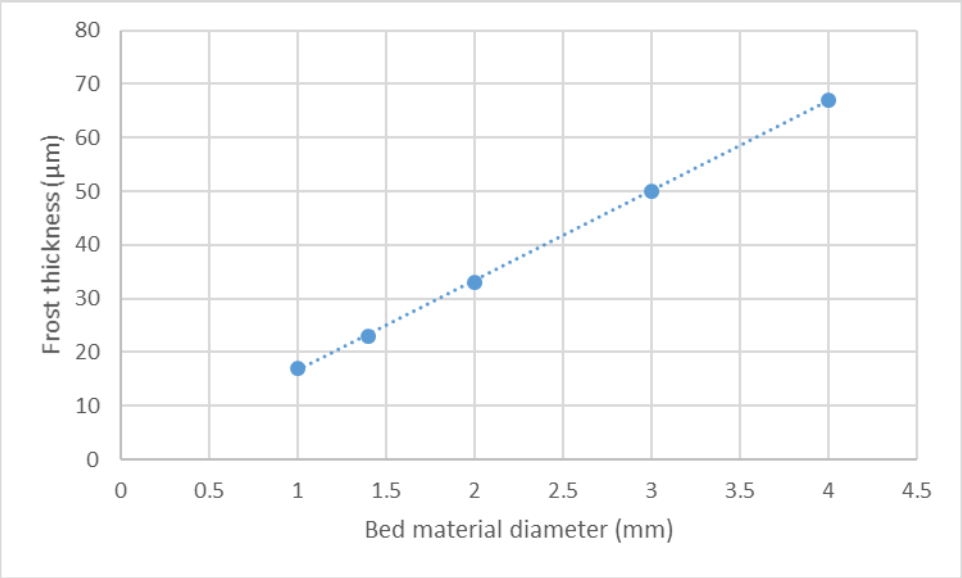

Figure 4.4. Graph of frost thickness vs bed material diameter.

The frost thickness will influence the bed porosity, as frost forms on the surface of the bed material there will be less empty space within the column for the gas to flow through. The bed porosity is expected to remain constant, equation 77 can be used to determine bed porosity (Achenbach, 1995):

$$\varepsilon = \frac{0.78}{\left(\frac{D}{d_p}\right)^2} + 0.375\,, \qquad for\ \left(\frac{D}{d_p}\right)^2 > 2 \tag{80}$$

While this equation remains true so long as the diameter ratio remains greater than 2, for the purpose of allowing bed material to flow through the column as a moving bed, the diameter ratio would have to remain greater than 10. The effect of particle diameter on porosity has a negligible effect if this ratio is maintained.

Estimating the porosity of the frosted bed material can be achieved by assuming the bed material is evenly coated with frost of a uniform thickness around each bead, the desublimation of CO_2 on the bed material results in a bed material with an effective radius equal to the radius of the bed material and the thickness of the frost. Equation (80) gives a value for porosity with frosted bed material.

The bed porosity of the metal beads was experimentally determined to be 0.42, this is larger than the value of 0.37 that equation (80) predicts. The most likely reason for this is that the bed material is not perfectly spherical and not perfectly uniform in size. The capture column is expected, according to equation (80) to have a frosted bead radius of 0.78mm for higher density frost and 0.88m for lower density frost estimates, increasing very slightly from 0.7mm radius of fresh bed material once frost formation has occurred. This is expected to have a negligible impact on the pressure drop within the bed, as equation (80) does not predict any significant change in bed porosity from the increase in diameter.

4.3. CO_2 desublimation

The driving force for CO_2 desublimation is the difference between the partial pressure of CO_2 and the saturated pressure of CO_2. The saturated vapour pressure is modelled using the Span and Wagner equation of state (1996). Referring back to equation (57) provided in chapter 2.5.

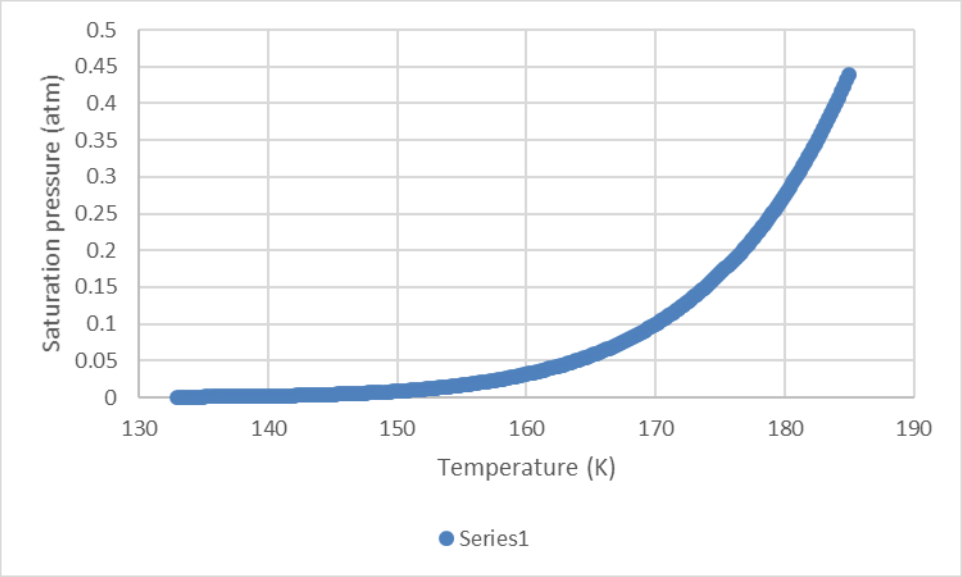

Figure 4.5. Saturation pressures of CO_2 at different temperatures (Span & Wagner, 1996).

As the partial pressure of CO_2 exceeds the saturation pressure, CO_2 will desublime out of the gas phase as a frost until the partial pressure matches the saturation pressure (Tuinier et al., 2010). The rate at which CO_2 desublimes and approaches the saturation pressure is dependent on the time constant.

The desublimation rate of CO_2 is dependent on the temperature of the gas phase in the bed material. Given the large heat transfer rates in packed beds, the temperature of the gas is considered to be equivalent to the temperature of the bed material at the same bed depth. The rapid change in temperature of the bed material once the frost front starts to form on it leads to an equally rapid decrease in frost desublimation rate.

The desublimation rate is largely unaffected by the conditions of the capture column itself. The difference in partial pressure and saturated vapour pressure is the driving force behind desublimation which relates to the rate at which the bed material at the boundary between frosted and fresh bed material heats up as well as the depth of the temperature gradient between the frost front boundary and fresh bed material.

Assuming a sharp frost front means that there is no temperature gradient. In other words, the temperature of the gas and the bed material sharply changes from conditions in the frosted bed material to the conditions beyond the frost front. This is further supported by observations in the experimental rig that heat transfer approached completion within a bed depth of 5mm.

As previously mentioned in the literature review, the introduction of a mass deposition rate constant g models the temperature gradient. Included in equation (59) provided in chapter 2.5. The mass deposition rate constant is calculated as (Tuinier, 2011):

$$g = \frac{M_{rCO_2} k_g}{\bar{T} R} \tag{81}$$

Where R is the universal gas constant, k_g is the gas-solid mass transfer coefficient and M_r is the molecular weight of CO_2. The g value can be adjusted to match the experimental results in order to accurately model the gradient on the frost front.

The column becomes saturated with frost once the frost has advanced 250mm up the column. This is due to insufficient cooling available within the cooling stage to sufficiently cool down bed material further up the column. Therefore the 250mm thermocouple can be considered the temperature of the outlet of the column. The theoretical model of frost deposition was measured against the experimental results from the rig. An example of such a comparison is provided in figure 4.6.

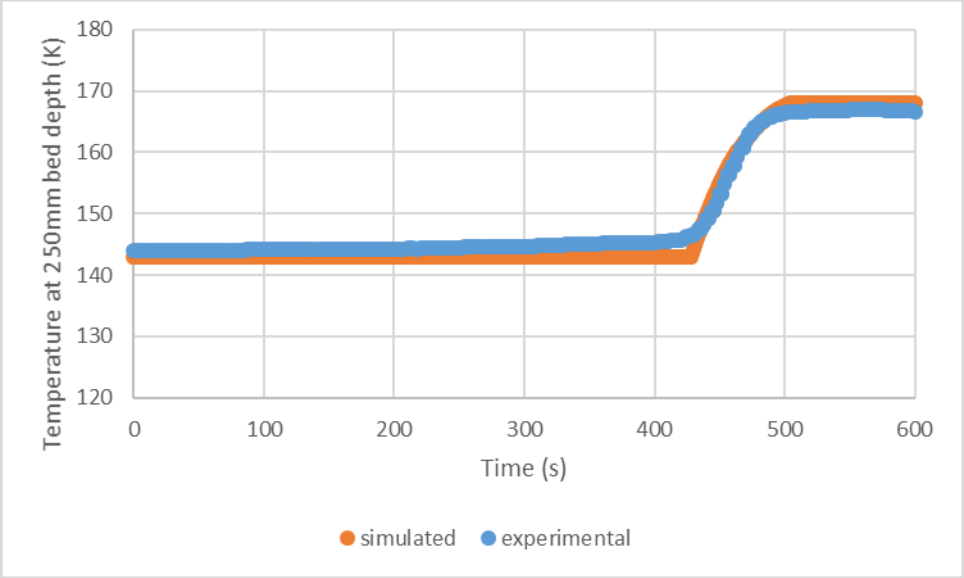

Figure 4.6. Experimental and simulated temperature profile at 250mm bed depth (100LPM, 8% CO_2).

The comparison provided in figure 4.6 represents a gas flow of 8% CO_2 purity at 100LPM, the 250mm thermocouple line in the simulated run represents the final 5mm of bed material given heat transfer occurs over roughly 5mm of bed depth. The experimental results show a more gradual advance of the frost front in comparison to the simulated results demonstrating a sharp initial change in temperature. The simulated and experimental results however match each other very well.

4.4. Moving bed theory

Introducing a moving bed would have an effect on the overall frost front velocity but the general energy balance equations for the frost velocity would not be dramatically affected. The general equations remain constant throughout the majority of operation of a cryogenic packed bed due to the

boundary conditions moving with the frost front plug flow. Deviations from the general equation would only occur once the bed is saturated with frost as the bed is no longer able to completely capture CO_2, the CO_2 concentration in the gas leaving the frosted region of the bed will begin to increase until matching the inlet CO_2 concentration. The introduction of a moving bed would allow the frosted region of the bed to remain stationary inside the column and thus the boundary conditions within the column will also remain stationary in the bed.

The energy balance equations will be affected by the introduction of a moving bed as the boundary conditions for the energy equation would include the entire column as opposed to just the frost front. The packed bed energy equations take into account the change of temperature over time and across the depth of the bed due to the advancement of the frost front within the column, whereas instead the moving bed energy balance would simplify the overall energy balance equation by replacing the differential equations with a static temperature gradient. This change would mainly be due to the moving bed introducing fresh bed material to the frosted region, which would maintain the thermal equilibrium within the frosted region of the bed.

Under fixed packed bed conditions, the frost front advances as the available cooling duty in the packed bed decreases over time. The bed material in the capture column has a finite amount of cooling duty that can be provided to the gas phase, the total cooling duty provided when the entire mass of bed material reaches the CO_2 desublimation temperature. As cooling duty is provided to the gas phase the CO_2 desublimes as a frost, CO_2 will continue to desublime as long as there is sufficient cooling from the packed bed material. The moving bed allows fresh bed material to replace frosted bed material within the capture column, providing extra cooling duty. When the rate of cooling duty added to the capture column (Q_{s+}) is in equilibrium with the rate of cooling duty required by the gas, the frost front should be in equilibrium. As there is no net loss in available cooling duty in the packed bed.

$$Q_{s+} = \dot{m}_s c_{ps} dT \tag{82}$$

$$Q_{s+} = Q_g \tag{83}$$

The cooling duty added to the column would have to be equal to the cooling duty required to desublime introduced CO_2 in order to create a thermal equilibrium. If the added cooling duty from bed material in insufficient, the frost front will continue to advance through the column at a slower frost front velocity. If the cooling duty added is in excess of what is required then the bed material is not fully saturated with frost, meaning cooling duty is being wasted and the frosted region within the bed material is expected to recede. The flow of bed material would therefore need to be set in order to maintain no net change in available cooling duty in the capture column. When this is achieved, then

the capture column would continue to desublime CO_2 frost without requiring a regeneration step within the capture column.

In an ideal case, the moving bed ensures no net cooling duty within the column is lost. Which is a result of the frost front velocity also approaching zero. If the moving bed flow rate is insufficient to offset the cooling duty lost by the bed due to heat transfer, then the temperature profiles shown in figure 4.7 should experience a delay in reaching the temperature plateau depending on how much the moving bed offsets the loss of available cooling duty.

For the profile in figure 4.6 the required cooling duty for the flow of CO_2 gas to desublime was approximately 230 J/s, so applying a moving bed so that the cooling duty added (Q_{s+}) approaches 230 would delay the temperature rise.

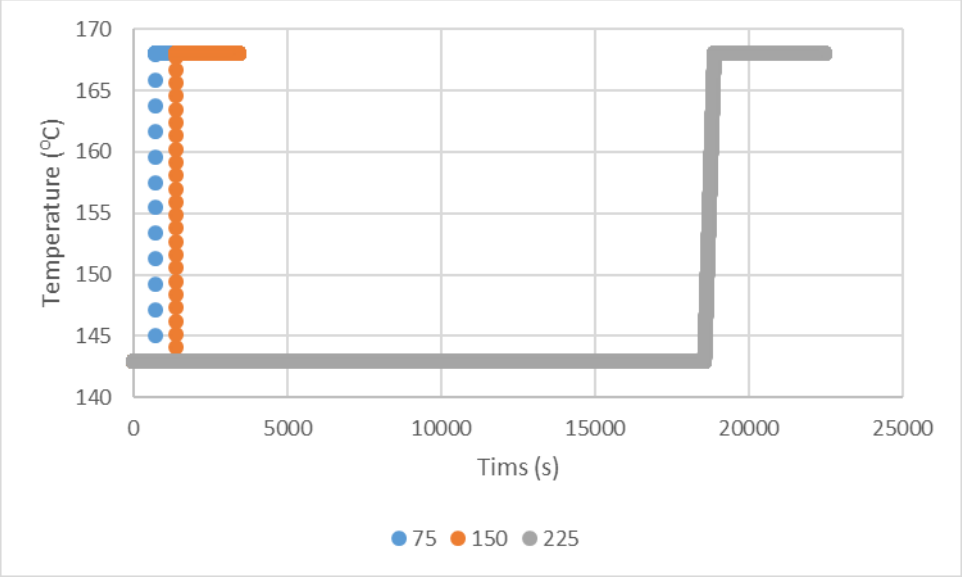

Figure 4.7 Temperature profiles for 250mm bed depth capture column for moving bed supplying differing values for Q_{s+}.

As figure 4.7 shows, the closer the bed material flow rate is able to offset the loss of cooling duty. The available time window for the capture step becomes larger before the capture column is saturated with frost and requires regeneration.

The desublimation of CO_2 should not be affected significantly by the introduction of the moving bed, the frost front should develop but not accumulate throughout the capture step. The moving bed may affect the availability of the nucleation zones for CO_2 in the capture column which may reduce the rate of CO_2 desublimation.

Conclusions

Results from the theoretical equations described in the literature provide acceptable results that align well with preliminary experimental results for frost front velocity profiles. This gives confidence that the capture column is working as designed.

Certain theoretical results have been pre-emptively compared with experimental results that are discussed in further detail in the next chapter. The results from the theoretical modelling chapter will further be compared with experimental results.

Chapter 5: Experimentation of fixed packed bed

Introduction

The theoretical modelling chapter adapts the available knowledge in the current literature to the design of the purpose built rig. The trends in frost front velocity that have been determined by the theory accurately match the results from the experimental work that have been conducted over the course of the PhD.

This chapter focuses on the experimental work performed under fixed packed bed conditions, assessing the frost front velocity with varying gas flow rates, CO_2 gas concentrations and bed materials. This chapter also provides comparisons between the experimental work and theoretical work both collected in the previous chapter in this thesis and theoretical work from the wider literature. As well as providing the necessary fundamental work for the advancement of experimental results towards the moving bed case.

5.1. Testing for fluidisation within packed bed material

Pressure drop would have an effect on the heat transfer performance of a packed bed, more so if the pressure drop is great enough to cause fluidisation within sections of the bed. Since pressure drop is dependent on the flow of gas through the bed, measuring the pressure drop across the bed was done by measuring pressure over a range of flow rates.

Figure 5.1 shows the results of the pressure drop experiments. The points show the experimental data with the solid line being the pressure drop prediction using equation (16) shown in chapter 2.3.1. It can be seen from the graph that increasing the gas flow rate results in an increased pressure drop across the column. Furthermore, the relationship between the gas flow rate and the pressure drop recorded follows closely to models found in the literature.

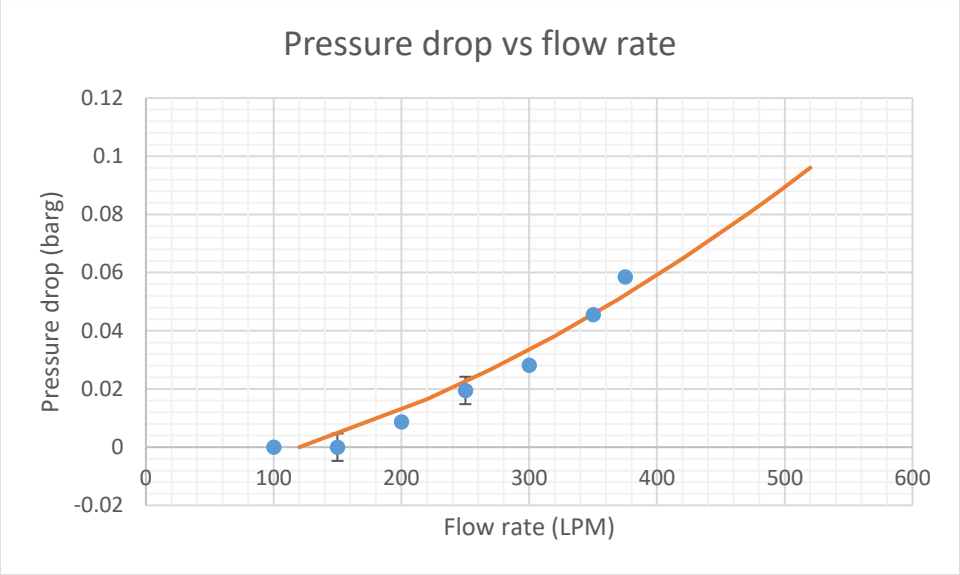

Figure 5.1. Pressure drop across packed bed material for varying flow rates. Blue points – experimental results, orange line – theoretical model prediction.

Since the experimental points follow closely the predicted line it would not seem that fluidisation is occurring, furthermore it could be observed that there was no evidence of local fluidisation near the gas injector. This evidence demonstrated that fluidisation would not occur during later experiments, there was no sign of fluidisation for gas flow rates up to 400LPM and further experiments would not subject the bed material to flow rates above 200LPM.

It should be noted that although the bed material does not experience fluidisation, the bed material does bounce quite significantly when dropped from a height. This could lead to complications in a moving bed system, designing the moving bed to not be dropped from significant heights would reduce the effect of the bouncing particles.

Since the bed material does not fluidise heat transfer between gas and the bed material should be stable and predictable. Further experimentation is required to understand the value of the heat transfer coefficient. Knowing the heat transfer coefficient will help to understand the nature of how heat transfer occurs within the bed material.

5.2 Calculating heat transfer coefficient of packed bed material

As stated previously, calculating the heat transfer coefficient between the bed material and a gas with a relatively simple experiment would provide help in designing the cryogenic capture column.

The main unknown in calculating the heat transfer coefficient is knowing what the temperature of the gas inside the bed material is. Due to the predicted heat transfer within the column being very high, it was expected that most of the heat transfer occurs across a small section of the bed. Thermocouples

were placed within the Perspex heat transfer column with one thermocouple in particular having a small covering over the end to prevent bed material from directly coming into contact with the thermocouple. The temperature difference between the covered thermocouple and another thermocouple of the same bed depth would allow the temperature approach to be measured.

It had been noticed that most heat transfer occurs over 5mm of bed material. This was therefore assumed to be the depth of the temperature gradient. Two thermocouples including the shrouded thermocouple were placed 5mm above the gas injector which allowed the heat transfer coefficient to be derived. The heat transfer coefficient is shown in table 5.1.

Table 5.1. Heat transfer experimental results from updated procedure.

Heat transfer coefficient (W/m^2K)	Uncertainty
148	$\pm$28

The results from these experiments give a clear temperature difference between the temperature of the bed material and the gas within the packed bed. This meant less uncertainty in the calculation of heat transfer coefficient in comparison to the previous method of estimating the temperature of the bulk gas phase found in appendix B. This previous method of assessing heat transfer did not use a shroud covered thermocouple, as a result the temperature difference between the gas phase and bed material was estimated as 1^oC, 2^oC and 5^oC. The use of a shroud covered thermocouple allows a more accurate estimate of the temperature difference between the gas and bed material.

Given that most heat transfer occurred across just 5mm of bed material, the heat transfer coefficient gave insight into the heat transfer of the packed bed column before advancing to cryogenic experiments. Using the results for heat transfer coefficient, the cryogenic rig was designed. The next stage of experiments in designing the moving cryogenic packed bed was understanding the behaviour of a fixed packed bed, which would both act as an important base to design the moving bed from and as a reference case to compare data from the later moving bed experiments with.

5.3 Cryogenic experiments of cooling column behaviour

The cryogenic experimental work was set out to establish two things. Firstly, establish how fast the frost advances through the column under a range of different conditions, so that the moving bed can be designed to match the rate of frost advance and establish an equilibrium. Secondly, to give a reference to compare the later moving bed experimental work with. Since the design of packed beds and moving packed beds is largely empirical, it is difficult to compare this work with the literature;

therefore collecting data regarding the fixed packed bed behaviour is required in order to have the clearest understanding of moving bed behaviour.

Initial cryogenic experiments focused on feeding cooled nitrogen gas into the packed bed column to see how the column cooled down. Figure 5.3 shows the raw temperature results from the thermocouples inside the column in place at set distances above the gas injector at the bottom of the column. The 5mm gas thermocouple has a small covering over the end to prevent direct contact between the bed material and the thermocouple. Which should highlight the difference in temperature between the gas and the bed material in the column. The high heat transfer coefficient should mean that the temperature difference between the gas and bed material is very small.

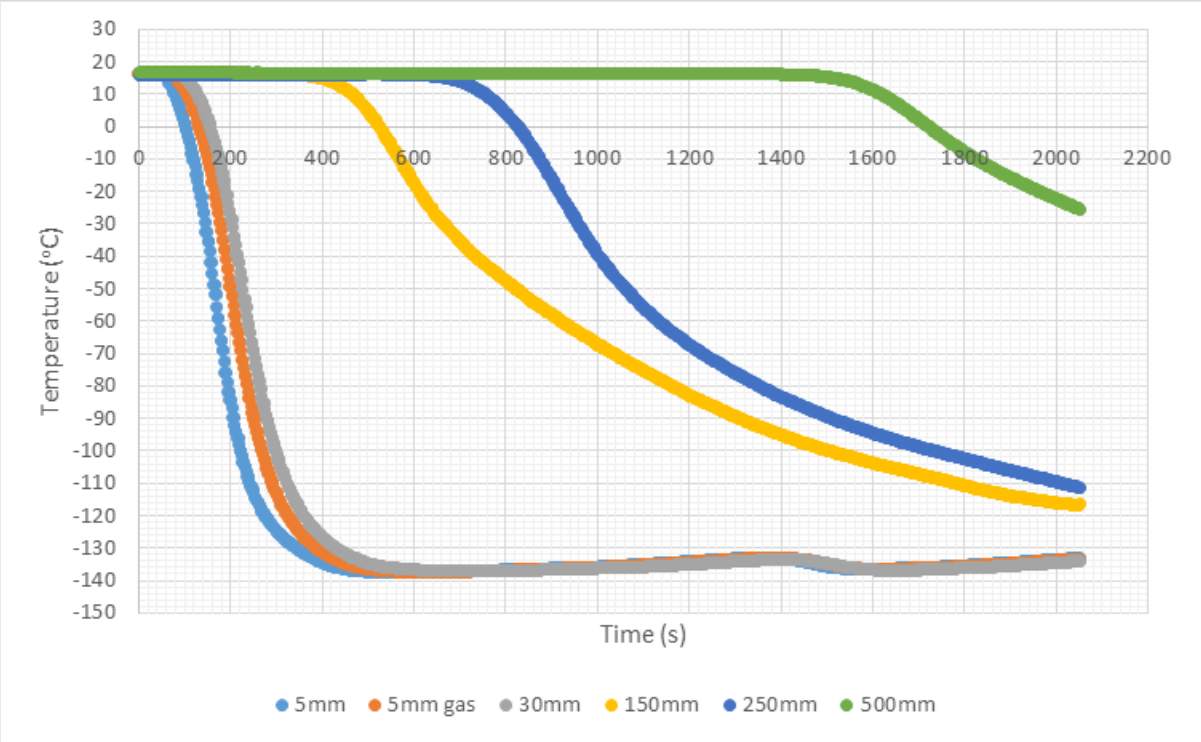

Figure 5.3. Temperature profiles from cryogenic cooling experiments.

The bed material close to the injector responds quickly to the introduction of the cold gas stream, however the thermocouples further away from the point of gas injection show a shallower gradient and less heat transfer occurring. The outcome of these results means that increasing the length of the cooling column leads to a much greater increase in time taken for the column to reach the desired temperature. Reduced heat transfer efficiency further away from the gas injector means scale up of this technology would be difficult. Scale up would require the increase of bed area close to the gas injector, meaning that rather than increasing the height of the capture column, increasing the diameter of the column would be key to scale up.

With the nature of cooling within the column better understood, experiments regarding the development of frost within the packed bed column was conducted.

5.4 Determining frost front velocity

The capture cycle of a cryogenic capture column causes CO_2 frost to desublime and form a frost on the heat transfer surface, due to the high heat transfer available in the packed bed column CO_2 frost will form very quickly within the bed. Over time the available surface area on bed material close to the gas injector will saturate with frost and the frosted region will begin to advance through the bed until the bed is fully saturated with frost. The frost front velocity shows how fast the capture column is becoming saturated with frost. The frost front velocity is important to the design of a moving bed as the moving bed must be set in order to balance the capture and removal rates of CO_2 frost. The frost front velocity would have to be stable and predictable under experimental conditions in order to allow a moving bed design to prevent excessive build-up of frost.

Due to the appearance of frost, it is expected that the temperature profiles would steadily increase as frost began to form and then plateau at a stable temperature (as shown in Figure 5.4ai), the temperature CO_2 desublimes at under the specified conditions, as the frost front had fully developed at that point. The appearance of these plateaus would indicate that the frost front is moving through the packed bed. This general trend of plateaus forming and temperatures of CO_2 desublimtation would be in agreement with similar results found in the literature (Eide et al., 2005; Tuinier et al., 2010).

Ai)

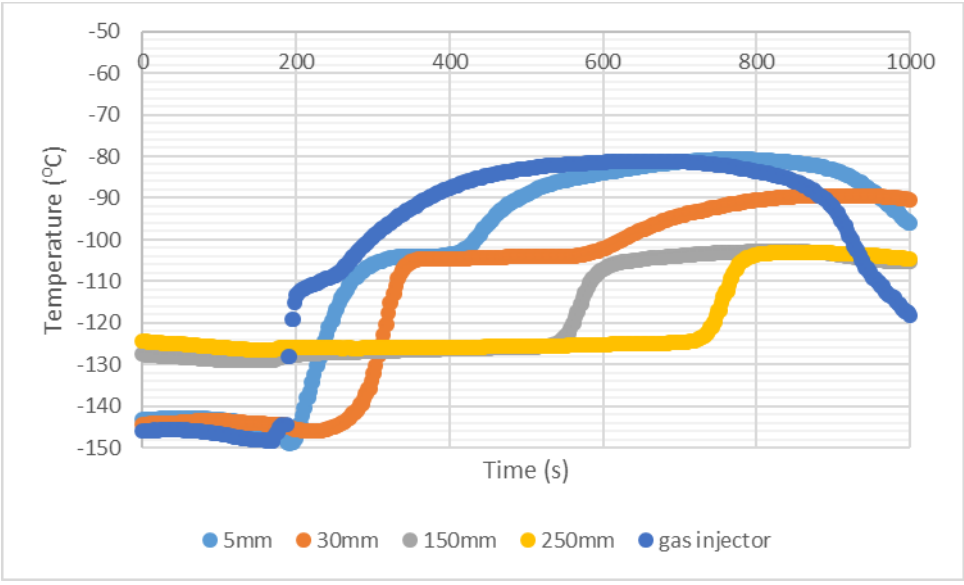

Aii)

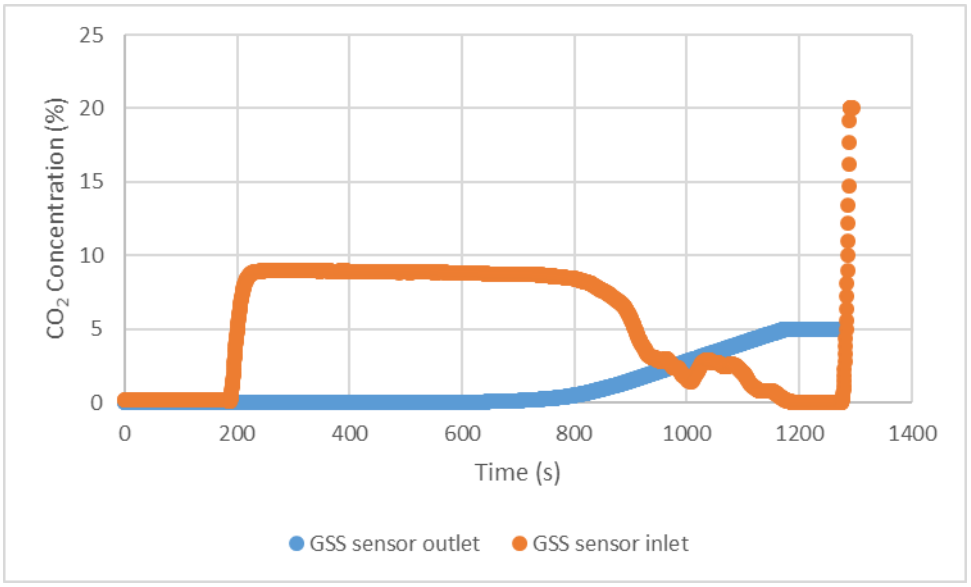
25
20
15
10
5
0
CO_2 Concentration (%)
0
200
400
600
800
1000
1200
1400
Time (s)
GSS sensor outlet
GSS sensor inlet

Bi)

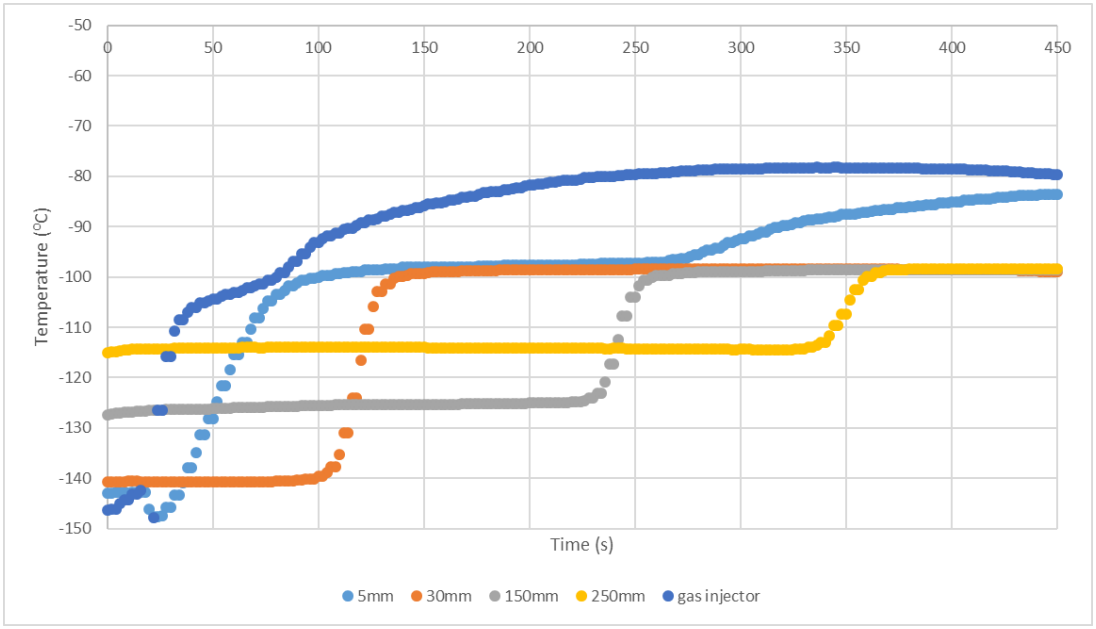
-50
-60
-70
-80
-90
-100
-110
-120
-130
-140
-150
Temperature (°C)
0
50
100
150
200
250
300
350
400
450
Time (s)
5mm
30mm
150mm
250mm
gas injector

Bii)

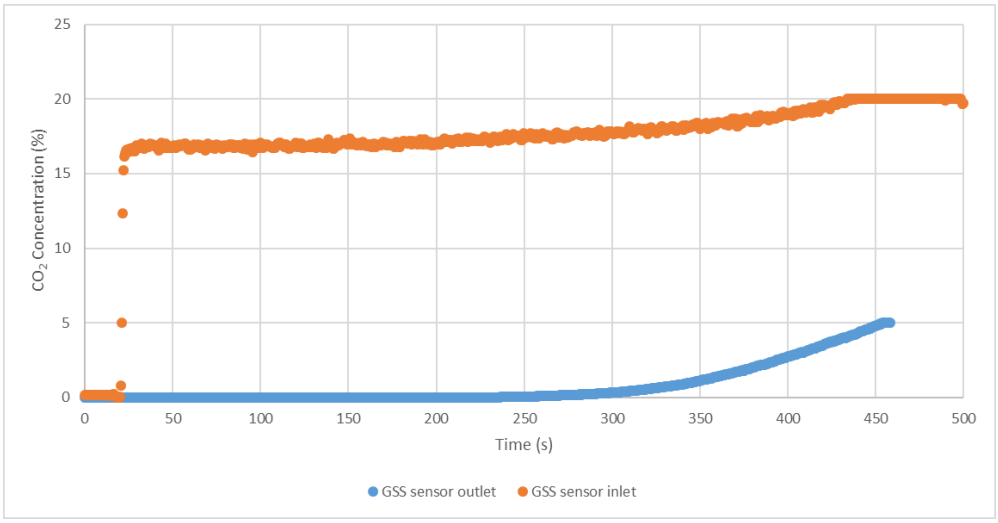
25
20
15
10
5
0
CO_2 Concentration (%)
0
50
100
150
200
250
300
350
400
450
500
Time (s)
GSS sensor outlet
GSS sensor inlet

ci)

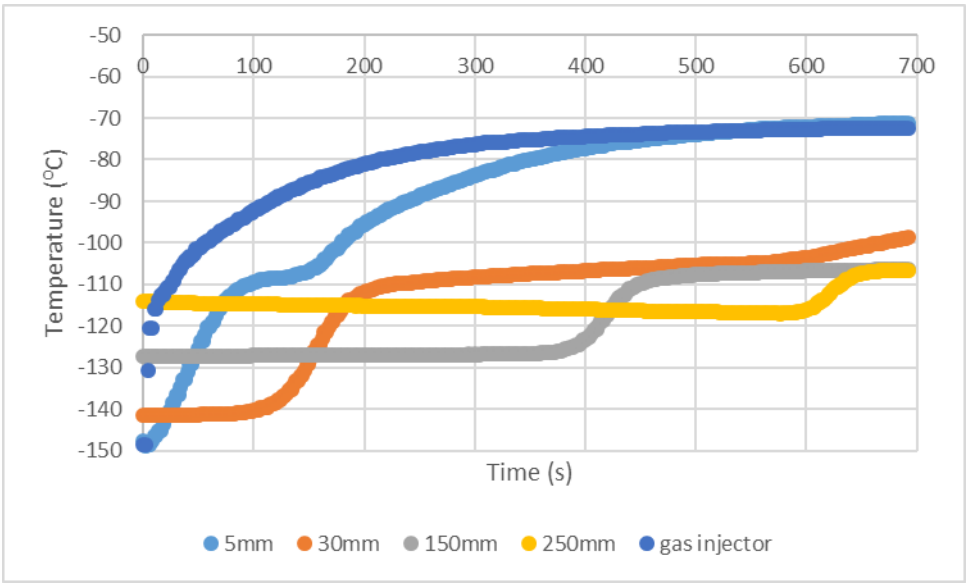

cii)

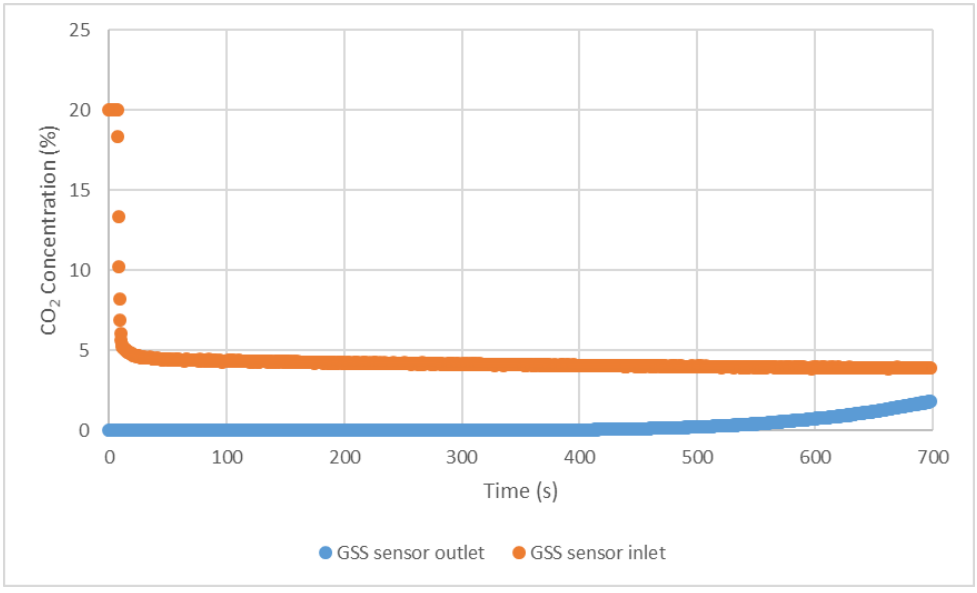

Figure 5.4. Temperature readings and CO_2 sensor measurements. ai) temperature profile 100LPM 8% CO_2 aii) CO_2 sensor measurements 100LPM 8% CO_2 bi) temperature profiles 100LPM 18% CO_2 bii) CO_2 sensor measurements 100LPM 18% CO_2 ci) temperature profile 100LPM 4% CO_2 experiment cii) CO_2 sensor measurements 100LPM 4% CO_2.

Figure 5.4 show examples of the experimental results of temperature profiles and CO_2 sensor measurements with differing CO_2 concentrations. The temperature profiles for varying gas flow rates can be found in appendix C. CO_2 outlet refers to the CO_2 concentration measured by the sensor leaving the column and CO_2 inlet refers to the concentration of CO_2 in the gas fed into the capture column. The frost front velocity is measured by judging from the temperature profiles how far the frost front has advanced up the column over time. The expected plateaus are easily identified from the graphs and can be seen to occur at different temperatures depending on the concentration of CO_2 present in the binary gas mixture. The results from the CO_2 measurements show the effectiveness of the CO_2

capture column by understanding the difference in CO_2 concentration (v/v) before and after the capture column.

The CO_2 concentration of the gas leaving the column is very low at first, in most cases the CO_2 concentration at the outlet is below the level of detection for the CO_2 sensor. The CO_2 sensors show that the cooled bed is causing CO_2 to desublime onto the packed bed, the CO_2 sensor at the outlet of the column did not detect CO_2 for most of the runs until the frost front approaches the 250mm mark. Indicating that the cooling column is able to capture CO_2 until the saturation point where no more frost can be formed onto the surface of the bed material. This is supported by evidence where samples of bed material were collected after the experiment was completed and measured with the same CO_2 sensor, over time the sensor would detect CO_2 concentrations exceeding the upper detection limit of the sensor. The CO_2 concentration of the gas flowing into the column slowly decreases or increases over time. This is believed to be the effect of CO_2 frost starting to build up within the pipeline or over the gas injector restricting the flow of mixed gas into the column.

Temperature results were then compared with results frost front velocity results from literature. Tuinier (2011) shows in figure 2.17 temperature profiles that would be expected from similar fixed packed bed experiments. Tuinier's results show the temperature profile across the entire column at specified times whereas results in this chapter record temperature profiles with time on the x-axis. However comparisons can still be made. The experimental results both show plateaus at roughly similar temperatures roughly -95^{o}C and -100^{o}C for Tuinier et al.'s results for 20% and 10% CO_2 respectively and roughly -97^{o}C and -105^{o}C from this work for 18% and 8% CO_2 results respectively, this gives confidence that the plateaus are indicative of frost formation.

The experimental runs individually present very clear isotherms as the frost front advances up the column. The point at which the isotherm appears is considered to be the point when the frost front has advanced to that distance within the column. A common occurrence among most experimental runs is the destabilisation of these isotherms close to the injector before the frost front has advanced 250mm up the column.

The CO_2 sensors show that the cooled bed is causing CO_2 to desublime onto the packed bed, the CO_2 sensor at the outlet of the column did not detect CO_2 for most of the runs until the frost front approaches the 250mm mark. Indicating that the cooling column is able to capture CO_2 until the saturation point where no more frost can be formed onto the surface of the bed material. This is supported by evidence where samples of bed material were collected after the experiment was completed and measured with the same CO_2 sensor, over time the sensor would detect CO_2 concentrations exceeding the upper detection limit of the sensor. The CO_2 sensor measuring the

concentration of the gas flowing into the column slowly decreases or increases over time, this occurs at the same time that the pressure gauge measuring the pressure of the gas flow starts to rise slowly and the rotameters measuring flow slowly fall throughout the experiment. This is believed to be the effect of CO_2 frost starting to build up within the pipeline or over the gas injector restricting the flow of mixed gas into the column.

Under repeated experiments, the frost front velocity was measured as described in the methodology chapter. The results for the frost front velocity with varying CO_2 concentration and flue gas flow rate are shown in figure 5.5.

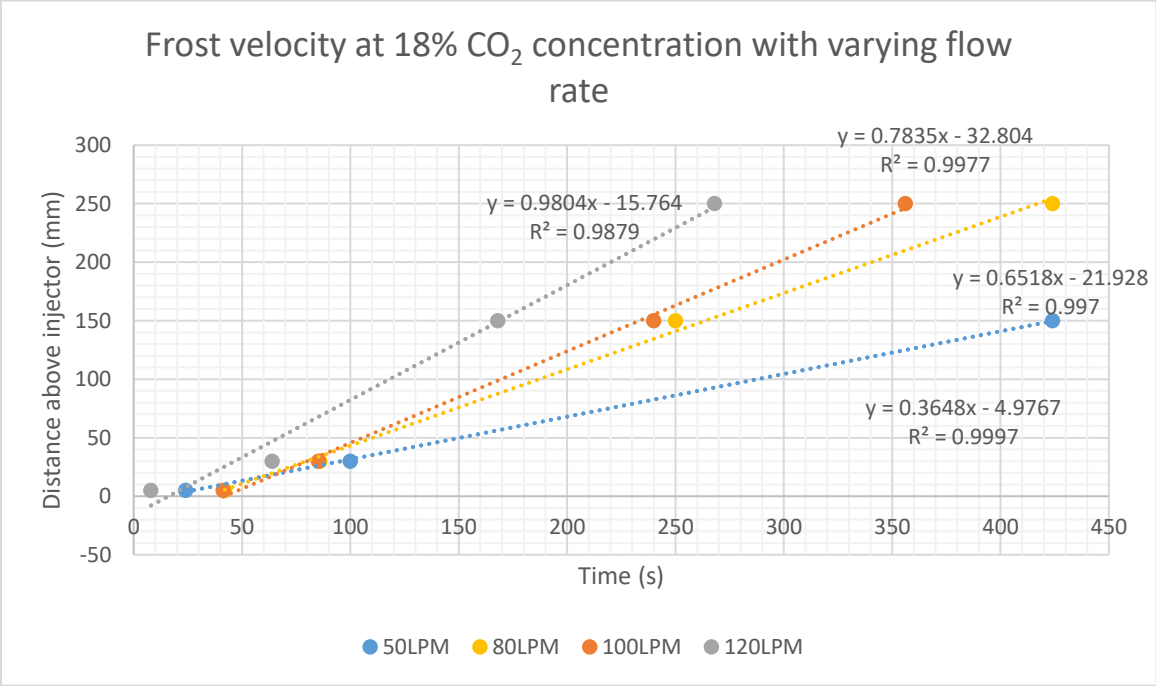

a)

b)

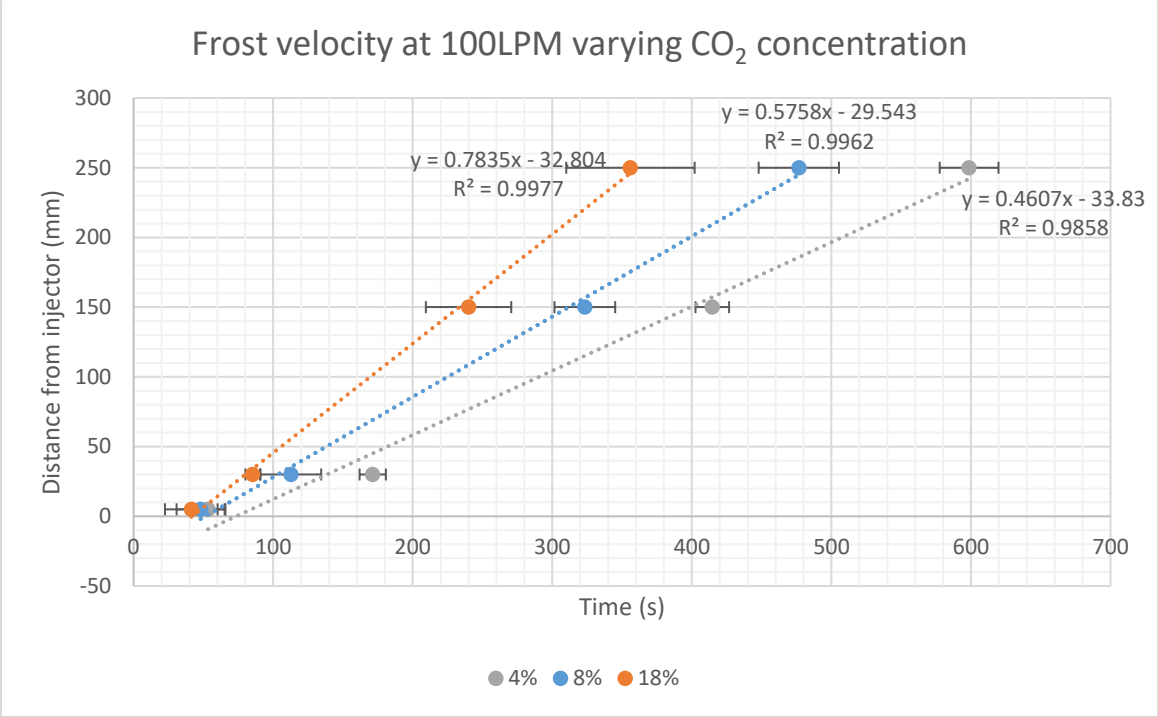

Figure 5.5. Frost front velocities under different conditions.

The frost front seems to advance to the specified distances in the column and the time at which the frost front advance to these locations seems to be constant throughout each experiment as can be seen by the linear trend line for each experiment in figure 4.5. The gradient for each line represents the velocity of the frost front within the column in mm/s. So the overall range of velocities under the conditions used are between 0.36-1 mm/s.

For most experimental runs, the frost advance seems to be slower from 5mm to 30mm, this is likely due to the frost either not being fully developed as per the frost growth stages described by Song et al (2013) or due to an effect of supercooling within the column. The trendlines shown do not intercept the axis at (0,0) which could also indicate supercooling phenomenon which would cause disturbance in the formation of frost at the early stages. However the deviation from how far the trendlines intercept the axis is mostly dependent on the assumption of what point in the experiment is t0. The data shown assumes that t0 is the point at which the gas being injected reached the temperature equivalent to the desublimation temperature of CO_2, the temperature that the isotherm forms at. If t0 is considered to be the point at which the frost front advances 5mm up the column then the trendlines will intercept the y axis much closer to (0,0). This would have to be taken into account for experimental runs utilising a moving bed, bed flow would have to be delayed until the frost front had fully developed.

The experimental results collected so far were used to develop calibration curves which were used to balance bed flow rates and frost front velocity. The calibration curves are shown, alongside the theoretically derived calibration curves from the previous chapter in figure 4.2, in figure 5.7.

a)

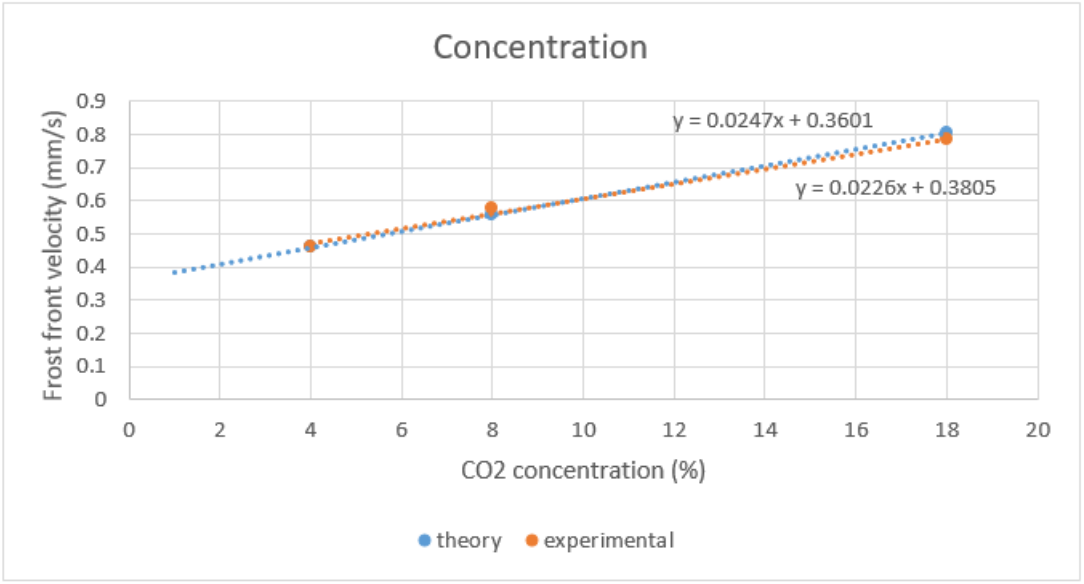

b)

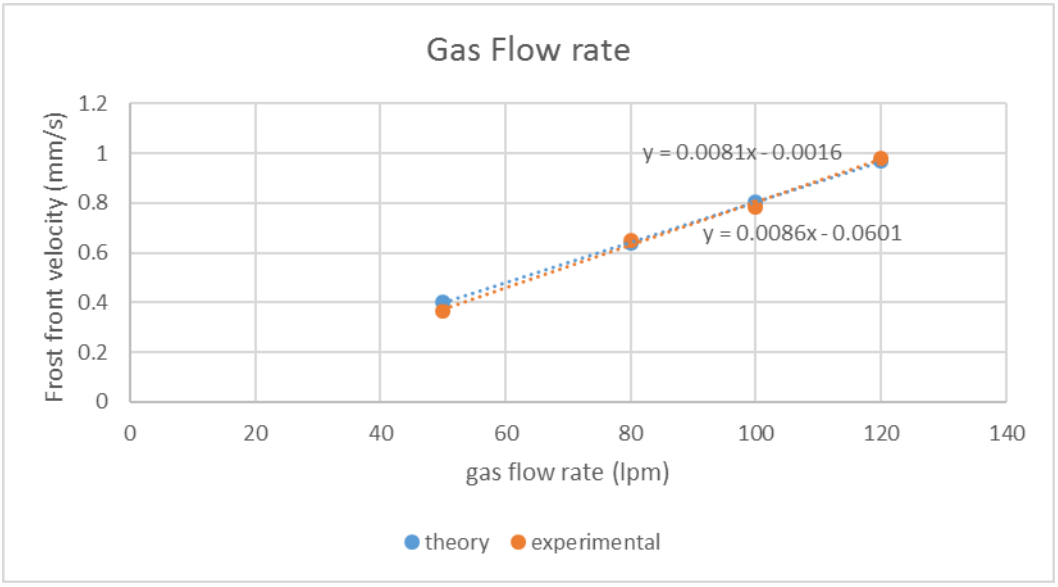

Figure 5.7. Variation of frost front velocity under different conditions a) calibration curve for CO_2 concentration b) calibration curve for gas flow rate.

The frost front velocities from the theoretical model match up very well with the experimental results for varying gas flow rates and CO_2 concentrations. The gas flow rate shows a linear relationship with the frost front velocity that closely intercepts the (0,0) point, and the effect of changing concentration on the frost front velocity similarly shows a linear relationship but does not intercept the y axis close to (0,0). The closely matching trends for the theoretical and experimental results support the

argument that the reason for this is the nitrogen concentration in the gas phase being responsible for wasted cooling duty from the bed material.

Comparing the results from this chapter with work from Tuinier et al. (Tuinier, 2011; Tuinier et al., 2010) requires an understanding of frost formation. The reason is that the experimental set up between the two sets of experimental work varies in terms of flow rates, capture column dimensions and packing material. Estimating frost front velocity from Tuinier et al.'s work (Tuinier et al., 2010) (figure 5) at 1.36 mm/s, involved converting this to an equivalent frost front velocity for this work's rig at 100 LPM, 18% CO_2 through conversion factors of heat transfer.

$$Q = mc_p\Delta T \tag{82}$$

Given that the CO_2 frost will form at roughly the same temperature for both 20% and 18% CO_2 concentrations and the starting temperature for Tuinier's bed material is roughly equivalent at -140^{o}C, it was considered that the temperature change and specific heat capacity of the gas should be the same in both experiments as they are similar in composition; however the bed material is of a different density and diameter, along with a larger bed diameter the mass of bed material in this work is roughly 10 times higher than in Tuinier's work. Along with a specific heat capacity 1.09 times higher in this work's metal bead compared to Tuinier's glass beads.

Comparing the flow rate of CO_2 into the capture columns, Tuinier's experimental set up feeds in 10 LPM gas containing 20% CO_2, converting to 100LPM 18% CO_2 means increasing the equilibrium temperature for the desublimation of CO_2 very slightly. This conversion become less accurate the larger the difference in concentration is as a result, as the difference in equilibrium temperature will have a larger impact on frost front velocity when the concentration difference in larger.

Table 5.2 Correction factors between thesis experimental work and Tuinier et al's work (2010).

Characteristic	Tuinier	Thesis	Conversion
Flow rate	10 LPM	100 LPM	10
CO_2 composition	20%	18%	0.9
Density of bed material	2547 kg/m^3	7850 kg/m^3	3.08
Specific heat capacity during capture step	365.4 J/kgK	400 J/kgK	1.09
Cross sectional area	0.00096 m^2	0.00407	4.23

The flow rate and composition would affect how fast the CO_2 would desublime onto the bed material, greater quantities of CO_2 desublimating would mean frost front would advance faster. The mass and heat capacity of the bed material would increase the amount of frost each m^2 of bed material can desublime before reaching equilibrium temperature. So the overall conversion rate estimate was considered to be:

$$\frac{d\dot{Q}dy}{d\rho\ dA\ dc_p} \tag{84}$$

The work from Tuinier was converted to match this work's 18% CO_2 experimental work at 120, 100, 80 and 50LPM. The estimate of frost front velocity from converting Tuinier's work was compared with experimental results in Table 5.3.

Table 5.3. Comparison between frost front velocities (mm/s) in experimental work and extrapolation from work by Tuinier et al (2011).

	120LPM	100LPM	80LPM	50LPM
Tuinier	1.0214	0.8514	0.6814	0.4257
This work	0.9854	0.7835	0.6843	0.3667
Difference (%)	4%	9%	1%	16%

Table 5.3 shows that the experimental results and estimates from literature is roughly comparable, it appears to be that estimating frost front velocity from altering gas flow rates is possible. To further test the comparisons between experimental work in this thesis and literature, the changes of frost front velocity by altering concentration must be compared. Tuinier's work includes experimental results considering 10% as well as 20% CO_2 (Tuinier, 2011). Interpreting data from Tuinier's work estimates frost front velocities of 0.8 and 1.4mm/s for 10% and 20% CO_2 respectively. Converting this data for frost front velocity for 100LPM 8% and 18% CO_2 gives frost front velocities 0.473 and 0.851mm/s respectively. Comparing 10% Tuinier and 8% thesis shows that the frost front velocity Tuinier's work would predict from conversion factor is 1.38 times higher than experimental results from this work.

a)

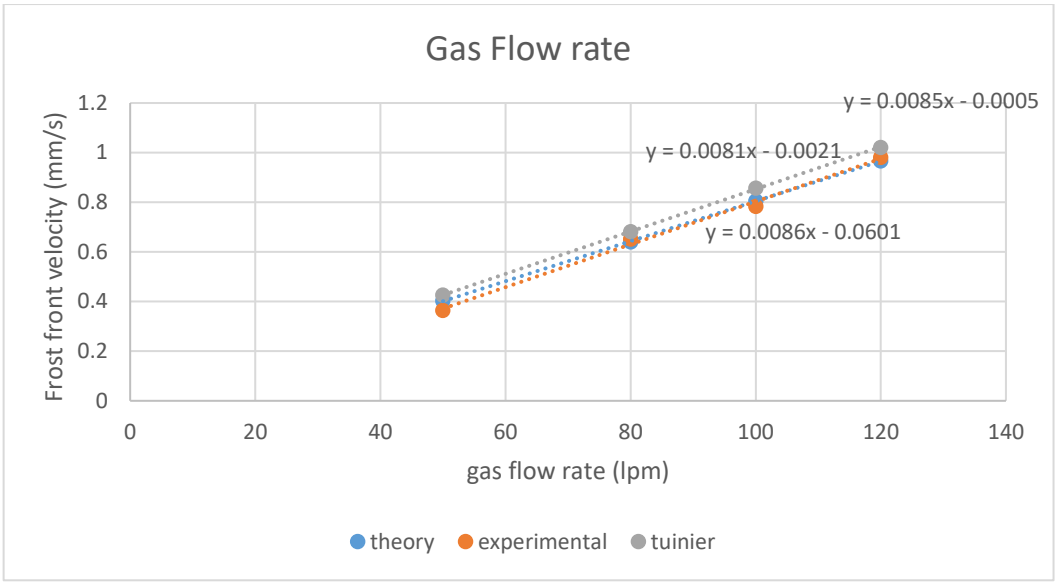

b)

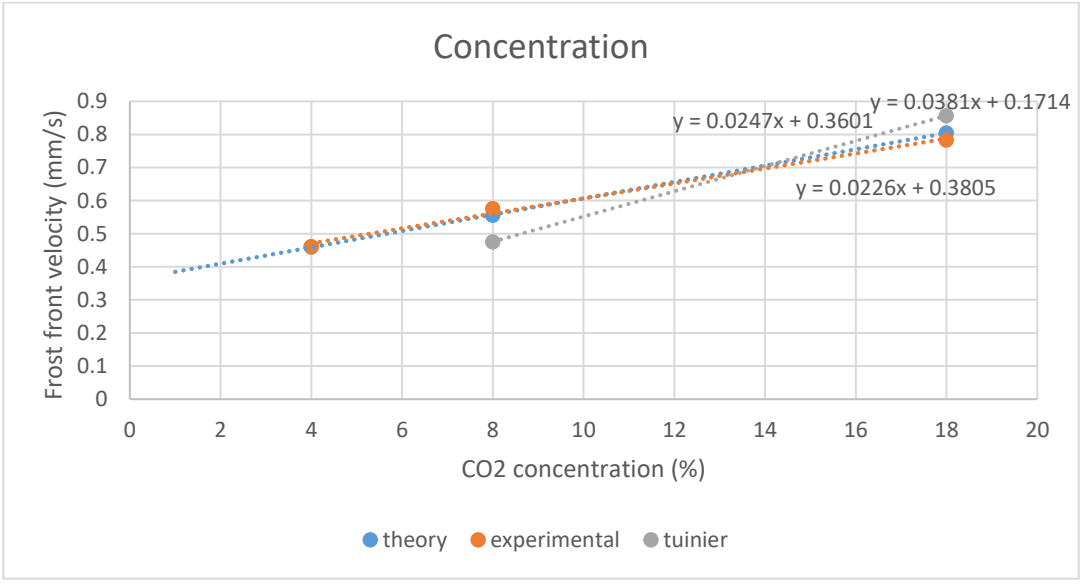

Figure 5.8. Comparative work between experimental results and estimates from Tuinier's work. a) comparative work on gas flow rates b) comparative work on CO_2 concentrations.

Comparing the results shows a similar trend between work in the literature and the work done in Figure 5.8a, however there is less reliability in comparisons between experimental and predictive work and the literature when changing concentration shown in Figure 5.8b. The comparisons show that it is possible to make a relatively simple comparison between different sets of experimental results as long as concentration of CO_2 in the flue gas and initial bed temperatures are similar. This method of using conversion factors to accommodate for discrepancies in CO_2 concentration are only suitable for relatively small changes in concentration, as altering the CO_2 concentration in the flue gas will alter the desublimation temperature of the CO_2, which then affects the temperature change of the bed material and gas phase through the capture column.

The experimental conditions for Tuinier et al.'s work can be incorporated into the theoretical frost front model in order to provide data for comparison. The theoretical model can predict the frost front velocity for a capture column similar to the one used by Tunier et al. which can then be converted to compare with results from this thesis. Figure 5.9 shows a comparison between the theoretical model's prediction for frost front velocity under different initial bed temperatures for both the capture column used in this project and used by Tunier et al.

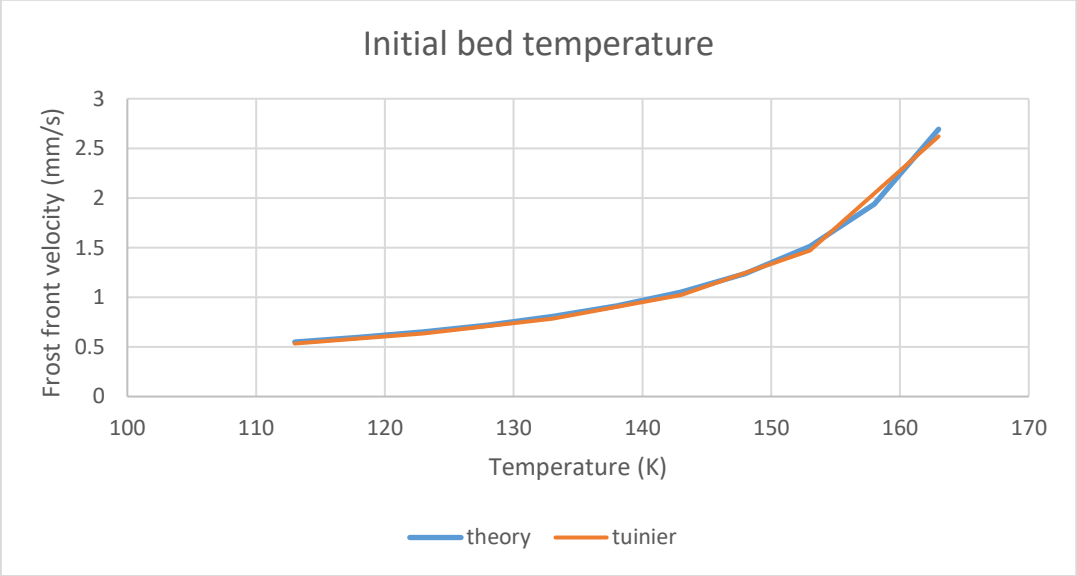

Figure 5.9. Comparisons between theoretical modelling of different capture column frost front velocities under different initial bed temperatures.

From the high level of agreement between the experimental results, theoretical modelling work and data from literature, the capture column is suitably validated. Experimental work on fixed packed bed can therefore be expanded in scope beyond the variation of gas flow rates and CO_2 concentrations and investigate different bed materials. Different bed materials were assessed for suitability based on density, specific heat capacity and bed material size, bed materials that had qualities similar in scale to the steel bed material should produce frost front velocity results comparable to the steel bed material.

Frost front velocity experiments were conducted using a high density ceramic bed material. The ceramic bed material has a more consistent spherical shape and size distribution in comparison to the steel bed material while still maintaining a comparable density and specific heat capacity. The physical properties of the steel and ceramic bed material that are expected to affect the frost front velocity are listed in table 5.1.

Table 5.1. Comparison between steel and ceramic bed material.

	Steel	Ceramic	Reference

Density (kg/m^3)	7850	5900	Steel supplier Pometon particles, Ceramic supplier Chemco beads (Tojo, Atake, Mori, & Yamamura, 1999)
Specific Heat Capacity during capture step (J/kgK)	400	420	
Particle Diameter (mm)	1.4-1.7	1.4-1.7	

The difference in the densities of the ceramic and steel bed material is expected to have an impact on the frost front velocity, the ceramic bed material has a lower available cooling duty which will increase the frost front velocity accordingly. The experimental comparisons between the ceramic and steel bed material are shown in figure 5.6 with simulated frost front velocities to compare with the given results.

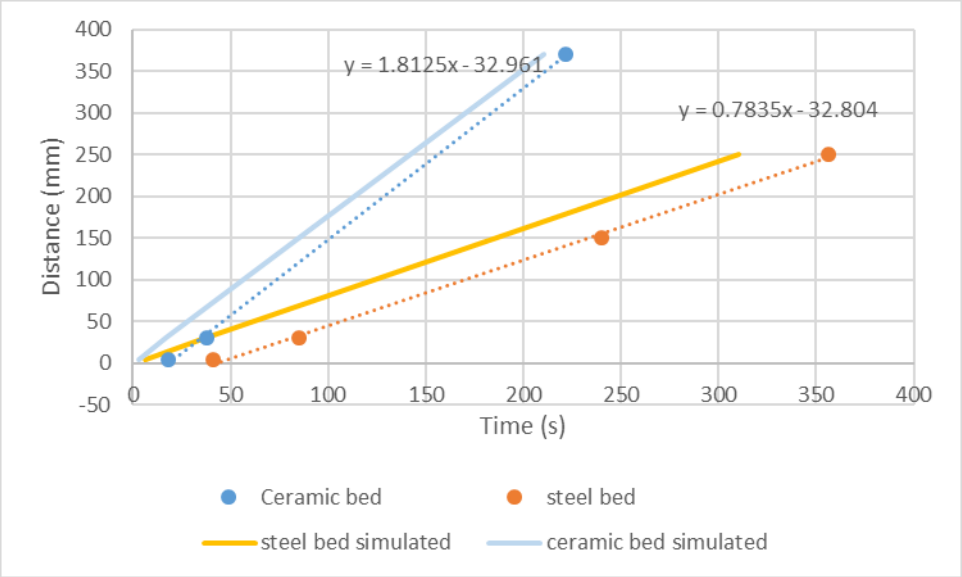

Figure 5.6. Comparison between ceramic and steel bed material 100LPM 18% CO_2.

The frost front velocities for the ceramic bed material and steel bed material match the trend lines of what the simulated frost front velocities predict, the major difference between the experimental and simulated lines is that the simulated lines are not taking any potential supercooling effects into account so they intercept the y axis at (0,0). Given the translational difference between the ceramic frost front velocities compared to the steel frost front velocities, it is likely that the frost is able to nucleate on the ceramic bed material more readily than on the steel bed.

These experimental results give confidence and provide a basis for the development of a moving bed to prevent the accumulation of frost using the gas flow rate calibration curve. Therefore, the experimental work in future stays at 18% CO_2 altering gas flow rate. Since the velocity of the frost front is very low, a hopper design to allow bed velocity to flow at the same speed would require an exit orifice small enough to cause arching. Therefore, a different design would have to be

implemented. The chosen design was a small screw conveyor that would be manufactured to provide the required column flow rate with a hopper design feeding into the conveyor.

Conclusions

The experimental work on the fixed bed behaviour of the capture column has been discussed in this chapter and has been compared with both the theoretical work from the previous chapter as well as information available in the literature.

The fixed bed experimental work has provided sufficient information about the behaviour of the packed bed column in order to progress the experimental work, by expanding the scope of the experimental work to start investigating the impact of the moving bed on frost formation within the column.

Chapter 6: Moving bed preparatory experiments

Introduction

The results from the experimental work focused on the fixed packed bed, discussed in the previous chapter, closely match the theoretically derived results. This provides confidence that the experimental rig is operating as intended and, given the predictability of the fixed packed bed results, provides a good basis for the moving bed experimental work.

The following chapter provides experimental results regarding moving packed bed scenarios. The chapter provides an explanation of the expected trends from temperature profiles in comparison to the temperature profiles observed in experiments from chapter 5, as well as discussing the results observed within this chapter.

6.1 Introducing the moving bed

Developing an understanding of the frost front velocity allows the design of a mechanism allowing bed material to flow at a matching speed to create an equilibrium. Since the bed velocity required was too small to achieve using a hopper design, a small screw conveyor was constructed and attached to the outlet of the column (shown in Figure 3.4). The conveyor was powered by a small motor with a variable RPM to allow adjustments in the bed flow in order to achieve equilibrium.

The moving bed experimental procedure, same as previously described in the methodology chapter, follows the same experimental procedure as in the previous cryogenic experiments with the exception that after the bed material is sufficiently cooled by the cooling gas, the screw conveyor is turned on and allowed to begin to shift bed material before the gas mixture is introduced.

It would be expected that even with the moving bed preventing the excessive build-up of CO_2 frost in the capture column, a frosted bed material region would still form in the column close to the injector. The CO_2 gas entering the column would flash freeze onto the bed material close to the injector. Temperature profiles from thermocouples above the frost region of the capture column are expected to stay relatively stable, temperature readings should not follow the same trend in theory as CO_2 should not be desublimating. Heat transfer may still occur but the gas flow above the frosted region should be CO_2 lean gas. Which would mean that the plateau that identifies the presence of CO_2 frost should not be present.

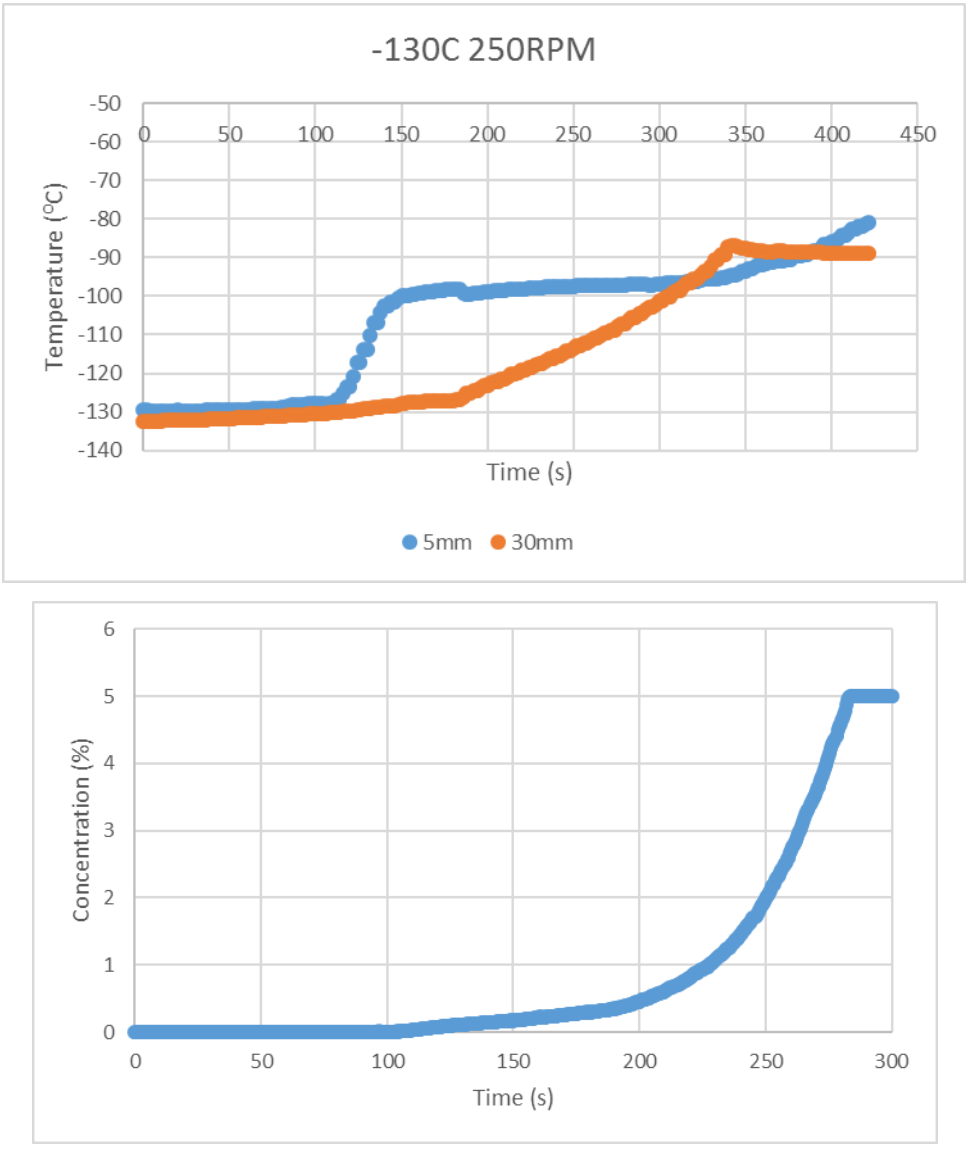

Figure 6.1. a) Thermocouple measurements from moving bed experiment b) CO_2 concentration measurements from moving bed experiment, initial bed temperature -130°C, 250RPM conveyor motor speed.

Figure 6.1 shows how the introduction of a moving bed affected the measured results from the cryogenic column. The 30mm thermocouple (orange data) was indicative of the temperature gradient of the bed after cooling. Due to the cooling gas being injected near the bottom of the column, the bed material further up the column is not cooled as substantially as bed material within a close proximity to the injector.

Compared to the typical experimental results shown in Chapter 5, results from figure 6.1a shows the 30mm thermocouple does not follow the fixed bed trend of plateauing shortly after the 5mm temperature profile, which indicates that the frost front was delayed in reaching the 30mm point or did not reach the 30mm point at all throughout the experiment. The 30mm thermocouple increases in temperature throughout the course of the experiment which was likely due to the falling bed material being cooled less substantially than bed material closer to the injector.

The CO_2 concentration measurements are different from results in Chapter 5, which showed results of a near zero concentration for CO_2 at the outlet of the injector until the column is saturated with frost. In contrast, figure 6.1b shows that there is a trace amount of CO_2 being detected shortly after CO_2 is being injected into the column. With the CO_2 concentration rising over time along with the temperature of the 30mm thermocouple.

To investigate this further, the outlet gas CO_2 composition was applied to the Span and Wagner (1996) equation of state for CO_2 desublimation (57) and the theoretical temperature profiles were compared to the measured temperature profiles from the thermocouples closer to the frost front. The theoretical temperature profiles were created by using equation (57) to calculate the temperature that corresponds to the CO_2 saturation pressure. Within the capture column the saturation pressure and partial pressure of CO_2 would be equivalent when the gas is sufficiently cooled, CO_2 will desublime out of the gas phase until the partial pressure of CO_2 is equivalent to the saturation pressure.

It was predicted that the theoretical temperature profile would follow a similar trend to the 5mm and 30mm moving bed temperature profiles. This is due to these thermocouples being located closest to the equilibrium frost front, temperatures at the frost front are expected to be within a few degrees of either the 5mm or 30mm thermocouple depending on whether the frost front reaches the 5mm thermocouple.

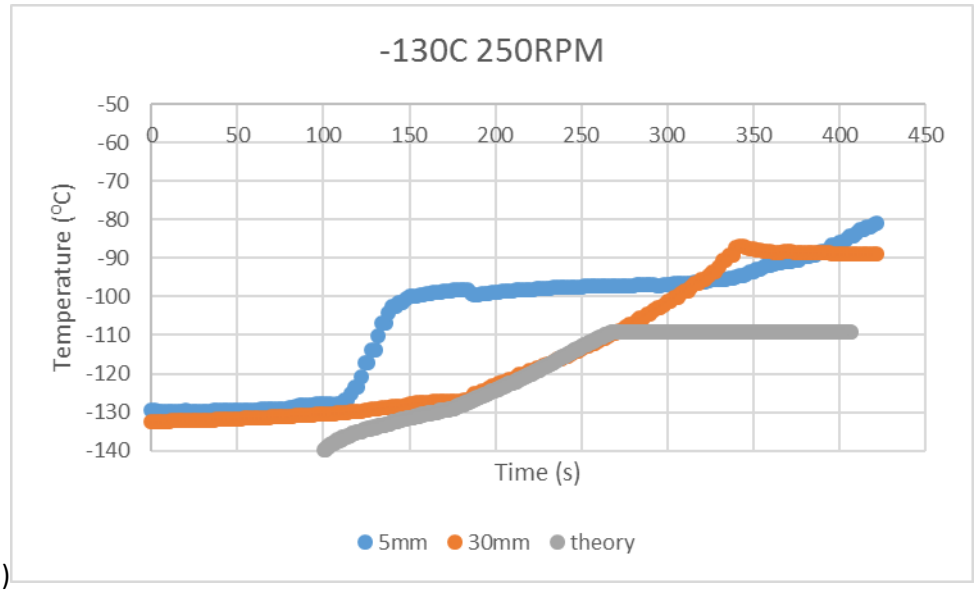
-130C 250RPM
-50
-60
-70
-80
-90
-100
-110
-120
-130
-140
0
50
100
150
200
250
300
350
400
450
Temperature (°C)
Time (s)
5mm
30mm
theory

a)

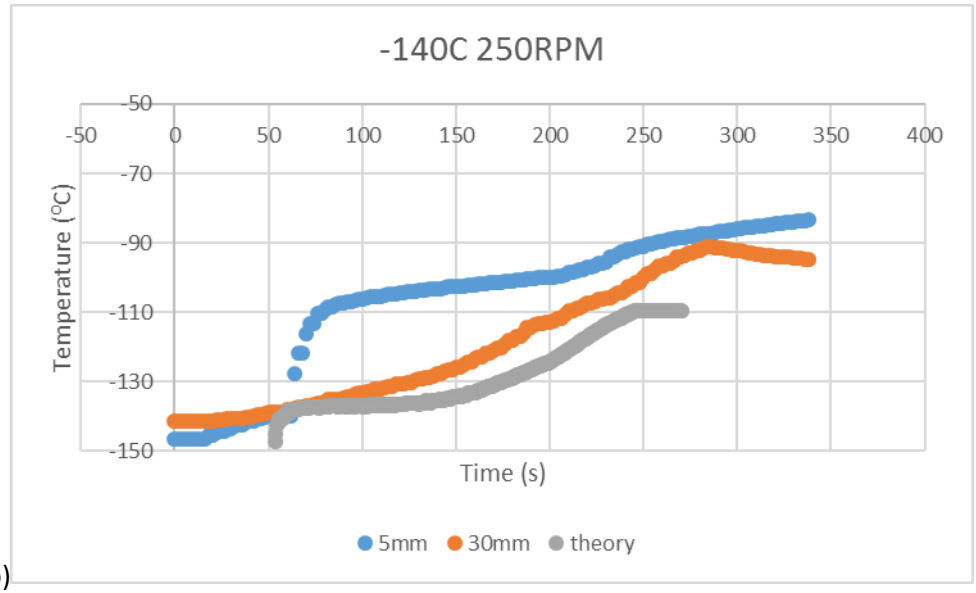
-140C 250RPM
-50
-70
-90
-110
-130
-150
-50
0
50
100
150
200
250
300
350
400
Temperature (°C)
Time (s)
5mm
30mm
theory

b)

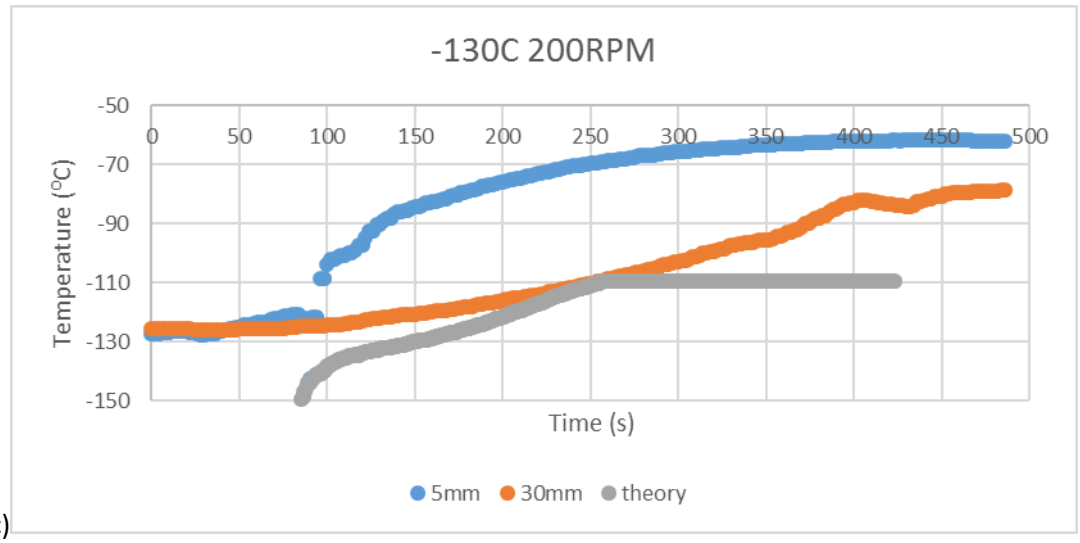
-130C 200RPM
-50
-70
-90
-110
-130
-150
0
50
100
150
200
250
300
350
400
450
500
Temperature (°C)
Time (s)
5mm
30mm
theory

c)

d)

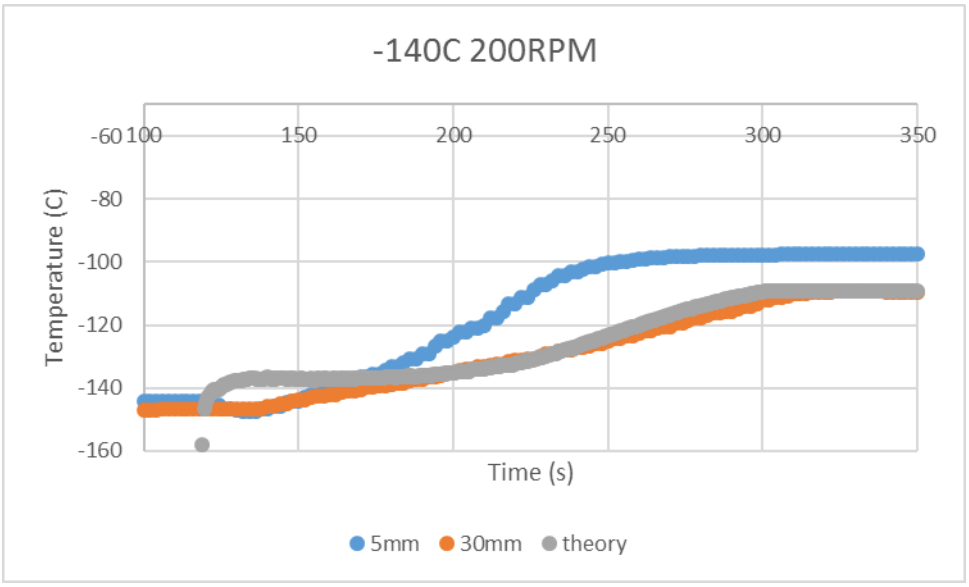

Figure 6.2. Comparison of temperature profiles with theoretical Span and Wagner (1996) model. a)-130C, 250rpm b) -140C, 250rpm c) -130C, 200rpm d) -140, 200rpm.

The theoretical temperature profiles in figure 6.2 show the temperature profiles calculated the Span and Wagner (1996) equation of state and CO_2 concentration results from the outlet gas sensor. Due to the nature of the equation of state, step changes in temperature at colder temperatures result in relatively low changes in CO_2 concentration, whereas step changes in temperature at higher changes result in larger changes in concentration. This explains the initial noise seen in the theoretical temperature profile.

From figure 6.2 it can be seen that the theoretical line roughly follows a similar trend as the 30mm thermocouple, therefore exhibiting qualities identified in moving bed temperature profiles. In most cases the theoretical temperature profile is slightly colder than the temperature profiles provided by the thermocouples. It is infeasible that moving bed temperature profiles would be colder than the theoretical line in practice as the theoretical line would estimate the saturated gas composition, a reduced temperature would force CO_2 to desublime and reduce the gas composition. The Span and Wagner (1996) equation of state shows a high level of precision for CO_2 sublimation pressures at relatively cold temperatures, meaning that the same magnitude of step change in measured CO_2 concentration can correspond to a relatively large change in temperature. A change in concentration of 0.1% to 0.3% v/v is a change in sublimation temperature from 137K to 143K whereas a change from 2% to 2.2% v/v is a temperature change from 156.5K to 157K. So at the early stages of the experiment, minor fluctuations in CO_2 concentration can have a notably large impact on the simulated temperature profile.

For the purpose of comparison, the theoretical temperature profile was constructed for the fixed bed experimental data. Which can be seen in figure 6.3. If the assumption that the temperature profile indicates the coldest temperature the gas could be is correct. Then the theoretical temperature profile would reflect that.

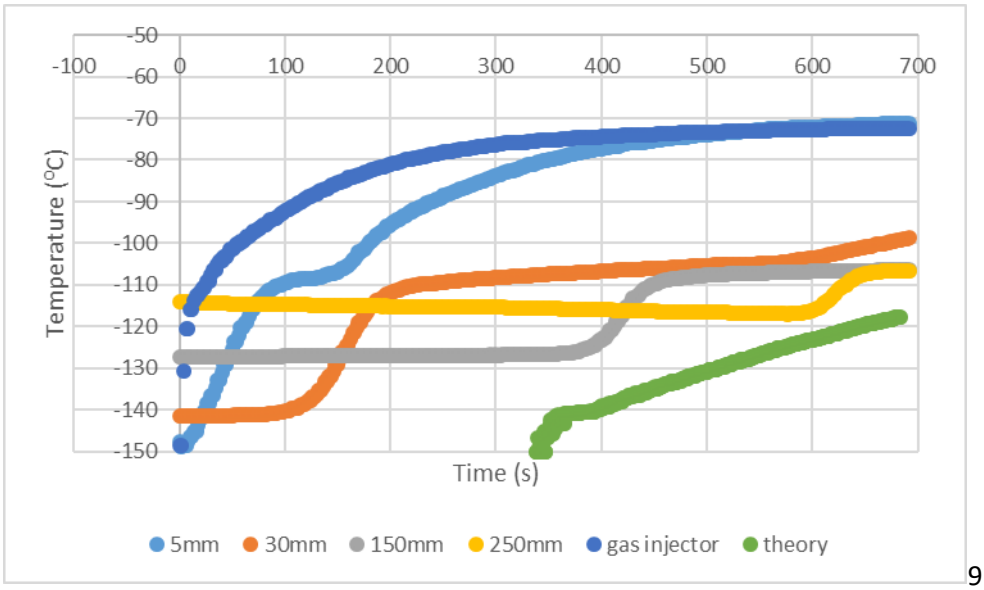

9

Figure 6.3. Fixed bed temperature profile with theoretical temperature profile (100LPM, 4% CO_2).

The theoretical temperature profile under fixed bed conditions confidently shows that for the majority of the experimental run, the theoretical temperature profile does not overtake any other temperature profiles. The theoretical temperature profile for the fixed packed bed results does not appear until after 300s, before this time the CO_2 sensor does not detect any CO_2 present in the sampled gas meaning the theoretical temperature profile cannot be constructed at this point. It is clear that the moving bed causes some level of instability of the frosted bed material region as the moving bed conditions show that CO_2 is detected for most of the experimental run time. The theoretical temperature profile is limited to a maximum value of -109°C due to the CO_2 sensor at the outlet recording a maximum of 5% CO_2. For the 4% CO_2 experiment it is most likely that if the experimental run were to continue after 700s, the theoretical temperature profile would eventually increase to -111°C where it would plateau due to saturation of the gas phase. In other words, the theoretical temperature profile should reach a plateau at the same temperature as the thermocouple plateaus. This would indicate that the capture column is fully saturated as the concentration of CO_2 entering and leaving the column is equivalent.

In an effort to eliminate the uncertainty in the results in figure 6.2, a new method of measuring CO_2 concentration near the frost front was constructed, as explained next.

6.2 Eliminating uncertainty in outlet gas CO_2 composition

For the new method of measuring CO_2 concentration near the frost front, a 6mm OD pipe was inserted into the capture column 30mm above the injector. The purpose of the pipe was to collect gas samples closer to the frost front boundary layer given reasonable assurance that the frost front could be controlled. A thermocouple was inserted inside the pipe in order to measure the temperature of the gas that passed through the pipe, being sheathed inside the pipe sheltered the thermocouple from interaction with the bed material.

In the new method of gas sampling there was an issue to be addressed. The temperature of the gas sample collected was colder than the gas being measured at the outlet. This led to erroneous results from the CO_2 sensor where the cold temperature would cause the sensor to record CO_2 compositions far higher than should be expected. Thus, a small heating unit was put in place to prevent the outlet GSS sensor chamber from becoming frosted up.

The new sensor arrangement was used to obtain CO_2 concentration results close to the frost front. The frost front is expected to be within the bed depth of 5mm to 30mm due to the results form figure 6.2 showing the theoretical temperature profile following the general trend of the 30mm thermocouple. The results from the new sensor arrangement were expected to be the temperature profile of the 30mm thermocouple sheathed inside the gas sampling pipe matching the temperature profile derived from the CO_2 outlet concentration more accurately than in the previous stage. Further experimental results for the new sampling method are performed under the same conditions to establish the repeatability of the updated gas sampling method, the graphical results from the other experiments can be found in appendix D.

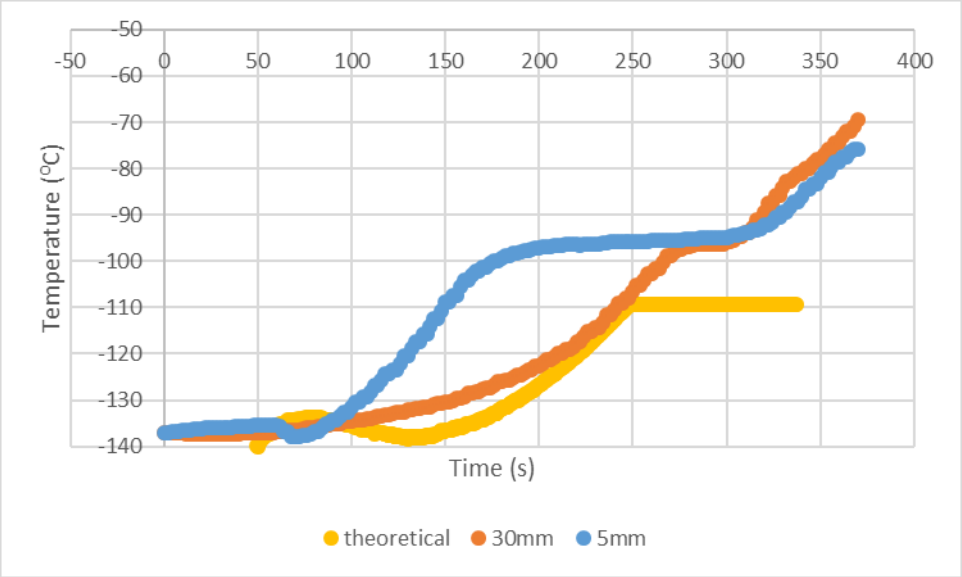

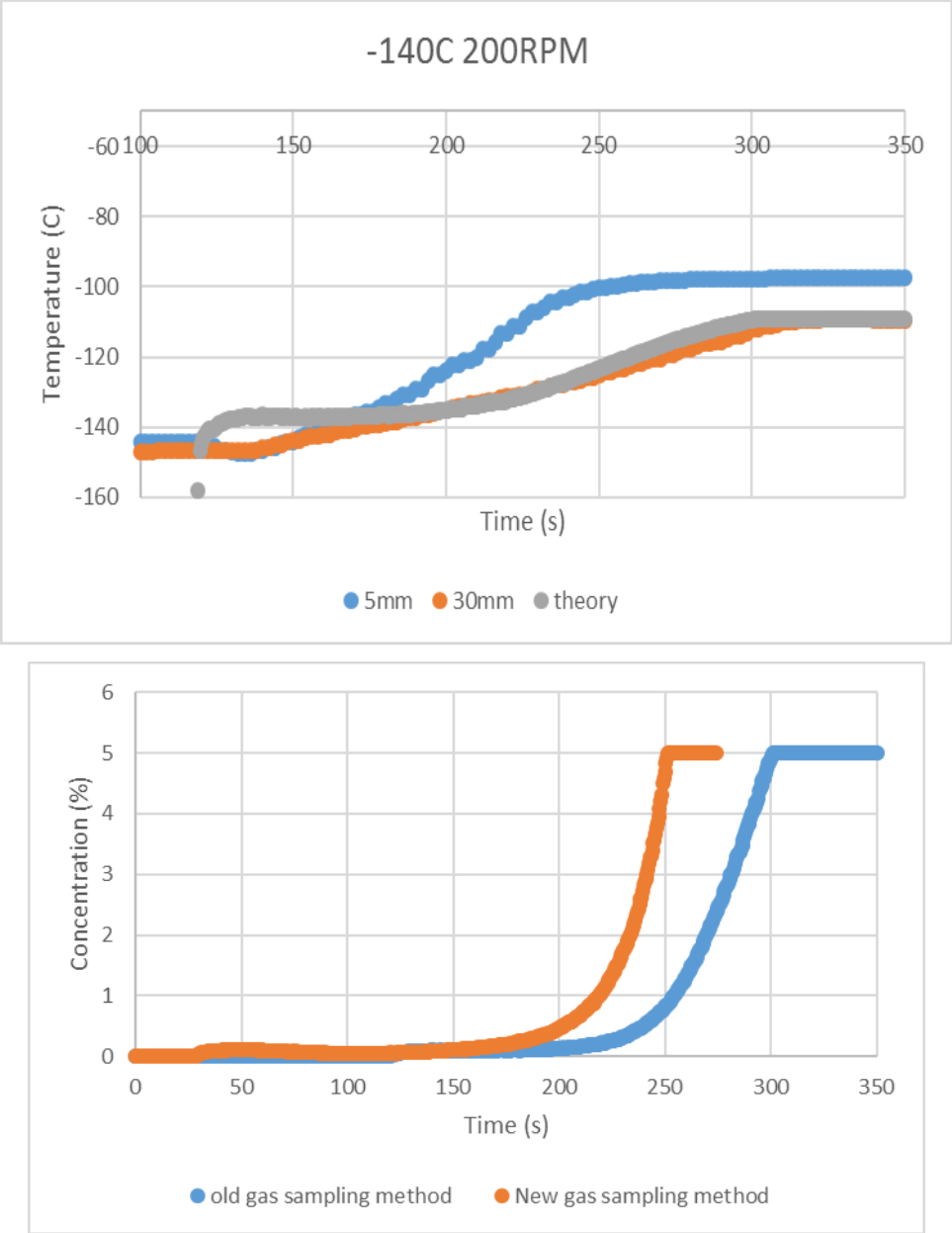

Figure 6.4. Comparison between theoretical and thermocouple temperature profiles. a) updated gas sampling method (-140°C 200RPM) b) previous gas sampling method (-140°C 200RPM) c) comparison of raw concentration readings from outlet CO_2 gas sensor.

The 30mm temperature profile in figure 6.4 represents the temperature of the thermocouple sheathed inside the 6mm OD pipe that the gas analysed by the sensor will pass through. The 30mm thermocouple measures the temperature of the gas being sampled by the CO_2 sensor and the gas passing through the bulk of the bed material.

The new gas sampling method gives a clear representation of the frost front boundary as well as providing context regarding the trace CO_2 being recorded by the outlet sensor. Figure 6.4 shows the

theoretical and sheathed 30mm temperature profiles being much more defined and comparable at the beginning and end of the experimental run. The theoretical temperature profile is consistently a few degrees colder than the temperature of the 30mm thermocouple outside of the beginning and ending section of the experiments. Which could show that the flue gas is not saturated with CO_2 when being recorded by the sensor, while still supporting the argument that the CO_2 concentration being recorded gives an approximate temperature of the gas at the equilibrium frost front which would be located near the 30mm point. The frost front still shows signs of instability in a moving bed due to the presence of CO_2 in the early stages of the capture step and the resulting spike in temperature early on in the temperature profile, the reasoning for this has not yet been determined.

The theoretical temperature profile shows a clear picture of conditions at the frost front and the relationship between the real and theoretical temperature profile of gas being measured close to the frost front. However, there are concerns that the process has not yet been fully understood. As seen by the region of instability at the early stages of the experiment and the temperature gradient within the column due to uneven cooling. The next stage of experiments involved updating the capture column itself with a second injector and allowing the capture step and cooling step to be performed simultaneously.

Conclusions

The experimental work involving the moving bed has been discussed in this chapter. Overall the general trends for the temperature profiles near the frost front appear to follow the expected trends, however there are greater discrepancies and uncertainty due to the transient nature of the experimental work.

Attempts to provide greater clarity to the experimental results were made by the alteration of the experimental methodology as well as a more focused display of results.

Chapter 7: Combining the capture and cooling step.

Introduction

Experimental results in the previous chapter focus on the previously unknown behaviours of frost formation within a moving bed. The experimental work matches the general trends that are expected from theoretical work but does not match the theoretical trends as closely as has been observed in fixed packed bed scenarios.

This chapter focuses on advancing the moving bed experimental work by introducing a second injector. The lack of uniform temperature within the bed material in the capture column during the

precool stage leads to uncertainty in measurement of results. The introduction of the second injector allows the precool stage and the capture stage to be run simultaneously. It is believed that the second injector running during the capture stage and well as the precool stage will keep the bed material at a more stable temperature as opposed to temperature profile results seen in chapter 6.

7.1 Introducing the second injector

The nature of experiments in the previous chapters has led to data that is difficult to interpret. The transient nature of the experimental procedure for the moving bed experiments, with cooling steps and capture steps performed sequentially, compounded with time required for the system to reach an equilibrium means that only a small section of experimental data is suitable for analysis.

The plan to introduce a second injector into the column means that the cooling step and capture step can be performed simultaneously, which is a step towards achieving a continuous cryogenic carbon capture system as the capture column would not be required to alternate between cooling and capture cycles. The second injector is positioned vertically within the radial centre of the column with the length of the perforated section of the injector reaching 250mm. This length of pipe for the gas injector was designed by heat transfer calculations required to sufficiently cool the bed material as the moving bed flows past the vertical gas injector. A sketch of the updated experimental rig is shown in figure 7.1. This would allow a more uniform temperature within the bed. For these moving bed experiments, ceramic bed material was used in favour of the steel bed material. Ceramic bed material was available in greater quantity in comparison to steel bed material after sifting to the specified size range, furthermore results from chapter 5 suggest that there is less of a supercooling effect which allows CO_2 frost to nucleate on the ceramic bed material faster in comparison to the steel bed material. The trace amount of CO_2 being detected by the outlet CO_2 sensor indicates that the steel moving bed could be seeing some small level of supercooling effect. Therefore, ceramic bed material was used in order to properly demonstrate that the length of time for the capture step is increased using the double gas injector set up by balancing the capture rate and removal rate of CO_2.

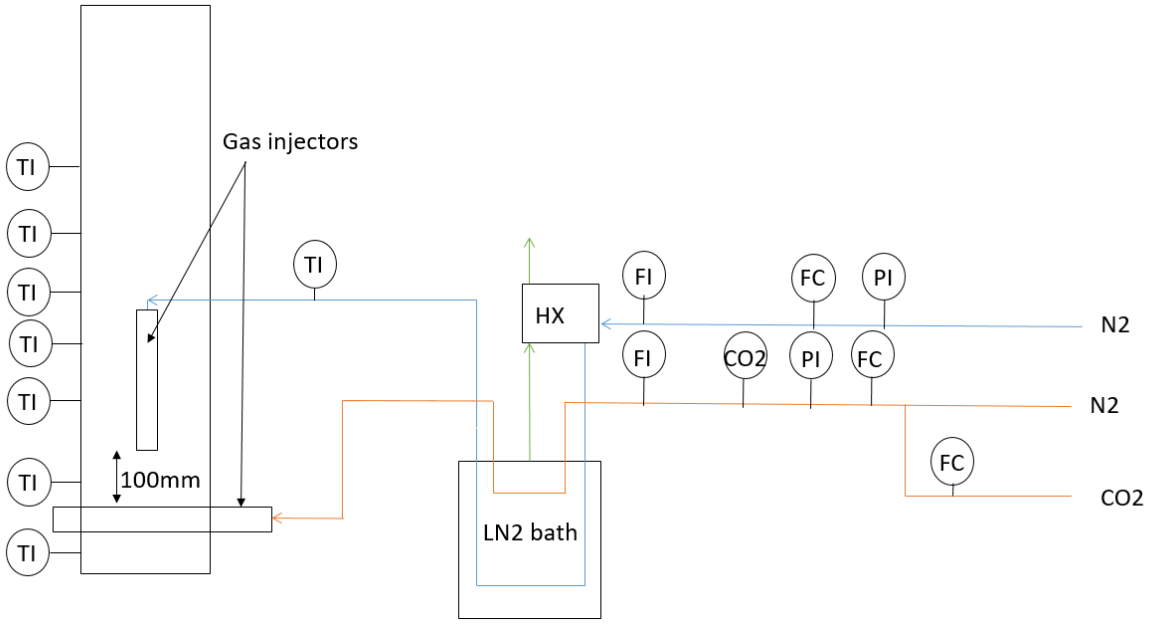

Figure 7.1. Sketch of experimental rig with second gas injector, distance between horizontal and vertical injectors is 100mm.

As the bed is moving, bed that is further up the column will pass the vertical cooling injector before interacting with the binary gas from the horizontal injector. Between the horizontal injector at the bottom of the column and the bottom of the vertical injector, there is a100mm spacing. This 100mm depth of bed material between the two gas injectors is expected to be the region of the bed where frost deposition will occur during the capture step.

The placement of the cylindrical injector inside the radial centre of the column makes the heat transfer close to the vertical injector difficult to predict due to the flow of gasses from both gas injectors. Whereas the horizontal injector can be represented by a 1D heat transfer equation up the height of the column, the vertical injector will instead inject cooling gas radially through a certain depth of bed before the gas begins to flow up and down the column. Furthermore, there will be some level of interference due to the flow of gas from the horizontal injector below the vertical injector. The two gas flow will interact with each other inside the capture column which could cause instability of the frost within the frosted region of the capture column.

Testing the vertical injector revealed that there was insufficient cooling from the vertical injector during the precooling step. Radial heat transfer appeared insufficient in comparison to the axial heat transfer within the system. Which resulted in the column a band of relatively warm bed material close to the bottom tip of the vertical injector. This warm band consisted of bed material mostly located in between the two gas injectors where the frosted bed zone is designed to occur.

The vertical injector was tested experimentally in the capture column, using ceramic bed material in the column. The ceramic bed material was cooled down using cryogenically cooled nitrogen gas fed into the column through the vertical injector. Once the column was cooled down sufficiently, the flow of nitrogen gas from the vertical injector was stopped and binary gas of CO_2 and N_2 was fed into the bottom of the column through the horizontal injector.

At first, it was observed that cryogenic cooling from the vertical injector was insufficient close to the wall in the bed depth below where the vertical injector is placed. Thermocouples close to the horizontal injector would reduce in temperature at a slower rate than observed from thermocouples recording temperatures further up the column. The temperature profiles in figure 7.2 also show this relatively warm band of bed material during the cooling step. The reason for this is unknown however it is known that the placement of the thermocouples around the circumference of the column would affect the temperature results which would point to one of two potential factors. The first being that the cooling effect within the column is uneven due to imperfect placement or set up of the vertical injector, in other words one sector of the bed near the wall is cooled more substantially than the rest of the bed material due to the injector not being placed in the exact centre of the column. The second being that the flow of cooling gas near the bottom of the vertical injector does not effectively cool bed material close to the wall, where most thermocouples in the column are located.

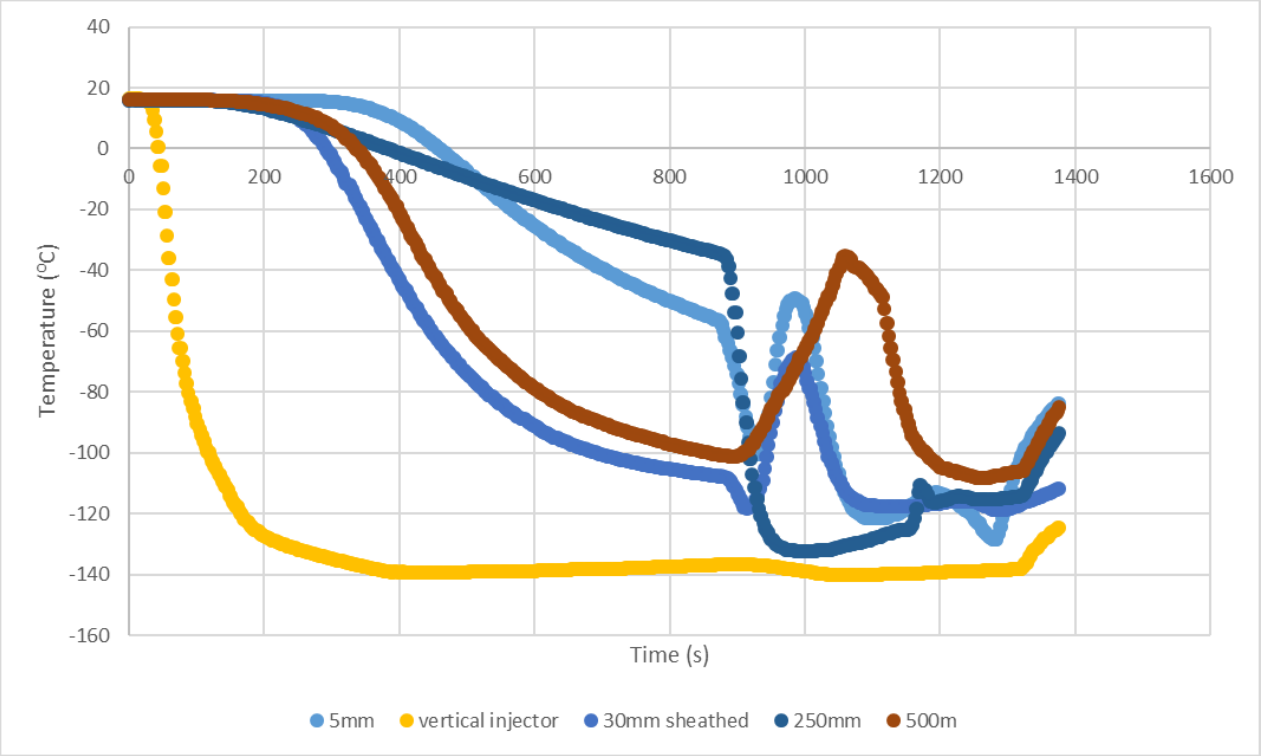

Figure 7.2. Temperature profiles from second injector precooling step.

The 250mm temperature profile is located within the depth of bed material that the vertical injector is submerged in. In comparison to figure 5.3, the cooling temperature profiles for the fixed bed horizontal injector, temperature profiles close to the injector cool down at a faster rather rate due to the high level of heat transfer between the gas and the bed material. As previously noted, the vertical injector cooling profile demonstrates a relatively warm band. In figure 7.2, the screw conveyor starts the moving bed at approximately 900s, where the temperature profiles for 30mm and 250mm show a sharp decline in temperature. The temperature profiles then rise and demonstrate a peak, showcasing the relatively warm section of the bed. Temperature profiles begin to stabilise for a while after the warm section of bed material has passed through the column.

The design of the second injector creating a region of insufficiently cooled bed material showcases room for improvement in the design of the cooling gas injector. The design of a single gas injector may be insufficient to rapidly cool down the bed material due to the high level of heat transfer within the column. The high level of heat transfer means that most heat transfer occurs close to the injector, with less efficient cooling further away from the source of the cooling gas and in potential areas of lower gas flow within the column. The fixed bed experiments using the single horizontal gas injector for cooling also shows a clear temperature gradient throughout the bed material with bed material further from the gas injector being progressively warmer.

The temperature profiles after the insufficiently cooled bed material band has passed shows that the temperature of the bed material can remain relatively stable. CO_2 desublimation runs with the moving bed were tested with particular interest in the temperature profiles after the warm bed material region has passed through the column.

The moving bed was tested with both the vertical cooling gas injector and the horizontal mixed gas injector both feeding gas into the column at the same time. The region of bed material between the two injectors will form the frosted region of the bed material. The interaction of the two gas phases inside the frosted region of the bed could affect the stability of the frost front. It is expected that the cooling gas flow rate and feed pressure needs to be controlled in order to prevent the mixed gas from being flushed out of the column.

Figure 7.3 shows an example of a moving bed experiment where the feed pressure of the cooling gas injector is disrupting the flow pattern of the mixed gas injector, this figure 7.3 the feed pressure of the cooling gas is 2 barg.

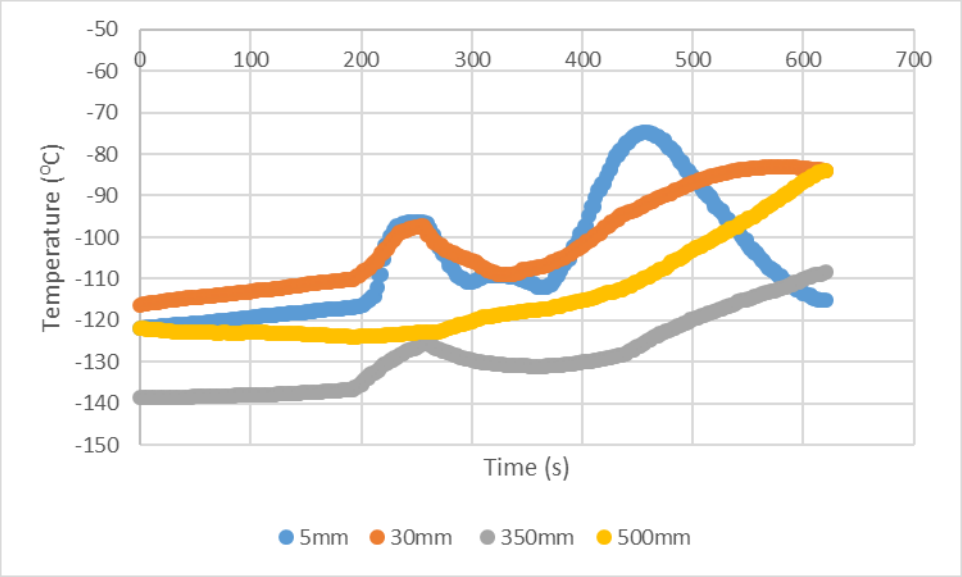

Figure 7.3. Double gas injector moving bed experiment – cooling gas flow dominant (40LPM, 18% CO_2).

In figure 7.3, the cooling gas line is shut off at 200s once the bed material is cooled down, the mixed gas line feeds through CO_2 mixed gas at 40LPM 18% CO_2. The mixed gas stream is fed into the column at approximately 200s, the frost front plateaus start forming shortly afterwards. The cooling gas stream is fed into the column again after the 5mm and 30mm temperature profiles plateau at 250s and the screw conveyor is started at the same time in order to begin the moving bed. The re-introduction of the cooling gas stream disrupts the frost front. The cooling gas flow down the column is dominant over the mixed gas flow up the column.

Figure 7.4 in comparison shows an experimental run where the mixed gas stream is not disrupted by the cooling gas line. The total flow rate of the mixed gas stream is increased to 100 LPM and the feed pressure of the cooling gas stream is decreased to 0.5 barg in order to reduce the flow rate.

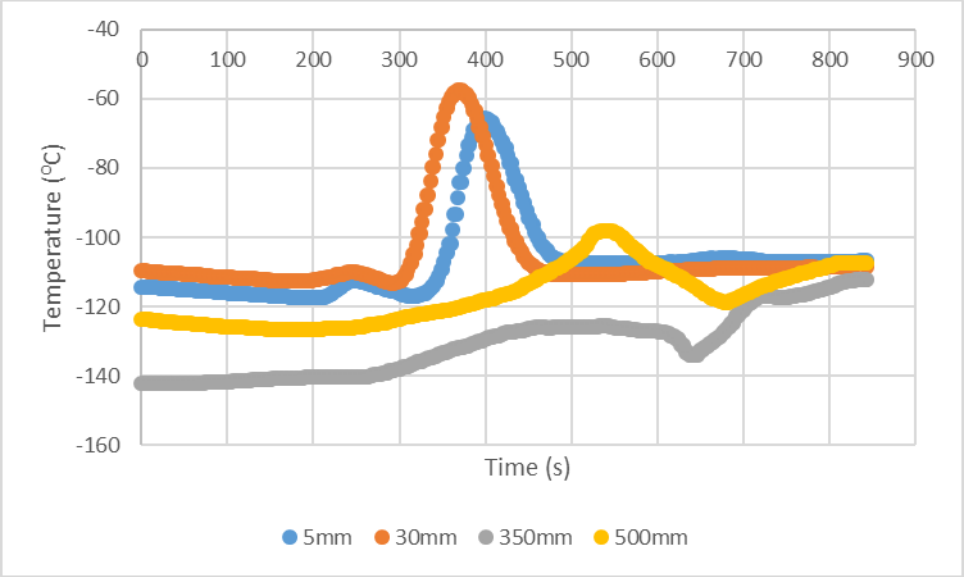

Figure 7.4. Double gas injector moving bed experiment – stable frost front (100LPM, 4% CO_2).

In figure 7.4 the cooling gas stream flow rate is reduced after the bed material is sufficiently cooled, the screw conveyor and the mixed gas stream are both started at the same time when. After the warm band of bed material is passed through the column, the temperature profiles of the 5mm and 30mm thermocouples remain stable at the desublimation temperature for CO_2. The frost front remains stable with the double gas injector set up for a period of 5 minutes, which is considerably longer than previous moving bed experiments.

The temperature profiles throughout the column are more stable in temperature using the double gas injector set up. For comparison in temperature profiles throughout the bed, figure 7.5 shows an example of the temperature profiles during the capture step when using only the horizontal injector, results from chapter 6 (figure 6.2d) which includes temperature profiles in the column further away from the frosted bed material region.

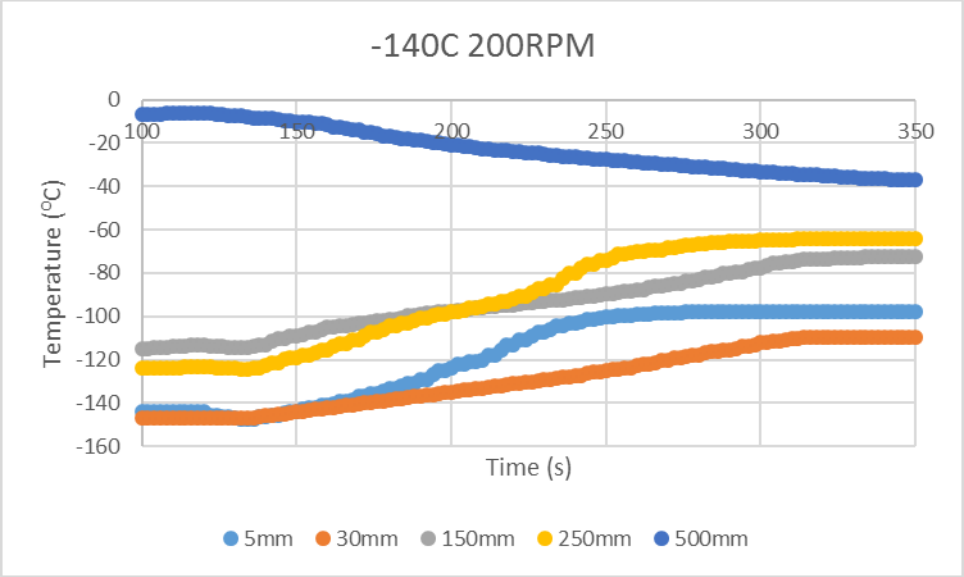

Figure 7.5. Horizontal gas injector moving bed experiment (100LPM, 18% CO_2).

From figure 7.5 in comparison to figures 7.3 and 7.4, it is clear that temperature profiles using the double gas injector set up and continuing the flow of cooling gas during the capture step improve the temperature profiles at different points in the bed. As a result this also allows for a greater period of time for which the capture step can continue to run when using the double gas injector set up.

Figure 7.6 shows experiments following the same experimental procedure as in figure 7.4 for different flow rates and CO_2 concentration.

a)

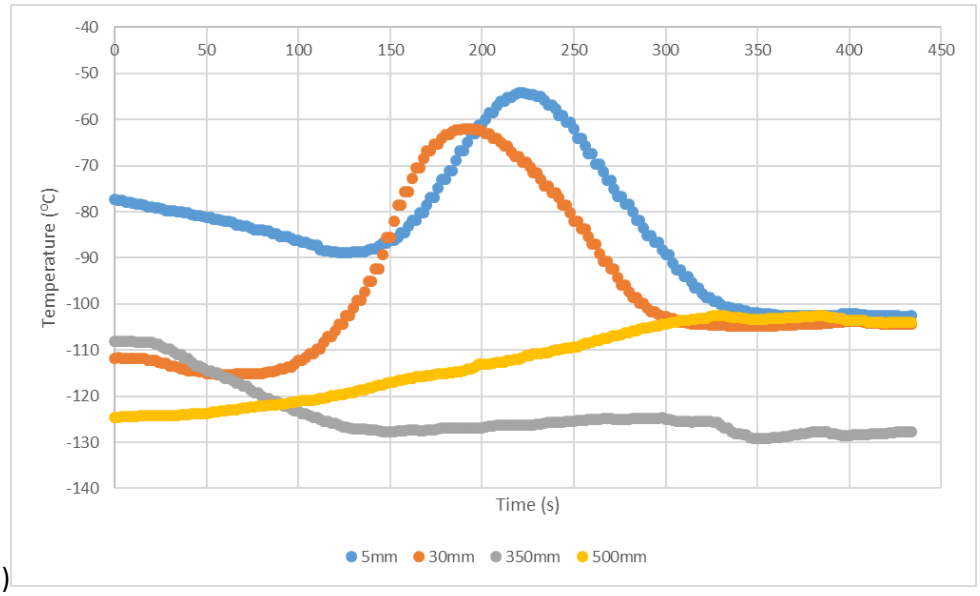

Figure 7.6. Double gas injector moving bed experiment (100LPM, 8% CO_2).

Figure 7.6a shows the temperature profiles stabilising at the CO_2 desublimation temperature after the warm section of bed material has passed through the column. The temperature front was not as stable

as in previous experiments with the double gas injector set up, this was due to operational issues with the screw conveyor during the experiment. The same general temperature profile patterns that were seen in figure 7.4 can also be seen in figure 7.6a for the 5mm and 30mm temperature profiles. The 350mm temperature profile remains colder than the other thermocouples as is typically the case with previous experiments, however the temperature profile did not show a rise in temperature as the cooling gas was adjusted or the moving bed was started in contrast with other figures. A decrease in temperature is observed instead, the cause for this is not certain. The temperature profile typically increases once the cooling gas flow pressure reduced or stopped in order to accommodate for the introduction of the mixed gas line. A change in temperature can also be due to the activation of the screw conveyor to start the moving bed, similar to what is seen with the 5mm and 30mm thermocouples detecting a band of relatively warm bed material. The precooling stage creates a temperature gradient within the bed material, due to issues with the screw conveyor during the experiments, the typical trends in the temperature profile due to a cascade of bed material are affected by the irregularity of bed flow in this particular experiment.

The double gas injector set up shows that the cooling stage and capture stage can be achieved simultaneously within the moving bed. The addition of the cooling gas stream during the capture stage must be accounted for in order to not disrupt the flow of the mixed gas stream, this is achievable by reducing the feed pressure of the cooling gas stream during the capture stage. This can be done in these experiments as the cooling stage cools the majority of the bed present within the column; the cooling gas stream during the capture stage serves to maintain a stable temperature of the bed material in the column as it travels down the column. In the operation of a more robust design, which would include a sublimation stage to recover the frosted CO_2 and a method of recirculating bed material to the capture column, the cooling gas would similarly only be required to deliver a relatively small amount of cooling duty to the bed material. Assuming the sublimation of CO_2 from the bed material left the bed material at a temperature of -90^{o}C, the cooling gas from the precooling gas injector would need to cool down recirculated bed material from -90^{o}C to -140^{o}C as opposed to cooling fresh bed material from room temperature to -140^{o}C, a cooling duty of 640MJ compared to 1,790GJ. The bed material would be recirculated at a temperature warm enough to regenerate CO_2 frost from the surface, so would only be required to be cooled down from desublimation temperature to initial bed temperature.

Concluding remarks

The introduction of a second injector to the capture column allowed the bed material to continue to be cooled by the cooling gas stream during the capture step. The second injector allowed the

experimental run time of the capture step to be increased which extended the period of time that the frost front was stable within the column.

Increasing the time span of the capture step signifies that the second injector is able to keep bed temperatures stable without disrupting the desublimation mechanism. Increasing the time span of the capture step utilising a double injector set up and a moving bed demonstrates that the moving bed concept can successfully extend the operation of the capture step.

Conclusions

This thesis has presented the first attempt of a moving packed bed for the purpose of cryogenic carbon capture. A purpose built rig was designed to capture CO_2 frost from a simulated flue gas of nitrogen and CO_2 and varying gas flow rates and CO_2 concentrations.

The objectives of this work were to used fixed packed bed experimental work to compare with experimental work done by Tuinier et al. (2011) for validation of theoretical models and design of the capture column. The objective of the moving bed experiments was to demonstrate that the moving bed can prevent the excessive build-up of CO_2 frost within the capture column. Here the main findings are summarised.

Fixed bed findings

The design and construction of the moving bed experimental rig was mostly successful, theoretical modelling and experimental results indicate that the design of the rig has been successful. However, the methods of controlling gas flow rates and bed flow rates could be improved to be more precise in order to more accurately balance the bed and frost front flow rates.

The first experimental results discussed focused on testing the suitability of the steel bed material chosen for the capture column. Pressure drop tests set out to identify whether the bed material experienced fluidisation at gas flow rates of up to 400 LPM and preliminary heat transfer experiments were performed to estimate the heat transfer coefficient between the steel bed material and the gas phase. Overall the steel bed material was found to be suitable for cryogenic experiments, as long as the issue of the bed material bouncing when falling from a height is kept under control. This issue was not noticed during moving bed experiments due to the design of the capture column, bed material was dropped from a mechanical screw conveyor a small height into a tray to collect the bed material.

The theoretical modelling work for the fixed packed bed has been shown to be accurate in predicting the behaviour of the fixed packed bed column, aligning well with experimentally constructed calibration curves for varying CO_2 gas concentration v/v and gas flow rates. Furthermore the results

also align well with fixed bed experimental work by Tuinier et al. (2011) when correction factors are applied. This work has provided a simple but effective method of comparing two sets of empirical data from different packed bed columns.

The frost front velocity was a key parameter for the operation of the moving bed. Experimental results show that the frost front velocity is predictable and has produced calibration curves for frost front velocity within the capture column for varying CO_2 concentrations and gas flow rates. Frost front velocity 0.4607-0.7835 mm/s for varying CO_2 concentrations between 4-18 % and between 0.3648-0.9804 mm/s for gas flow rates between 50-120 LPM. Overall the objectives set for the fixed bed experimental work have been achieved with success.

This work has provided a comparison between two different bed materials inside the cryogenic fixed packed bed column. A stainless steel and a high density ceramic bed material were compared with each other and against theoretical models. The high density ceramic had thermal properties similar to the steel bed material; with a slightly lower density 5900 kg/m^3 - 7850 kg/m^3, particle size distribution and specific heat capacity. Density and specific heat capacity were chosen to be similar in order to be certain that the ceramic bed material would meet the same suitability criteria as the steel bed material in the initial tests for fluidisation and heat transfer coefficient. Both bed materials provide a frost front velocity comparable in magnitude to the theoretical model predictions, with the ceramic bed material resulting in a faster frost front velocity due to the slightly lower density of the bed material in comparison to steel. In future work a greater variety of bed materials could be tested, density and specific heat capacity appear to have the greatest influence on frost front velocity.

Moving bed outcomes

The moving bed experimental work successfully demonstrates that the frost front velocity can be controlled and that the accumulation of frost within the capture column can be prevented. Moving bed experimental work however had shown a small decrease in the effectiveness of CO_2 capture which was seen by trace amounts of CO_2 being detected leaving the capture column. In order to validate CO_2 frost deposition in the moving bed experiments, trace CO_2 concentrations of the CO_2 lean gas were used to calculate the temperature of the gas at saturated vapour pressure for CO_2 and compared with the temperature profiles from thermocouples within the capture column.

The predicted saturation temperature profiles were then compared with temperature profiles close to the frost front. Data was collected for the CO_2 concentration in the lean gas exiting the capture column by two different methods. The first method placed the CO_2 sensor at the outlet of the capture column in line with the gas leaving the column, the second method inserted a small metal pipe close to the frost front to collect gas samples close to the frost front, the temperature of this gas sample

was measured by a thermocouple sheathed inside the small metal pipe and CO_2 concentration was measured by gas flowing through the small metal pipe. The gas sampling method using the small metal pipe generally showed more consistent results for predicted temperature which aligned better with the temperature profiles from the thermocouples. Evaluation of these two temperature profiles showed that the two temperature profiles follow similar trends, showing that the temperature of the frost front and the CO_2 concentration in the gas phase were linked.

One issue with these experiments is the presence of a small peak in the temperature profile at the beginning of the experiments, where the temperature predicted by the CO_2 concentration measurements is greater than the temperature measurements from the thermocouples. This would indicate that the CO_2 vapour pressure in the gas phase measured by the CO_2 sensor is greater than the saturated vapour pressure. A large increase in the CO_2 concentration at the beginning of the experiments could indicate a period of time when the gas phase is supercooled and thus CO_2 is not desubliming out of the gas phase. It should be noted that the relationship between CO_2 saturated vapour pressure and temperature is more sensitive at lower temperatures, this means that when measuring trace amounts of CO_2 relatively small fluctuations in concentration can result in a larger temperature difference. Investigating further into this period of possible supercooling in the moving bed would be potentially useful future work beyond this thesis.

The progression to the introduction of the vertical gas injector to provide cooling gas is an advancement towards a continuous capture process. The vertical gas injector provides cooling duty to the bed material while the original horizontal gas injector feeds the CO_2 mixed gas which desublimes onto the bed material. The experimental set up shows an extension of the available capture time of the capture column.

Experimental work utilising the combined vertical and horizontal gas injector set up has shown promising results, by extending the period of stable frost front temperatures around the 5mm and 30mm thermocouple points to approximately 5 minutes of CO_2 capture; however there is limited experimental work and robust data in this chapter due to restrictions imposed by Covid-19 lockdown. The injector testing would benefit from a larger range of experimental conditions to fully analyse the double gas injector set up. There is a need for further work to expand on the work done in this chapter.

Future work

The first cryogenic moving bed experiments have been demonstrated in this work. The experimental work demonstrates that the temperature profiles from moving bed experiments follow a different pattern in comparison to the fixed bed pattern. Temperature profiles for the 30mm thermocouple in moving bed experiments follow closely with temperature profiles calculated from the CO_2

concentration in the outlet of the capture column. The moving bed experimental runs show a general pattern of temperature profiles to expect from utilising the moving bed, there is however an opportunity to investigate how the temperature profiles adjust based on bed flow rate. Further work could investigate how the temperature profiles are affected when the moving bed flow rate matches frost front velocity, is less than frost front velocity and/or when the bed flow rate is greater than frost front velocity. If these conditions were to demonstrate different identifiable patterns for the temperature profiles then it would be possible to identify how closely frost front velocity and bed flow rate match by measuring temperature profiles.

The moving bed experiments that include the vertical gas injector for precooling stage and horizontal gas injector for injection of CO_2 mixed gas can easily be expanded upon. In particular, there is a need for investigation on balancing the flows of cooling gas from the vertical injector and mixed gas from the horizontal injector. This work has shown that balancing the flows through feed pressure of the gas flows is required in order to prevent the frost formation mechanisms within the moving bed from being affected.

Experimental work has sufficiently demonstrated the working principle of the moving packed bed capture system. CO_2 capture represents a single unit operation in a complete moving bed CCC system. The other unit operations; cooler-drier step, sublimation and recirculation of bed material into the capture column still require investigation and the combination of all unit operations to create a fully continuous process has yet to be achieved experimentally.

Appendix A – Further analysis on energy efficiency of carbon capture technologies

Chapter 2 focuses on the energy duty of carbon dioxide capture from an economic perspective. Appendix A gives an overview of the most typical carbon capture technologies and provides a range of energy duties associated with the technology from literature.

Table A.1. Energy duty values for different CO_2 capture technologies.

Technology	Energy duty (MJ/kg CO_2)	Reference
Oxy-Fuel Combustion	1.15-2.02	(Jensen, 2015)
Absorption	0.87-4.2	(Hussin & Aroua, 2020)
Adsorption	0.36-4.2	(Jensen, 2015)
Membranes	0.239-1	(Khalilpour et al., 2015)
Cryogenics	0.74-1.18	(Jensen, 2015)

The energy duty for membranes has decreased in recent years, patents utilise vaccum pumps to achieve the driving force. This adaptation makes membrane capture more appealing (Khalilpour et al., 2015).

The energy duty of cryogenic carbon capture is competitive compared to the presented capture technologies.

Appendix B – Heat transfer coefficient with estimate of thermal pinch point

This is a summary of experimental work performed on heat transfer coefficient within the ambient condition Perspex capture column. The introduction of the shroud covered thermocouple allowed an estimate of the gas temperature within the column. Figure B1 shows the results for heat transfer coefficient when estimating the gas temperature within the bed as being a fixed temperature difference, or pinch point, from the bed temperature.

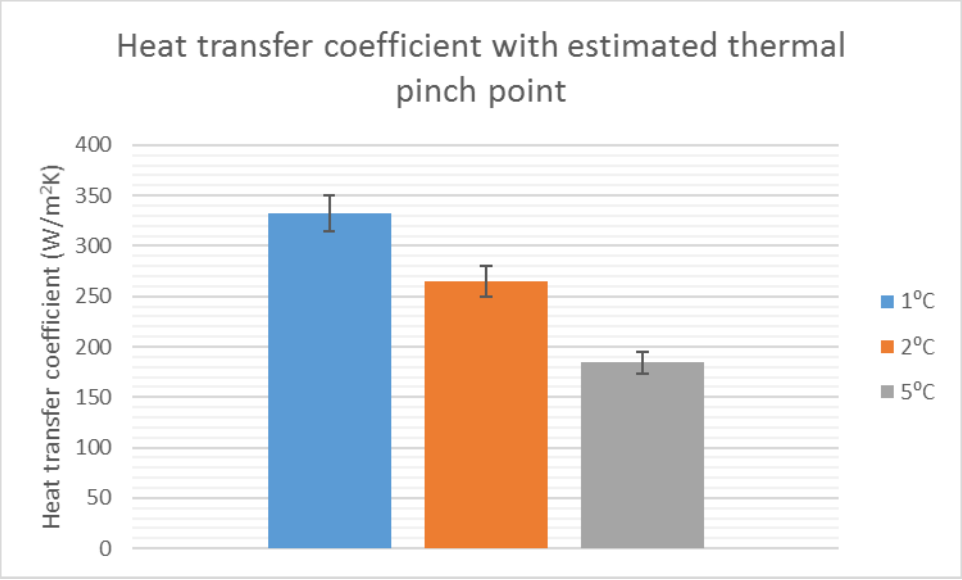

Figure B.1. Heat transfer coefficient with estimated thermal pinch point.

Comparison between results in figures B.1 and 5.2 shows that the heat transfer estimate using the shrouded thermocouple is similar to the heat transfer estimate using a fixed 5°C temperature difference. The heat transfer coefficient uncertainty is smaller for results in figure B.1 due to the variance in the thermal pinch point between the gas and bed material being ignored. Since the

temperature of the gas was not measured and was instead assumed to be a range of potential values there was less measurement uncertainty.

Appendix C – Fixed bed temperature profiles with varying gas flow rates

Figure 5.4 shows results for frost front velocities and CO_2 concentration measurements in fixed packed bed experiments with varying CO_2 concentration. Varying concentration affects the desublimation temperature of CO_2 in accordance with the difference in saturation pressure and partial pressure of CO_2. Varying concentration also affects how fast the frost front advances through the bed with a higher concentration of CO_2 leads to a higher frost front velocity.

Results in figure C.1 shows the same temperature profiles and CO_2 concentrations experiments with varying total gas flow rates at 18% CO_2 v/v concentration. The desublimation temperature does not vary significantly as the desublimation temperature for CO_2 is not dependent on the total flow rate of the gas. For 18% CO_2 v/v concentration, the desublimation temperature is approximately -97°C.

Ai)

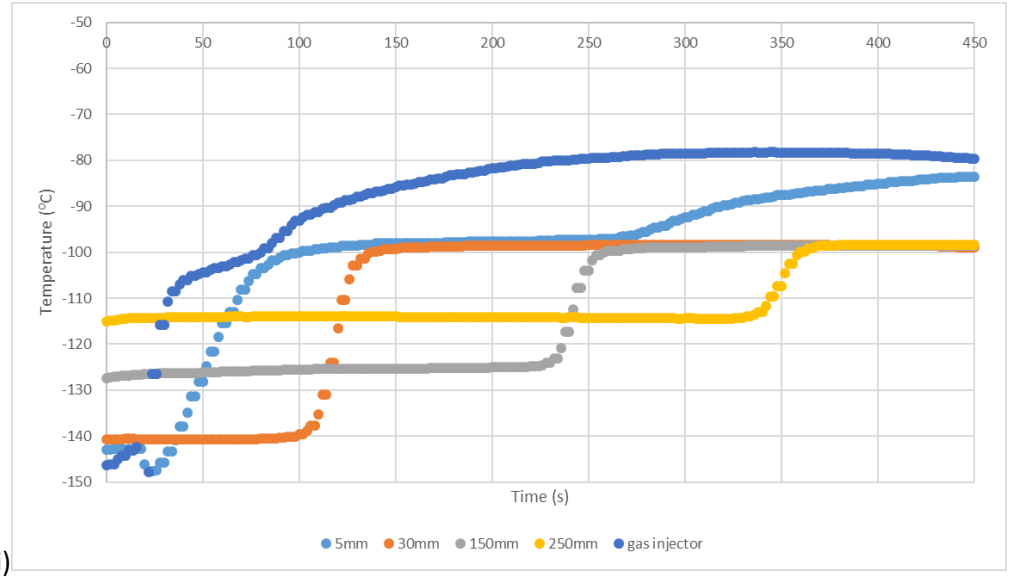

aii)

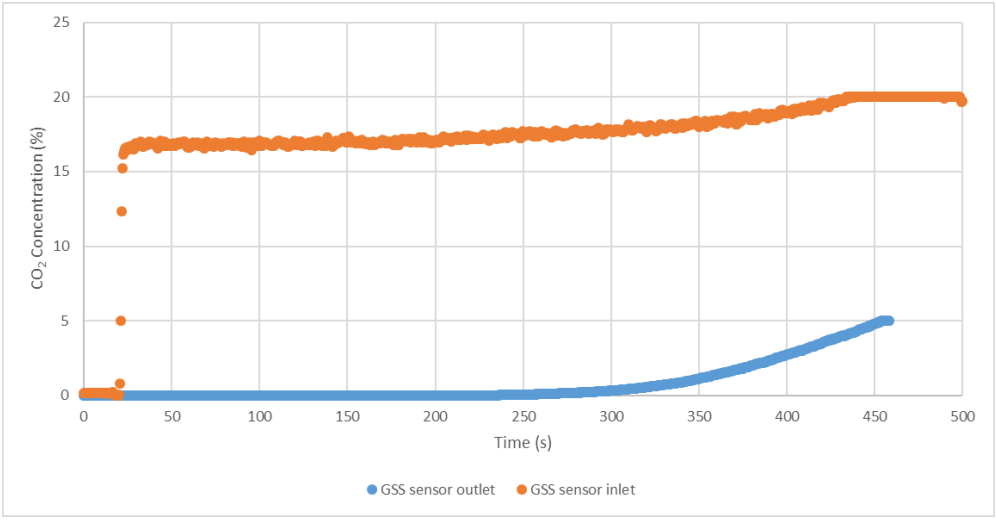
25
20
15
10
5
0
CO_2 Concentration (%)
0
50
100
150
200
250
300
350
400
450
500
Time (s)
GSS sensor outlet
GSS sensor inlet

bi)

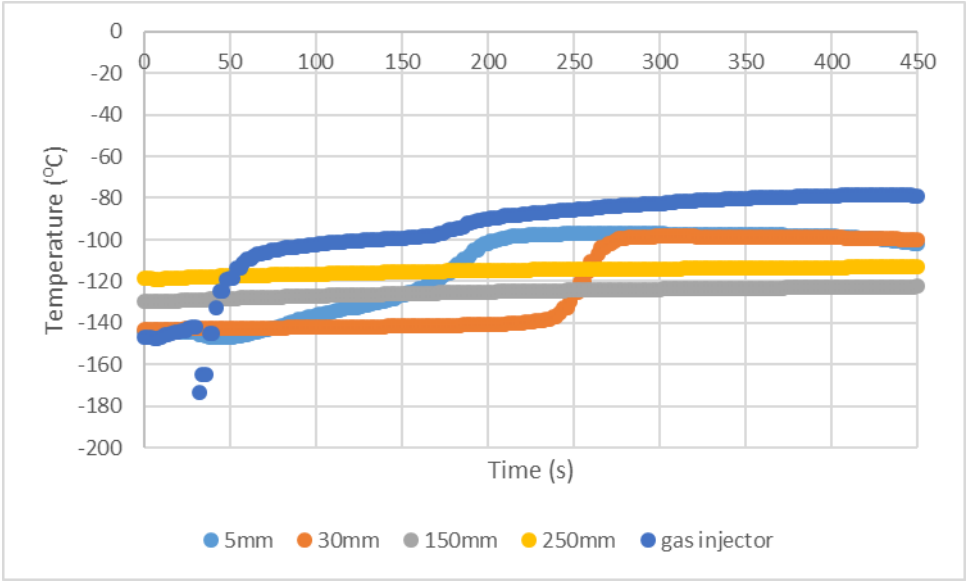
0
-20
-40
-60
-80
-100
-120
-140
-160
-180
-200
Temperature (°C)
0
50
100
150
200
250
300
350
400
450
Time (s)
5mm
30mm
150mm
250mm
gas injector

bii)

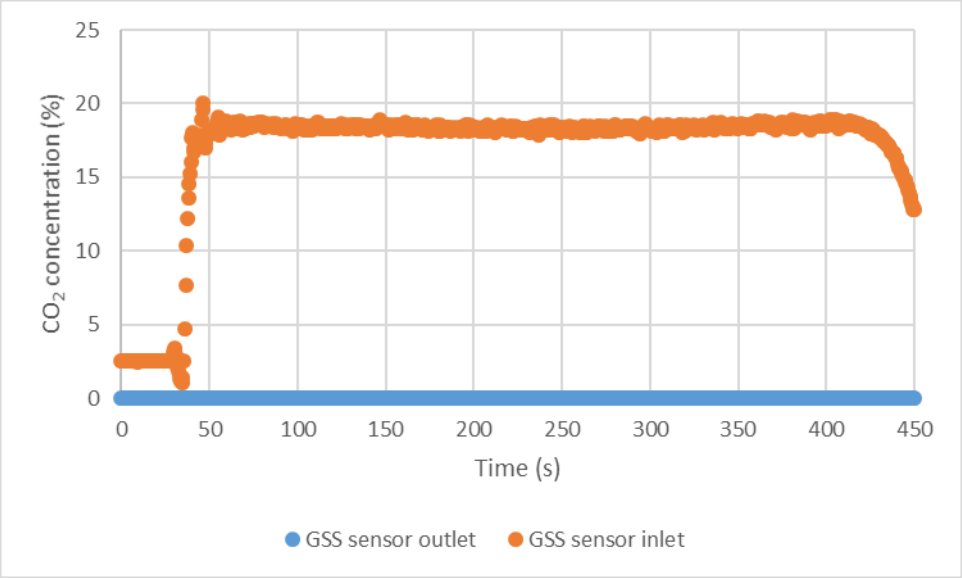
25
20
15
10
5
0
CO_2 concentration (%)
0
50
100
150
200
250
300
350
400
450
Time (s)
GSS sensor outlet
GSS sensor inlet

ci)

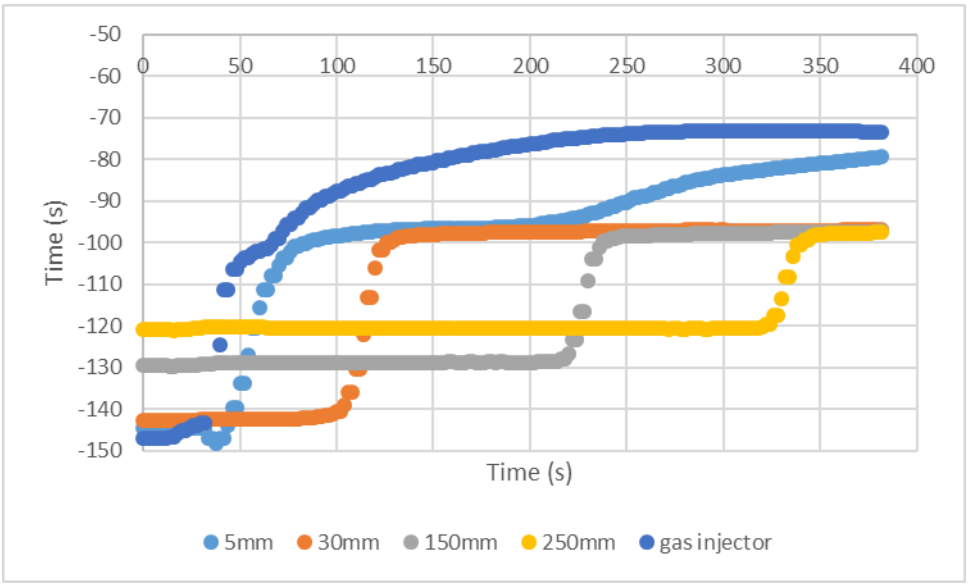

cii)

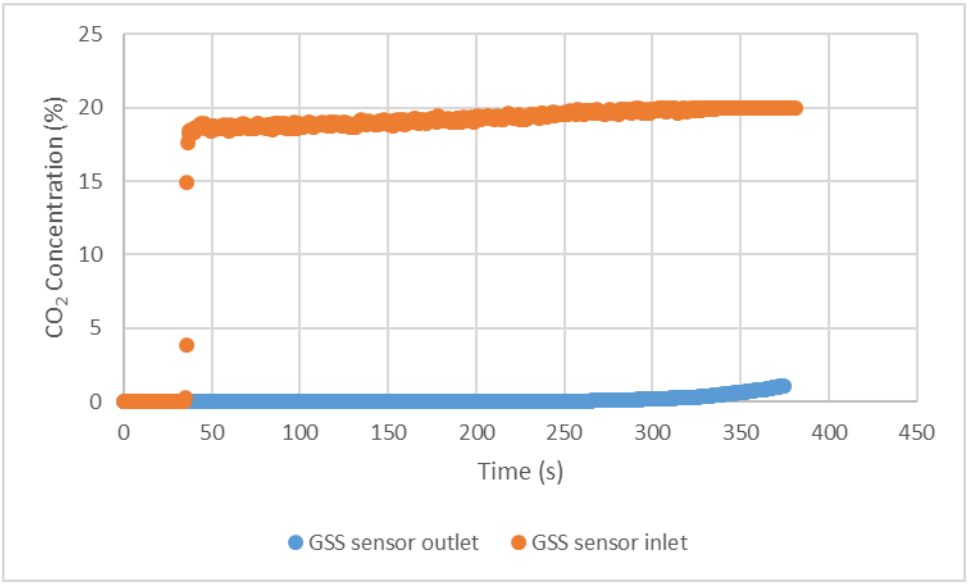

Figure C.1. Frost front velocity and CO_2 concentration results for fixed packed bed experiments with varying flow rates. ai) temperature profiles 100LPM 18%CO_2 aii) CO_2 sensor measurements 50LPM 18% CO_2 bi) temperature profiles 50LPM 18%CO_2 bii) CO_2 sensor measurements 100LPM 18% CO_2 ci) temperature profiles 120LPM 18%CO_2 cii) CO_2 sensor measurements 120LPM 18% CO_2.

The frost front velocity shows a proportional dependency on the total gas flow rate, the change from 100LPM to 50LPM halves the gas flow rate, which roughly halves the frost front velocity. The frost front velocity is therefore easy to predict when varying the total gas flow rate into the capture column.

Appendix D – Repeat experiments for comparison between theoretical and experimental temperature profiles with updated gas sampling method

The moving bed experimental results showed a variation in results. The old gas sampling method showed a variance in the comparisons between the 30mm experimental temperature profile and simulated temperature profile.

These differences lead to a new strategy for gas sampling to be developed. The gas sampling method using a small pipe inserted 30mm above the horizontal gas injector would feed gas from the frost front directly to the GSS gas sensor. The grey temperature profile in figure D.1 is measured by a thermocouple that is sheathed inside the gas sampling pipe.

Due to the nature of the moving bed experiments being prone to uncertainty, results from multiple experiments the new gas sampling method under the same conditions are compared. Results from further experiments to compare with figure 6.4 are shown in figure D.1.

a)

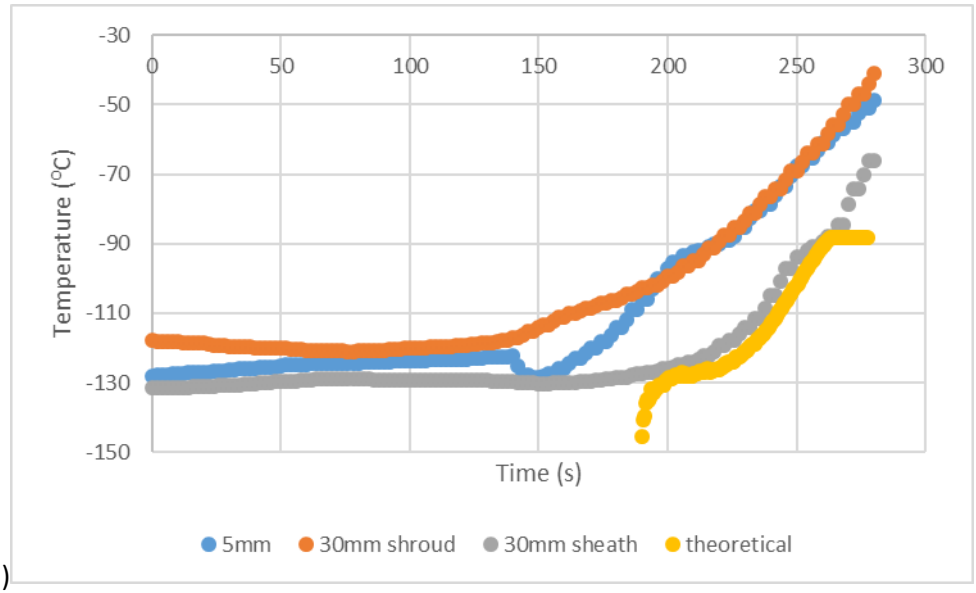

b)

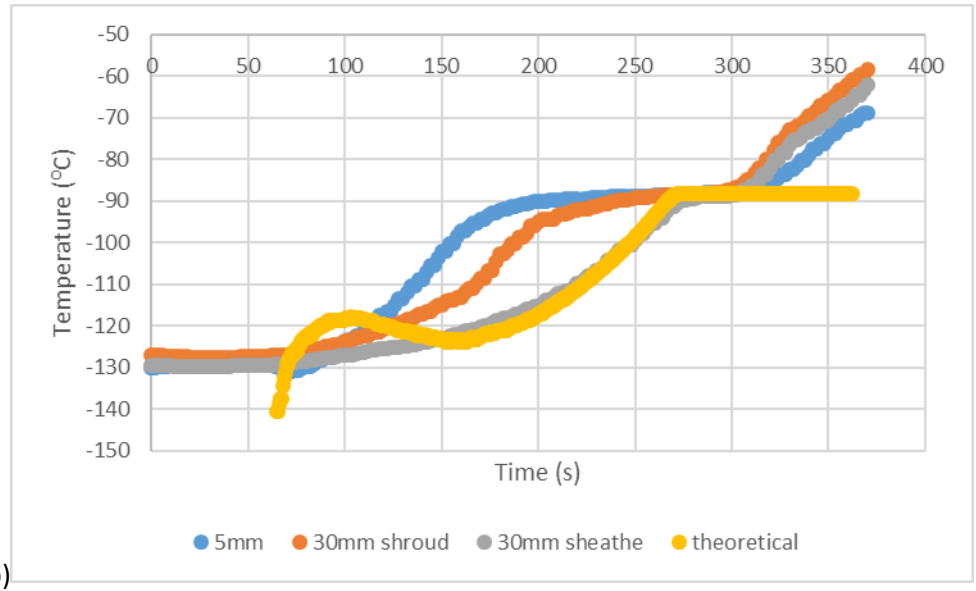

Figure D.1. Experimental results for updated gas sampling method (-130°C, 200RPM).

The resulting difference in the simulated temperature profile shows an improved correlation between the 30mm temperature profile and the simulated temperature profile. Figure D.1 b shows the simulated temperature profile increasing at the start of the experiment after the mixed gas is fed into the capture column. This initial rise in CO_2 concentration is most likely an effect of supercooling, where the CO_2 frost struggles to nucleate on the moving bed material in comparison to a fixed bed.

Overall, the stronger correlation between simulated and experimental temperature profiles puts greater confidence in the updated gas sampling method as a more reliable representation of what is happening close to the frost front boundary.

References

Aaron, D., & Tsouris, C. (2005). Separation of CO2 from flue gas: A review. *Separation Science and Technology, 40*(1-3), 321-348. doi:10.1081/ss-200042244

Abdulmohsin, R. (2013). *Gas dynamics and heat transfer in a packed pebble-bed reactor for the 4th generation nuclear energy.* (doctor of philosophy PhD Thesis), Missouri university of science and technology.

Achenbach, E. (1995). HEAT AND FLOW CHARACTERISTICS OF PACKED-BEDS. *Experimental Thermal and Fluid Science, 10*(1), 17-27. doi:10.1016/0894-1777(94)00077-l

Adams, T. A., Hoseinzade, L., Madabhushi, P. B., & Okeke, I. J. (2017). Comparison of CO2 Capture Approaches for Fossil-Based Power Generation: Review and Meta-Study. *Processes, 5*(3), 37. doi:10.3390/pr5030044

Ali, A., Maqsood, K., Syahera, N., Shariff, A. B. M., & Ganguly, S. (2014). Energy Minimization in Cryogenic Packed Beds during Purification of Natural Gas with High CO2 Content. *Chemical Engineering & Technology, 37*(10), 1675-1685. doi:10.1002/ceat.201400215

Allam, R., Martin, S., Forrest, B., Fetvedt, J., Lu, X. J., Freed, D., . . . Manning, J. (2017). Demonstration of the Allam Cycle: An update on the development status of a high efficiency supercritical carbon dioxide power process employing full carbon capture. In T. Dixon, L. Laloui, & S.

Twinning (Eds.), *13th International Conference on Greenhouse Gas Control Technologies, Ghgt-13* (Vol. 114, pp. 5948-5966). Amsterdam: Elsevier Science Bv.

Allen, K. G., von Backstrom, T. W., & Kroger, D. G. (2013). Packed bed pressure drop dependence on particle shape, size distribution, packing arrangement and roughness. *Powder Technology, 246*, 590-600. doi:10.1016/j.powtec.2013.06.022

Almendros-Ibáñez, J. A., Soria-Verdugo, A., Ruiz-Rivas, U., & Santana, D. (2011). Solid conduction effects and design criteria in moving bed heat exchangers. *Applied Thermal Engineering, 31*(6), 1200-1207. doi:https://doi.org/10.1016/j.applthermaleng.2010.12.021

Ambrose, D. (1956). The vapour pressures and critical temperatures of acetylene and carbon dioxide. *Transactions of the Faraday Society, 52*(0), 772-781. doi:10.1039/TF9565200772

Aouini, I., Ledoux, A., Estel, L., & Mary, S. (2014). Pilot Plant Studies for CO2 Capture from Waste Incinerator Flue Gas Using MEA Based Solvent. *Oil & Gas Science and Technology - Revue de l IFP, 69*, 1091-1104. doi:10.2516/ogst/2013205

Aronu, U. E., Gondal, S., Hessen, E. T., Haug-Warberg, T., Hartono, A., Hoff, K. A., & Svendsen, H. F. (2011). Solubility of CO2 in 15, 30, 45 and 60 mass% MEA from 40 to 120°C and model representation using the extended UNIQUAC framework. *Chemical Engineering Science, 66*(24), 6393-6406. doi:https://doi.org/10.1016/j.ces.2011.08.042

Baird, M. H. I., Rao, N. V. R., Tackie, E., & Vahed, A. (2008). Heat transfer to a moving packed bed of nickel pellets. *Canadian Journal of Chemical Engineering, 86*(2), 142-150. doi:10.1002/cjce.20023

Baxter, L., Baxter, A., & Burt, S. (2009). Cryogenic CO2 Capture as a Cost-Effective CO2 Capture Process.

Baxter, L., & Stitt, K. (2016). Cryogenic Carbon Capture Development.

Ben-Mansour, R., Habib, M. A., Bamidele, O. E., Basha, M., Qasem, N. A. A., Peedikakkal, A., . . . Ali, M. (2016). Carbon capture by physical adsorption: Materials, experimental investigations and numerical modeling and simulations - A review. *Applied Energy, 161*, 225-255. doi:10.1016/j.apenergy.2015.10.011

Beverloo, W. A., Leniger, H. A., & van de Velde, J. (1961). The flow of granular solids through orifices. *Chemical Engineering Science, 15*(3), 260-269. doi:https://doi.org/10.1016/0009-2509(61)85030-6

Bosoaga, A., Masek, O., & Oakey, J. E. (2009). CO2 Capture Technologies for Cement Industry. In J. Gale, H. Herzog, & J. Braitsch (Eds.), *Greenhouse Gas Control Technologies 9* (Vol. 1, pp. 133-140). Amsterdam: Elsevier Science Bv.

Bryson, C. E., Cazcarra, V., & Levenson, L. L. (1974). Sublimation rates and vapor pressures of water, carbon dioxide, nitrous oxide, and xenon. *Journal of Chemical & Engineering Data, 19*(2), 107-110. doi:10.1021/je60061a021

Calderón, C. A., Villagrán Olivares, M. C., Uñac, R. O., & Vidales, A. M. (2017). Correlations between flow rate parameters and the shape of the grains in a silo discharge. *Powder Technology, 320*, 43-50. doi:https://doi.org/10.1016/j.powtec.2017.07.004

Chen, X., Vinh, H., Avalos Ramirez, A., Rodrigue, D., & Kaliaguine, S. (2015). Membrane gas separation technologies for biogas upgrading. *RSC Adv., 5*. doi:10.1039/C5RA00666J

Chhabra, R. P., & Shankar, V. (2017). *Coulson and Richardson's Chemical Engineering : Volume 1B: Heat and Mass Transfer: Fundamentals and Applications*. San Diego, UNITED KINGDOM: Elsevier Science & Technology.

Clodic, D., El Hitti, R., Younes, M., Bill, A., & Casier, F. (2005). *CO2 capture by anti-sublimation Thermo-economic process evaluation*.

Crawford, C. W., & Plumb, O. A. (1986). The Influence of Surface Roughness on Resistance to Flow Through Packed Beds. *Journal of Fluids Engineering, 108*(3), 343-347. doi:10.1115/1.3242584

Crawshaw, J. P., Paterson, W. R., & Scott, D. M. (2000). Gas channelling and heat transfer in moving beds of spherical particles. *Chemical Engineering Research & Design, 78*(A3), 465-472. doi:Doi 10.1205/026387600527365

Diego, M. E., Arias, B., & Abanades, J. C. (2020). Investigation of the dynamic evolution of the CO2 carrying capacity of solids with time in La Pereda 1.7 MWth calcium looping pilot plant. *International Journal of Greenhouse Gas Control, 92*, 102856. doi:https://doi.org/10.1016/j.ijggc.2019.102856

Eide, L. I., Anheden, M., Lyngfelt, A., Abanades, C., Younes, M., Clodic, D., . . . Giroudiere, F. (2005). Novel capture processes. *Oil & Gas Science and Technology-Revue D Ifp Energies Nouvelles, 60*(3), 497-508. doi:10.2516/ogst:2005031

Eisfeld, B., & Schnitzlein, K. (2001). The influence of confining walls on the pressure drop in packed beds. *Chemical Engineering Science, 56*(14), 4321-4329. doi:https://doi.org/10.1016/S0009-2509(00)00533-9

Ergun, S. (1952). Fluid flow through packed columns. *Chemical Engineering Progress*.

Fenech, H. (1981). *Heat transfer and fluid flow in nuclear systems*: Pergamon Press.

Feng, J. S., Dong, H., Gao, J. Y., Li, H. Z., & Liu, J. Y. (2016). Numerical investigation of gas-solid heat transfer process in vertical tank for sinter waste heat recovery. *Applied Thermal Engineering, 107*, 135-143. doi:10.1016/j.applthermaleng.2016.06.175

Figueroa, J. D., Fout, T., Plasynski, S., McIlvried, H., & Srivastava, R. D. (2008). Advances in CO2 capture technology—The U.S. Department of Energy's Carbon Sequestration Program. *International Journal of Greenhouse Gas Control, 2*(1), 9-20. doi:https://doi.org/10.1016/S1750-5836(07)00094-1

Fossa, M., & Tanda, G. (2002). Study of free convection frost formation on a vertical plate. *Experimental Thermal and Fluid Science, 26*(6-7), 661-668. doi:10.1016/s0894-1777(02)00173-5

Ghanbari, T., Abnisa, F., & Wan Daud, W. M. A. (2020). A review on production of metal organic frameworks (MOF) for CO2 adsorption. *Science of The Total Environment, 707*, 135090. doi:https://doi.org/10.1016/j.scitotenv.2019.135090

Giauque, W. F., & Egan, C. J. (1937). Carbon Dioxide. The Heat Capacity and Vapor Pressure of the Solid. The Heat of Sublimation. Thermodynamic and Spectroscopic Values of the Entropy. *The Journal of Chemical Physics, 5*(1), 45-54. doi:10.1063/1.1749929

Gnielinski, V. (1978). Correlations for Calculating Heat-Transfer of Single Rows of Tubes and Tube Bundles in Cross-Flow. *Forschung Im Ingenieurwesen-Engineering Research, 44*(1), 15-25. doi:Doi 10.1007/Bf02560750

Goto, K., Yogo, K., & Higashii, T. (2013). A review of efficiency penalty in a coal-fired power plant with post-combustion CO2 capture. *Applied Energy, 111*, 710-720. doi:10.1016/j.apenergy.2013.05.020

Govender, N., Wilke, D., Pizette, P., & Abriak, N.-E. A study of shape non-uniformity and poly-dispersity in hopper discharge of spherical and polyhedral particle systems using the Blaze-DEM GPU code.

Govender, N., Wilke, D. N., Pizette, P., & Abriak, N. E. (2018). A study of shape non-uniformity and poly-dispersity in hopper discharge of spherical and polyhedral particle systems using the Blaze-DEM GPU code. *Applied Mathematics and Computation, 319*, 318-336. doi:10.1016/j.amc.2017.03.037

Gunn, D. J. (1978). Transfer of Heat or Mass to Particles in Fixed and Fluidized-Beds. *International Journal of Heat and Mass Transfer, 21*(4), 467-476. doi:Doi 10.1016/0017-9310(78)90080-7

Hahn, W., & Achenbach, E. (1986). Determination of the wall heat transfer coefficient in pebble beds.

Happel, J. (1949). Pressure Drop Due to Vapor Flow through Moving Beds. *Industrial & Engineering Chemistry, 41*(6), 1161-1174. doi:10.1021/ie50474a009

Hart, A., & Gnanendran, N. (2009). Cryogenic CO2 capture in natural gas. *Energy Procedia, 1*(1), 697-706. doi:https://doi.org/10.1016/j.egypro.2009.01.092

Haszeldine, R. S. (2009). Carbon Capture and Storage: How Green Can Black Be? *Science, 325*(5948), 1647-1652. doi:10.1126/science.1172246

Haut, R. C., & Thomas, E. R. (1989). Development and Application of the Controlled-Freeze-Zone Process. *SPE Production Engineering, 4*(03), 265-271. doi:10.2118/17700-PA

The Climate Change Act 2008 (2050 amendment) order 2019, (2019).

Houghton, J. T., Meiro Filho, L. G., Callander, B. A., Harris, N., Kattenburg, A., & Maskell, K. (1996). Climate Change 1995: The Science of Climate Change.

Hui, L., Jia, Z., Gui-Ping, C., & Hai-Feng, L. (2018). Gravitational discharge of fine dry powders with asperities from a conical hopper. *Aiche Journal, 64*(2), 427-436. doi:doi:10.1002/aic.15954

Hussin, F., & Aroua, M. K. (2020). Recent trends in the development of adsorption technologies for carbon dioxide capture: A brief literature and patent reviews (2014–2018). *Journal of Cleaner Production, 253*, 119707. doi:https://doi.org/10.1016/j.jclepro.2019.119707

JapanCCS. (2016). Tomakomai CCS Demonstration project.

Jensen, M. (2015). *Energy Process Enabled by Cryogenic Carbon Capture.* Brigham Young University.

Jia, X. L., Gui, N., Yang, X. T., Tu, J. Y., Jia, H. J., & Jiang, S. Y. (2017). Experimental study of flow field characteristics on bed configurations in the pebble bed reactor. *Annals of Nuclear Energy, 102*, 1-10. doi:10.1016/j.anucene.2016.12.009

Jia, X. L., Gui, N., Yang, X. T., Tu, J. Y., & Jiang, S. Y. (2017). Fluctuation and arching formation of very dense and slow pebble flow in a silo bed. *Journal of Nuclear Science and Technology, 54*(1), 111-126. doi:10.1018/00223131.2016.1213671

Kárászová, M., Zach, B., Petrusová, Z., Červenka, V., Bobák, M., Šyc, M., & Izák, P. (2020). Post-combustion carbon capture by membrane separation, Review. *Separation and Purification Technology, 238*, 116448. doi:https://doi.org/10.1016/j.seppur.2019.116448

Kelley, B. T., Valencia, J. A., Northrop, P. S., & Mart, C. J. (2011). Controlled Freeze Zone™ for developing sour gas reserves. *Energy Procedia, 4*, 824-829. doi:https://doi.org/10.1016/j.egypro.2011.01.125

Khalilpour, R., Mumford, K., Zhai, H., Abbas, A., Stevens, G., & Rubin, E. S. (2015). Membrane-based carbon capture from flue gas: a review. *Journal of Cleaner Production, 103*, 286-300. doi:https://doi.org/10.1016/j.jclepro.2014.10.050

Krupiczka, R., Rotkegel, A., & Ziobrowski, Z. (2015). Comparative study of CO2 absorption in packed column using imidazolium based ionic liquids and MEA solution. *Separation and Purification Technology, 149*, 228-236. doi:https://doi.org/10.1016/j.seppur.2015.05.026

KTA. (1981). Reactor Core Design of High-Temperature Gas-Cooled Reactors Part 3: Loss of Pressure through Friction in Pebble Bed Cores.

KTA. (1983). Reactor Core Design of High-Temperature Gas-Cooled Reactors Part 2: Heat Transfer in Spherical Fuel Elements.

Lee, K.-S., Jhee, S., & Yang, D.-K. (2003). Prediction of the frost formation on a cold flat surface. *International Journal of Heat and Mass Transfer, 46*(20), 3789-3796. doi:https://doi.org/10.1016/S0017-9310(03)00195-9

Liu, J., Wang, S., Zhao, B., Tong, H., & Chen, C. (2009). Absorption of carbon dioxide in aqueous ammonia. *Energy Procedia, 1*(1), 933-940. doi:https://doi.org/10.1016/j.egypro.2009.01.124

Ma, Y., Gao, J., Wang, Y., Hu, J., & Cui, P. (2018). Ionic liquid-based CO2 capture in power plants for low carbon emissions. *International Journal of Greenhouse Gas Control, 75*, 134-139. doi:https://doi.org/10.1016/j.ijggc.2018.05.025

MacDowell, N., Florin, N., Buchard, A., Hallett, J., Galindo, A., Jackson, G., . . . Fennell, P. (2010). An overview of CO2 capture technologies. *Energy & Environmental Science, 3*(11), 1645-1669. doi:10.1039/c004106h

Mankoc, C., Janda, A., Arevalo, R., Pastor, J. M., Zuriguel, I., Garcimartin, A., & Maza, D. (2007). The flow rate of granular materials through an orifice. *Granular Matter, 9*(6), 407-414. doi:10.1007/s10035-007-0062-2

Maqsood, K., Pal, J., Turunawarasu, D., Pal, A. J., & Ganguly, S. (2014). Performance enhancement and energy reduction using hybrid cryogenic distillation networks for purification of natural gas

with high CO2 content. *Korean Journal of Chemical Engineering, 31*(7), 1120-1135. doi:10.1007/s11814-014-0038-y

McGrath, M. (2017). Climate's magic rabbit: Pulling CO2 out of thin air. *BBC.*

Michael E. Parker, P. E., Northrop, S., Valencia, J. A., Foglesong, R. E., & Duncan, W. T. (2011). CO2 management at ExxonMobil's LaBarge field, Wyoming, USA. *Energy Procedia, 4*, 5455-5470. doi:https://doi.org/10.1016/j.egypro.2011.02.531

NETL. (2016). *Cryogenic Carbon Capture Development*. Retrieved from https://www.netl.doe.gov/projects/files/FE0028697_SES_Cryogenic_tech%20sheet.pdf

Nicolas, A., Garcimartin, A., & Zuriguel, I. (2018). Trap Model for Clogging and Unclogging in Granular Hopper Flows. *Physical Review Letters, 120*(19), 5. doi:10.1103/PhysRevLett.120.198002

Ohlemuller, P., Strohle, J., & Epple, B. (2017). Chemical looping combustion of hard coal and torrefied biomass in a 1 MWth pilot plant. *International Journal of Greenhouse Gas Control, 65*, 149-159. doi:10.1016/j.ijggc.2017.08.013

Okeke, I. J., & Adams II, T. A. Advanced petroleum coke oxy-combustion power generation with carbon capture and sequestration: Part II—Environmental assessment and cost of CO2 avoided. *The Canadian Journal of Chemical Engineering, n/a*(n/a). doi:https://doi.org/10.1002/cjce.24023

Parmesan, C., & Yohe, G. (2003). A globally coherent fingerprint of climate change impacts across natural systems. *Nature, 421*(6918), 37-42.

Powell, C. E., & Qiao, G. G. (2006). Polymeric CO2/N-2 gas separation membranes for the capture of carbon dioxide from power plant flue gases. *Journal of Membrane Science, 279*(1-2), 1-49. doi:10.1016/j.memsci.2005.12.062

Rhodes, M. J. (2008). *Introduction to Particle Technology*. Chichester, UNITED KINGDOM: John Wiley & Sons, Incorporated.

Ribeiro, R. P. P. L., Grande, C. A., & Rodrigues, A. E. (2014). Electric Swing Adsorption for Gas Separation and Purification: A Review. *Separation Science and Technology, 49*(13), 1985-2002. doi:10.1080/01496395.2014.915854

Rochelle, G., Chen, E., Freeman, S., Van Wagener, D., Xu, Q., & Voice, A. (2011). Aqueous piperazine as the new standard for CO2 capture technology. *Chemical Engineering Journal, 171*(3), 725-733. doi:https://doi.org/10.1016/j.cej.2011.02.011

Sahoo, R. K., & Das, S. K. (1994). EXERGY MAXIMIZATION IN CRYOGENIC REGENERATORS. *Cryogenics, 34*(6), 475-482. doi:10.1016/0011-2275(94)90207-0

Sanders, C. T. (1974). Frost formation: The influence of frost formation and defrosting on the performance of air coolers.

Sanz-Perez, E. S., Murdock, C. R., Didas, S. A., & Jones, C. W. (2016). Direct Capture of CO2 from Ambient Air. *Chemical Reviews, 116*(19), 11840-11876. doi:10.1021/acs.chemrev.6b00173

Scaccabarozzi, R., Gatti, M., & Martelli, E. (2016). Thermodynamic analysis and numerical optimization of the NET Power oxy-combustion cycle. *Applied Energy, 178*, 505-526. doi:10.1016/j.apenergy.2016.06.060

Sharma, S., & Maréchal, F. (2019). Carbon Dioxide Capture From Internal Combustion Engine Exhaust Using Temperature Swing Adsorption. *Frontiers in Energy Research, 7*, 143. doi:10.3389/fenrg.2019.00143

Song, C.-F., Kitamura, Y., Li, S.-H., & Ogasawara, K. (2012). Design of a cryogenic CO2 capture system based on Stirling coolers. *International Journal of Greenhouse Gas Control, 7*, 107-114. doi:https://doi.org/10.1016/j.ijggc.2012.01.004

Song, C., Liu, Q., Deng, S., Li, H., & Kitamura, Y. (2019). Cryogenic-based CO2 capture technologies: State-of-the-art developments and current challenges. *Renewable and Sustainable Energy Reviews, 101*, 265-278. doi:https://doi.org/10.1016/j.rser.2018.11.018

Song, C. F., Kitamura, Y., & Li, S. H. (2012). Evaluation of Stirling cooler system for cryogenic CO2 capture. *Applied Energy, 98*, 491-501. doi:https://doi.org/10.1016/j.apenergy.2012.04.013

Song, C. F., Kitamura, Y., Li, S. H., & Jiang, W. Z. (2013). Analysis of CO2 frost formation properties in cryogenic capture process. *International Journal of Greenhouse Gas Control, 13*, 26-33. doi:10.1016/j.ijggc.2012.12.011

Soria, A., Almendros-Ibáñez, J. A., Ruiz-Rivas, U., & Santana, D. (2009). Exergy Optimization in a Steady Moving Bed Heat Exchanger. *Annals of the New York Academy of Sciences, 1161*, 584-600. doi:10.1111/j.1749-6632.2009.04091.x

Span, R., & Wagner, W. (1996). A new equation of state for carbon dioxide covering the fluid region from the triple-point temperature to 1100 K at pressures up to 800 MPa. *Journal of Physical and Chemical Reference Data, 25*(6), 1509-1596. doi:10.1063/1.555991

Spitoni, M., Pierantozzi, M., Comodi, G., Polonara, F., & Arteconi, A. (2019). Theoretical evaluation and optimization of a cryogenic technology for carbon dioxide separation and methane liquefaction from biogas. *Journal of Natural Gas Science and Engineering, 62*, 132-143. doi:10.1016/j.jngse.2018.12.007

Sreenivasulu, B., Gayatri, D. V., Sreedhar, I., & Raghavan, K. V. (2015). A journey into the process and engineering aspects of carbon capture technologies. *Renewable & Sustainable Energy Reviews, 41*, 1324-1350. doi:10.1016/j.rser.2014.09.029

Stull, D. R. (1947). Vapor Pressure of Pure Substances. Organic and Inorganic Compounds. *Industrial & Engineering Chemistry, 39*(4), 517-540. doi:10.1021/ie50448a022

Tan, Y. T., Nookuea, W., Li, H. L., Thorin, E., & Yan, J. Y. (2016). Property impacts on Carbon Capture and Storage (CCS) processes: A review. *Energy Conversion and Management, 118*, 204-222. doi:10.1016/j.enconman.2016.03.079

Tojo, T., Atake, T., Mori, T., & Yamamura, H. (1999). Heat capacity and thermodynamic functions of zirconia and yttria-stabilized zirconia. *The Journal of Chemical Thermodynamics, 31*(7), 831-845. doi:https://doi.org/10.1006/jcht.1998.0481

Tuinier, M. J. (2011). *Novel process concept for cryogenic CO2 capture.* Eindhoven: Technische Universiteit, Eindhoven.

Tuinier, M. J., Annaland, M. V., Kramer, G. J., & Kuipers, J. A. M. (2010). Cryogenic CO2 capture using dynamically operated packed beds. *Chemical Engineering Science, 65*(1), 114-119. doi:10.1016/j.ces.2009.01.055

Tuinier, M. J., Annaland, M. V., & Kuipers, J. A. M. (2011). A novel process for cryogenic CO2 capture using dynamically operated packed beds-An experimental and numerical study. *International Journal of Greenhouse Gas Control, 5*(4), 694-701. doi:10.1016/j.ijggc.2010.11.011

Tuinier, M. J., Hamers, H. P., & Annaland, M. V. (2011). Techno-economic evaluation of cryogenic CO2 capture-A comparison with absorption and membrane technology. *International Journal of Greenhouse Gas Control, 5*(6), 1559-1565. doi:10.1016/j.ijggc.2011.08.013

Wakao, N., & Kaguei, S. (1983). Heat and Mass Transfer in Packed Beds. *Volume 1*. doi:https://doi.org/10.1002/aic.690290627

Wang, Guo, Q. C., Feng, Y. C., Lu, W. P., Dong, X. G., & Zhu, J. H. (2013). Theoretical study on the critical heat and mass transfer characteristics of a frosting tube. *Applied Thermal Engineering, 54*(1), 153-160. doi:10.1016/j.applthermaleng.2013.01.040

Wang, R. J., Fan, Y. P., & Lu, C. X. (2017). Influences of different operating parameters and gas/solid properties in rectangular cross-flow moving bed. *Powder Technology, 318*, 135-150. doi:10.1016/j.powtec.2017.05.029

Willson, P., Lychnos, G., Clements, A., Michailos, S., Font-Palma, C., Diego, M. E., . . . Howe, J. (2019). Evaluation of the performance and economic viability of a novel low temperature carbon capture process. *International Journal of Greenhouse Gas Control, 86*, 1-9. doi:https://doi.org/10.1016/j.ijggc.2019.04.001

Xu, C., Sandali, Y., Sun, G., Zheng, N., & Shi, Q. F. (2017). Segregation patterns in binary granular mixtures with same layer-thickness under vertical vibration. *Powder Technology, 322*, 92-95. doi:10.1016/j.powtec.2017.07.010

Yonko, J. D., & Sepsy, C. F. (1967). An Investigation of the Thermal Conductivity of Frost while Forming on a Flat Horizontal Plate. *Energy and Power Enginering, Volume 5*.

Yoon, S. M., & Kunii, D. (1970). GAS FLOW AND PRESSURE DROP THROUGH MOVING BEDS. *Industrial & Engineering Chemistry Process Design and Development, 9*(4), 559-&. doi:10.1021/i260036a011

Yun, R., Kim, Y., & Min, M. K. (2002). Modeling of frost growth and frost properties with airflow over a flat plate. *International Journal of Refrigeration-Revue Internationale Du Froid, 25*(3), 362-371. doi:Pii S0140-7007(01)00026-3

Doi 10.1016/S0140-7007(01)00026-3

ZareNezhad, B., & Eggeman, T. (2006). Application of Peng-Rabinson equation of state for CO2 freezing prediction of hydrocarbon mixtures at cryogenic conditions of gas plants. *Cryogenics, 46*(12), 840-845. doi:10.1016/j.cryogenics.2006.07.010

Zhao, M., Minett, A. I., & Harris, A. T. (2013). A review of techno-economic models for the retrofitting of conventional pulverised-coal power plants for post-combustion capture (PCC) of CO2. *Energy & Environmental Science, 6*(1), 25-40. doi:10.1039/C2EE22890D

Zhao, Y., Yang, S. L., Zhang, L. Q., & Chew, J. W. (2018). DEM study on the discharge characteristics of lognormal particle size distributions from a conical hopper. *Aiche Journal, 64*(4), 1174-1190. doi:10.1002/aic.16026